

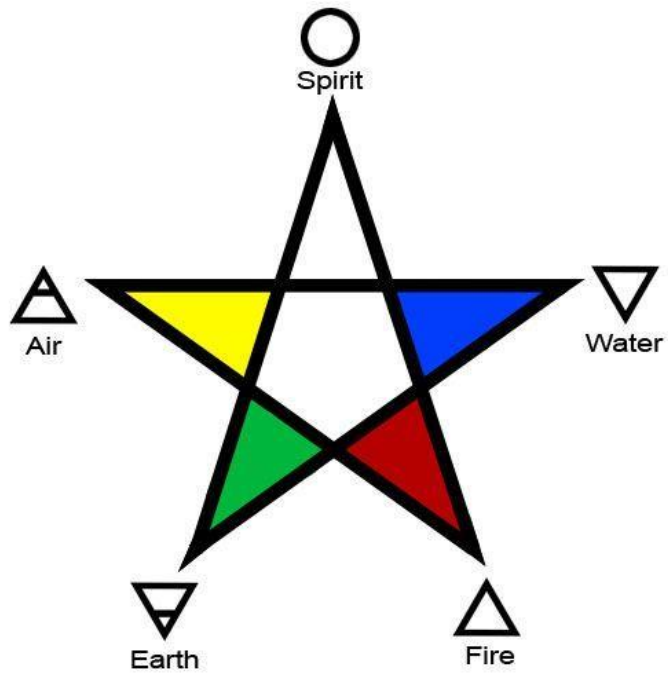
**A Novel Technique to Manufacture Carbon-free Gas Diffusion Layer
for Polymer Electrolyte Membrane Fuel Cell Application by a
Selective Laser Sintering (3D Printing)**

Arunkumar Jayakumar



**A Thesis submitted to
Auckland University of Technology
in fulfilment of the requirements for the degree of
Doctor of Philosophy (Ph.D.)
2018**

Nature is My Lord & Spirit



Abstract

A Gas Diffusion Layer (GDL) is an integral component of a PEM fuel cell stack, which plays a significant role in determining its performance, durability and the dynamic characteristics. An ideal GDL function to simultaneously transport three of the five essential elements, namely gas, water and heat involved in the electrochemical reaction. In addition, it also transports the electron produced in the electro chemical reaction and serves as an armour to safeguard the membrane (Nafion), which is a delicate and most expensive component of the PEM fuel cell stack. However, the conventional carbon-based GDL materials suffer from degradation issues during PEM fuel cell operation, and the predominant one is the electrochemical voltage oxidation.

The electrochemical degradation is due to the oxidation of the carbon present in the carbon paper to carbon dioxide especially at voltages greater than 0.207 V on a standard hydrogen electrode (SHE). Operating a PEM fuel cell stack at a low voltage (<0.207 V) is not practically possible since it can severely aggravate the operating efficiency and power density of the PEM fuel cell stack. Incorporating a GDL that is free from carbon can be a promising solution to circumvent these issues about the electrochemical oxidation. Also, the conventional GDL manufacturing technique had a tedious and complicated process, which involves multiple stages. These multiple production stages also led to its high manufacturing costs and increased lead-time.

The proposed research work is estimated to address both these issues of GDL durability and manufacturing costs. The additive manufacturing method incorporating selective laser sintering (SLS) technique aims to provide a comprehensive solution to address both these issues. The concept of SLS is that the laser beam robotically scans the composite powder (base and conductive powder) at points in a space defined by a 3D model, fusing and subsequently binding the composite material together to create a solid-state structure.

Thus, SLS can be a favourable route to fabricate a carbon-free GDL as well as to reduce its manufacturing costs and lead-time. At the end of the experimental investigation,

holistic characterisation studies were performed to have a general insight on the characteristics of the proposed material. Valuable information is extrapolated from the characterisation studies, which can assist, to fine-tune the material selection and SLS process parameter. In addition, ground-breaking findings from the perspective of the structural and functional relationship of the proposed GDL specimen had been made considering the first principles of the diverse field of engineering. Though the performance based on the experimental results are inferior, it gives us the buoyancy that the proposed proof of concept can be a promising route to fabricate durable and cost-effective gas diffusion layers based on the critical observations of the SLS process.

Acknowledgements

I express my sincere gratitude to the Auckland University of Technology (AUT) for the valuable learning prospects provided. I wish to express my thanks to Dr Maximiano Ramos, primary supervisor for providing an opportunity to experience an independent research. I would also like to thank my secondary supervisor Prof. Ahmed-Al-Jumaily for his assistance, and fruitful ideas to construct the thesis. I would also like to thank NZ product accelerator for partially funding the project. I am grateful to additional supervisor Prof. Sarat Singamneni for sharing his knowledge of selective laser sintering. I am also thankful to my Mentors Dr John Robertson and Dr Sashikumar Gangadharan and my friend Dr Sundar for sharing their expertise in Chemistry. Deepest gratitude is also due to Jo Stone for her assistance in proofreading the thesis in a professional manner.

I would like to thank Josephine Prasad and Prof. Zhan Chen who struggled hard to enrol me in the programme. I am also thankful to Liz Chandy and Leonie Duval who organised to purchase the components at the right time. I would also like to acknowledge Prof. Tek-Tjing Lie, Deputy Head of School - Engineering, Computer and Mathematical Sciences. I would also like to thank my fellow colleagues Dr Andrew Chalmers, Dr Rajkumar Velu, Udhaya Kumar and Dr Gautam Anand for productive discussions. The backing received from various staff from a diverse field of engineering, Brett Holden, Dave Crofts, Mark Masterton, Ross Jamieson, Jim Crossen, Tim Tuton, Dr Patrick Conor, Prof. Owen Young, Yuan Tao, Stefanie, and Yan Wang is absolutely worth specifying. I would also like to acknowledge Prof. Paul Kilmartin, Dr Karnika De Silva and Stephen Cawley from the University of Auckland and Garth Weinberg from Scion for assisting the conductivity and air permeability measurements. I would also like to acknowledge, NETZSCH, Germany for performing few thermal characterisation studies and Ingsman Energy and Fuel Cell Research Organization Private Limited, India.

I would also like to thank my parents Jayakumar and Lakshmi Bai for their affection and prayers throughout the period of my life. I would like to thank my brothers Lalithkumar and Rajkumar for their concrete support.

Contents

Abstract	iii
Acknowledgements	v
List of Figures	x
List of Tables.....	xii
List of Publications	xiii
List of Abbreviations and Acronyms	xvi
Chapter 1: Background	1
1.1 Introduction.....	1
1.2 Fuel Cell Fundamentals	1
1.3 Fuel Cell Reaction.....	3
1.4 Fuel Cell Classification.....	3
1.5 Polarisation Curve and its Significance	5
1.6 Fuel Cell Efficiency	7
1.7 PEM Fuel Cells: Principle and Integral Components	8
1.7.1 Membrane and Electrode Assembly (MEA)	8
1.7.2 Flow Field (Graphite) Plate	9
1.7.3 Electro-catalysts Layer and its Characteristics	9
1.7.4 Gas Diffusion Layer (GDL).....	10
1.8 Outline of the Thesis	10
Chapter 2: Literature Review	13
2.1 Introduction.....	13
2.2 Gas Diffusion and Structural Characteristics of GDL	13
2.3 Electrochemical Characteristics of GDL	16
2.4 Conventional Gas diffusion Medium (Carbon Paper vs. Carbon Cloth).....	17
2.5 Significance of Micro-Porous layer (MPL) and its Fabrication	19
2.6 Novel Gas Diffusion Medium.....	20
2.7 Durability of GDL.....	21
2.8 Conventional Manufacturing Technique of GDL.....	23

2.9	Research Questions	24
2.10	Contributions to knowledge	25
Chapter 3: Methodology and Materials.....		27
3.1	Introduction.....	27
3.2	Additive Manufacturing.....	29
3.2.1	Selective laser sintering	29
3.3	SLS Process parameters	31
3.4	Material Selection	31
3.4.1	Selection of Base Material	32
3.4.2	Selection of Conductive Filler Material.....	35
3.5	Experimental methods and equipment.....	38
3.6	Characterisation Techniques	39
3.6.1	Thickness and Surface Characterisation	39
3.6.2	Tensile characterisation	40
3.6.3	Porosity/Air-Permeability Measurement	41
3.6.4	Surface contact angle measurement.....	41
3.6.5	Electrical Characterisation	41
3.6.6	Thermal Characterisation.....	42
3.7	Closure	44
Chapter 4: Preliminary Investigation and Measurement Techniques		45
4.1	Introduction.....	45
4.2	Initial Investigation	45
4.3	Characterisation Techniques.....	48
4.3.1	Thickness and Surface Characterisation	48
4.3.2	Tensile characterisation	50
4.3.3	Porosity/Air-Permeability Measurement (Gurley Method).....	50
4.3.4	Surface contact angle measurement.....	51
4.3.5	Electrical Characterisation	52
4.3.6	Thermal Characterisation.....	53
4.4	Summary Initial Trial.....	53
4.5	Closure	54

Chapter 5: Experimental and Characterisation Studies.....	55
5.1 Introduction.....	55
5.2 Experimental Design.....	55
5.3 Experimental Iteration-I.....	57
5.4 Characterisation for Iteration-I	59
5.4.1 Thickness and Surface Characterisation- Iteration-I	59
5.4.2 Tensile Characterisation- Iteration-I.....	62
5.4.3 Porosity/Air permeability test- Iteration-I	62
5.4.4 Surface contact angle - Iteration-I	63
5.4.5 Electrical Characterisation- Iteration-I	63
5.4.6 Thermal Characterisation- Iteration-I.....	63
5.4.7 Summary- Iteration-I	64
5.5 Experimental Iteration-II	66
5.6 Characterisation for Iteration-II	67
5.6.1 Thickness and Surface Characterisation - Iteration-II	67
5.6.2 Tensile Characterisation- Iteration-II.....	68
5.6.3 Porosity/Air permeability test- Iteration-II.....	68
5.6.4 Surface contact angle - Iteration-II	68
5.6.5 Electrical Characterisation- Iteration-II	69
5.6.6 Thermal Characterisation- Iteration-II.....	69
5.6.7 Summary Iteration-II	69
5.7 Experimental Iteration-III	71
5.8 Characterisation for Iteration-III.....	72
5.8.1 Thickness and Surface Characterisation- Iteration-III.....	72
5.8.2 Tensile Characterisation- Iteration-III	74
5.8.3 Porosity/Air permeability test- Iteration-III.....	74
5.8.4 Surface contact angle- Iteration-III.....	74
5.8.5 Electrical Characterisation- Iteration-III.....	74
5.8.6 Thermal Characterisation- Iteration-III	74
5.8.7 Summary- Iteration-III.....	74
5.8.8 Significance of Laser Power	77

5.8.9	Balling Effect.....	78
5.9	PEM Fuel cell Experimental Set-up	79
5.10	Polarisation curve.....	82
5.11	Closure	83
Chapter 6: Discussions and Recommendations		84
6.1	Introduction.....	84
6.2	Structural and Functional Relationship.....	84
6.2.1	Structural-Mechanical-Electrical Relation	84
6.2.2	Hydrophobicity–Tensile Strength-Electrical Conductivity Relation.....	87
6.2.3	Porosity-Electrical Conductivity-Thermal Conductivity Relation	88
6.3	Challenges in Measurement System	88
6.3.1	Electrical and Thermal Measurements [Electrical Conductivity Vs. Thermal Conductivity]	89
6.3.2	Air porosity/Permeability measurement	92
6.3.3	Surface contact angle/Hydrophobicity measurement	92
6.3.4	Necessity for Real-Time Dynamic Measurement Technique.....	93
6.3.5	Uncertainty Analysis.....	93
6.4	Materials Limitation and Operational Environment	93
6.5	SLS Process Parameter Limitation	94
6.5.1	Causes of Improper Sintering	96
6.5.2	Balling effect Vs. Agglomeration.....	97
6.6	Repercussion of Wiedemann–Franz law	98
6.7	Critical Assessment.....	99
6.8	Presence of Zirconium in the proposed GDL specimen	101
6.9	Closure	103
Chapter 7: Conclusion and Future Work		104

List of Figures

Figure 1.1 Energy Conversion Path of Conventional Systems	2
Figure 1.2 V-I Characteristics of Fuel Cells	6
Figure 1.3 PEM fuel cell Stack Component and Ion transfer.	8
Figure 1.4 Conventional gas diffusion layer a) Carbon paper b) Carbon cloth.	10
Figure 2.1 Key Degradation factors for Gas Diffusion Layer	22
Figure 2.2 Manufacturing steps involved in the conventional GDL-SGL 39 BC [9].....	23
Figure 2.3 Functional chart on the contribution to Knowledge	25
Figure 3.1 Flowchart illustrating the methodology and material selection.....	28
Figure 3.2 Selective laser sintering process	30
Figure 3.3 SEM image of alumide	34
Figure 3.4 SEM image of polyamide	34
Figure 3.5 SEM image of Titanium (micron) Powder	37
Figure 3.6 SEM image of Titanium (nano) Powder.....	37
Figure 3.7 SEM with the integrated Energy Dispersive Spectrometer (EDX)	39
Figure 3.8 Texture analyser to perform Tensile Test.....	40
Figure 3.9 Digital Multimeter to measure the in-plane resistance	42
Figure 3.10 Laser flash apparatus NETZSCH	43
Figure 4.1 Line sketch of SLS experiment set-up [89]	46
Figure 4.2: Actual Photograph of Alumide Thin film	47
Figure 4.3: Spin coater used for Microfabrication.....	47
Figure 4.4 Surface morphology of graphene coated specimen	48
Figure 4.5 Cross-Sectional SEM of graphene coated on alumide specimen	49
Figure 4.6 EDX of the graphene-coated alumide surface	49
Figure 4.7 Surface Contact angle measurement a) Hydrophilic b) Hydrophobic.....	51
Figure 4.8 In-plane resistance measurement of graphene coated alumide specimen.	52
Figure 4.9 Cross-sectional image revealing graphene and alumide	53
Figure 5.1 Systematic procedure of Experimental Process.....	56
Figure 5.2 Functional chart of the experimental flow process.....	57
Figure 5.3 SEM of gas diffusion specimen fabricated with 90% alumide/10% Ti.....	59

Figure 5.4 Point analysis SEM image of 90% alumide/10% Ti.	60
Figure 5.5 SEM image of 80% alumide/20% Ti at various levels of magnification	61
Figure 5.6 SEM image of the GDL fabricated with 70% alumide/30% Ti.....	61
Figure 5.7 SEM image of the GDL with 90% PA/10% Ti (a) Surface View (b) Cross-sectional view	67
Figure 5.8 Cross-sectional view of the composite specimen with 80% PA/20% Ti.....	68
Figure 5.9 SEM of a GDL fabricated with 70% PA/30% Ti	71
Figure 5.10 GDL specimen formed with 90% PA/10% Ti (Nano).....	72
Figure 5.11 Low magnification SEM Images for 95% PA/5% Ti-Nano composites	73
Figure 5.12 High magnification SEM of 95% PA/5% Ti-Nano composites	73
Figure 5.13 SEM point analysis/Mapping of PA/Ti-Nano composites	75
Figure 5.14 Cross-Sectional View of the GDL for 95% PA/5% Ti (Nano).	76
Figure 5.15 GDL Specimen of 95% PA/5% Ti-Nano a) Cross-sectional view at Laser Power of 9 W b) Cross-sectional view at Laser Power of 12 W	77
Figure 5.16 Balling effect in SEM image for 95% PA/5% Ti-Nano	79
Figure 5.17 a) Line sketch of the Cell Assembly and b) Photograph of the Fuel cell experiment.....	81
Figure 5.18 PEM Fuel cell Polarisation Curve	82
Figure 6.1 SEM image of GDL with a) 90% Alumide/10% Ti [Micron] and b) 95% PA/5% Ti [Nano]	85
Figure 6.2 Role of Interconnector in Electrical Conductivity.....	86
Figure 6.3 Hydrophobicity nature of GDL specimen fabricated with (a) 70% PA/30% Ti (Micron) and (b) 95% PA/5% Ti (Nano)	88
Figure 6.4 In-plane Electrical Resistance Measurement technique	90
Figure 6.5 Armfield HT11 for Linear Heat Conductivity Measurement	91
Figure 6.6 Effect of various operating parameters on the energy input to surface	95
Figure 6.7 Improper SLS along the Bottom of the GDL specimen	96
Figure 6.8 Balling and Agglomeration Phenomenon GDL composition.....	98
Figure 6.9 Linear increase in the Thermal conductivity with Ti [Iteration II].....	99
Figure 6.10: V-I Characteristics of Fuel Cells	100
Figure 6.11 Zirconium presence in Alumide powder	101
Figure 6.12 Zirconium presence in Polyamide powder.	102

List of Tables

Table 1.1 Classification of Fuel cells [Organised from high to low temperature].....	4
Table 1.2 Integral Membrane and Electrode Components and their Function	9
Table 2.1 Physical characteristics of diffusion medium [25, 26].....	16
Table 2.2 Comparison of features of carbon paper and carbon cloth [28].....	17
Table 2.3 Physical properties of various carbon blacks used to fabricate MPL [42-45]	19
Table 2.4 Effect of PTFE content in MPL on PEMFC Performance [48, 50-52].....	20
Table 2.5 Properties of Carbon Aerogels [51].	21
Table 2.6 Properties of SGL 39 BC [Baseline-GDL]	24
Table 3.1 List of base polymer materials.	32
Table 3.2 List of base polymer materials (Contd...).....	33
Table 3.3 Corrosion rates of materials [73]	35
Table 3.4 Base polymer and conductive filler materials.....	37
Table 3.5 Characterisation Techniques and the related Measuring Instruments	38
Table 4.1 Porosity/air permeability measurement of the alumide/graphene specimen ..	50
Table 4.2 EDX cross-sectional analysis of the graphene coated alumide specimen	54
Table 5.1: Laser power required to sinter various configuration of Alumide/Titanium.	58
Table 5.2 EDX analysis of GDL fabricated with 90% alumide/10% Ti.....	60
Table 5.3 Weight % elemental composition of entire GDL for Iteration-I.....	62
Table 5.4 Surface contact angle measurement for Alumide/Titanium composition.....	63
Table 5.5: Laser power to sinter Polyamide/Titanium composite powder	66
Table 5.6 Thermal conductivity of GDL specimen fabricated with PA/Titanium composite.	69
Table 5.7 EDX analysis of the GDL specimen sintered with 80% PA/20% Ti.....	70
Table 5.8 EDX analysis of various zones of the sintered GDL for the 95% PA/5% Ti (Nano) composition.....	76
Table 7.1 Research Questions, Outcomes and its Implications	104
Table 7.2 Quantitative Results of the Proposed GDL Material.....	105

List of Publications

The following Book Chapters, Journal papers, and Conference papers have been published over the Ph.D. research duration. Though mostly covered by this thesis, they form an additional body of work, and the reader may refer it. However, two of the primary publications are listed in Appendix B and C. There is also one U.S patent to be filed.

Book Chapter

Arunkumar Jayakumar, An Assessment on Polymer Electrolyte Membrane (PEM) Fuel Cell Stack Components, Applied Physical Chemistry with Multidisciplinary Approaches, Apple Academic Press, Book Chapter, E-Book ISBN: 9781315169415, 14 May 2018.

Selected Journals

Arunkumar Jayakumar, “A Comprehensive Assessment on the Durability of Gas Diffusion Electrode Materials in PEM fuel cell Stack”, *Frontiers in Energy* [Accepted]

Arunkumar Jayakumar, Sarat Singamneni, Maximiano Ramos, Ahmed M Al-Jumaily, Sethu Sundar Pethaiah, “Manufacturing the Gas Diffusion Layer for PEM Fuel Cell Using a Novel 3D Printing Technique and Critical Assessment on the Challenges Encountered”, *Materials*, Special Issue "Advanced Materials in Polymer Electrolyte Fuel Cells, 14 July 2017.

S. Pethaiah, **Arunkumar Jayakumar**, Maximiano Ramos, Ahmed Al-Jumaily, “The impact of anode design on fuel crossover of direct ethanol fuel cell,” *Bulletin of Materials Science*, Volume 39, Issue 1, 2016, pp 273-278.

Arunkumar Jayakumar, S. Pethaiah, Maximiano Ramos, John Robertson and Ahmed, Al-Jumaily, “A Technical Review on Gas Diffusion, Mechanism and Medium of PEM Fuel Cell,” *Ionics*, Volume 21, Issue 1, 2015, Page 1-18.

Selected Conferences

Arunkumar Jayakumar “PEM fuel cell gas diffusion layers through Selective Laser Sintering: Scopes and Challenges,”[Accepted] June 28-July 2, The ASME 2018, ASME Power & Energy Conference, 2018, June 24-28, 2018, Lake Buena Vista, Florida, USA.

Arunkumar Jayakumar, “An Assessment on Additive Manufacturing Technique to Fabricate Integral PEM Fuel Cell/Electrolyser Component” 3rd International Conference on Design, Analysis, Manufacturing & Simulation (ICDAMS 2018) at Saveetha University, Chennai, India. 6–7 April 2018.

Arunkumar Jayakumar, “Measurement Techniques and Related Challenges Involved in the Gas Diffusion Electrode Characterization of PEM fuel cell Stack,” 2nd International Conference on Battery & Fuel Cell Technology, July 27-28, 2017 Rome, Italy.

Arunkumar Jayakumar, et al., “Real-Time Applications of Electrochemical Impedance Spectroscopy” - A Technical Assessment, ENZCON, November 17-18, 2016, Wellington, NZ.

Arunkumar Jayakumar, et al., “A Durable Gas Diffusion Medium Synthesized by 3D Printing”, November 11 – 17, 2016, The ASME 2016, International Mechanical Engineering Congress & Exposition, Phoenix Convention Center, Phoenix, Arizona, USA.

Arunkumar Jayakumar, et al., “A Novel Gas Diffusion Material for PEM Fuel Cell Application by 3D Printing Technique”, International Conference of Young Researchers

on Advanced Materials (IUMRS-ICYRAM. 11 to 15 Dec 2016), Indian Institute of Science, Bangalore, India.

Arunkumar Jayakumar, et al., “Correlation of Heat and Current Distribution in the GDL of a PEMFC Stack”, International Conference of Young Researchers on Advanced Materials (IUMRS-ICYRAM. 11 to 15 Dec 2016), Indian Institute of Science, Bangalore, India.

Arunkumar Jayakumar, et al., “A Novel Fuzzy Schema to Control the Temperature and Humidification of PEM Fuel Cell System,” June 28-July 2, The ASME 2015, 13th Fuel Cell Science, Engineering, and Technology Conference, San Diego, USA.

Patent

Arunkumar Jayakumar, et al., “Next Generation Gas Diffusion Electrodes for High Power Density PEM Fuel Cell Application by 3D Printing Technique”, US Patent to be filed.

List of Abbreviations and Acronyms

PEM	Polymer Electrolyte Membrane
AFC	Alkaline Fuel Cell
SOFC	Solid Oxide Fuel Cell
MCFC	Molten Carbonate Fuel Cell
PAFC	Phosphoric Acid Fuel Cell
IC	Internal Combustion
3D	Three Dimensional
SLS	Selective Laser Sintering
LASER	Light Amplification by Stimulated Emission of Radiation
SCR	scan radius
SS	step size
SP	step period
SCSP	scan spacing
MEA	Membrane and Electrode Assembly
GDL	Gas Diffusion Layer
CL	Catalyst Layer
MPL	Micro Porous Layer
SHE	Standard Hydrogen Electrode
psi	Pounds per square inch
kgf	kilogram-force
RPM	revolutions per minute
ASTM	American Society for Testing and Materials
ISO	International Organization for Standardization

CVD	Chemical vapor deposition
MD	Machine direction
PA	Polyamide
Ti	Titanium
Pt	Platinum
CO ₂	Carbon dioxide
CO	Carbon monoxide
PTFE	Poly Tetra Fluro Ethylene
Ca.	Circa [approximate]
CAD	Computer-aided design
CAM	Computer-aided manufacturing
US-DoE	United States Department of Energy
SEM	Scanning Electron Microscope
EDX	Energy Dispersive X-ray Spectrometry

School of Engineering, Computer, and Mathematical Sciences
Auckland University of Technology

‘I hereby declare that this submission is my own work and to the best of my knowledge and belief, it contains no material previously published or written by another person nor material which to a substantial extent has been accepted for the qualification of any other degree or diploma of a university or other institution of higher learning, except where due acknowledgement is made in the acknowledgments.’

Full name

Arunkumar Jayakumar

Signature

Date: 28/05/2018

Chapter 1: Background

“Thousand Miles Journey Begins with the First Step”

Lao Tzu

1.1 Introduction

Energy is an indispensable constituent and key driver for the sustainable growth of any nation. Conventional energy systems, though highly reliable, pose devastating consequences due to toxic gas emission. To circumvent this effect, the use of alternative energy systems has been significantly increasing over the last few decades. Regrettably, the most accredited clean systems, such as wind and solar power systems pose concerns due to their intermittent nature, causing a mismatch between the energy supply and demand. Fuel cells can be a promising solution to address these issues, as they have the potential to be both a clean and reliable power system. In addition, their operating efficiency can be as high as 85% for combined heat and power [1]. Furthermore, fuel cells have economic implications for petroleum importing nations by reducing a dependency on imported petroleum and enhancing the energy security. The present chapter deals with the fuel cell fundamentals, fuel cell types, fuel cell performance characteristics, fuel cell efficiency, advantages of PEM fuel cells, and various key components of the PEM fuel cell stack. The chapter also includes an outline of the thesis.

1.2 Fuel Cell Fundamentals

Fuel cells have been in existence since 1838 a few decades before Nikolaus Otto designed the Internal Combustion (IC) engine. In the December 1838 edition of The London and Edinburgh Philosophical Magazine and Journal of Science, Welsh physicist William Grove explained the basic concept of fuel cell [2] operation. Grove used a combination of sheet iron, copper and porcelain plates, and a solution of sulphate of copper and diluted acid.

In a fuel cell, the chemical energy of the fuel is converted directly to electrical energy, unlike traditional generators, where the chemical energy is first converted to the mechanical energy (by IC engine) and then to electrical energy (by generator) as illustrated in Figure 1.1.

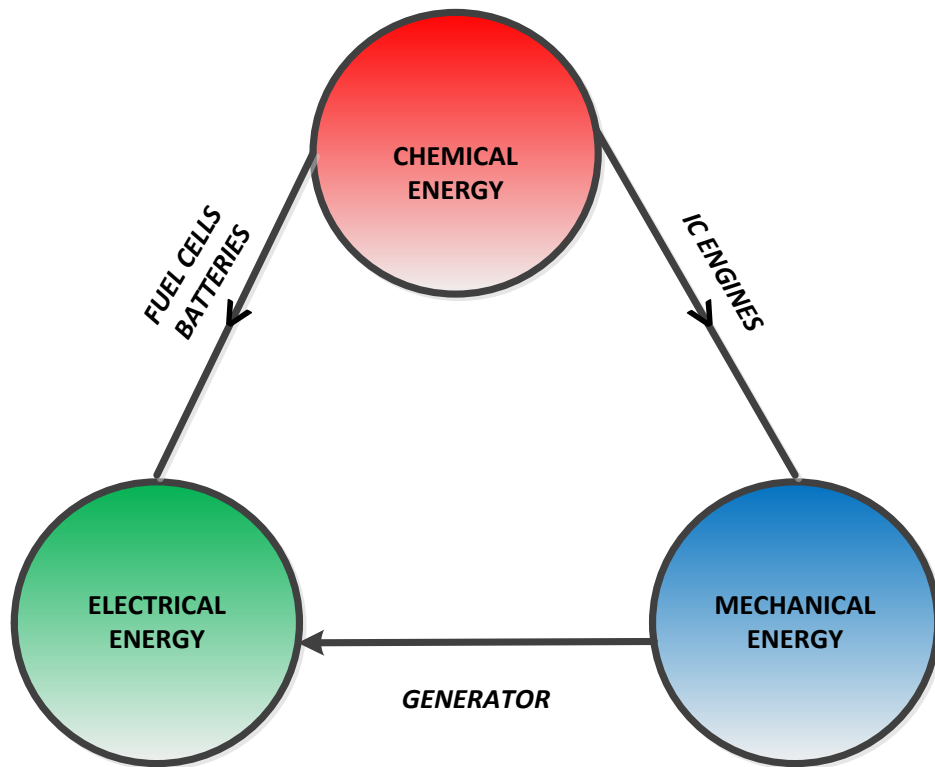


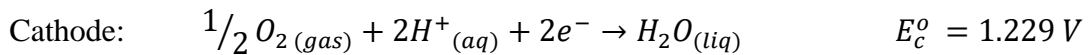
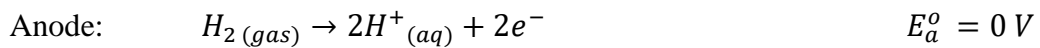
Figure 1.1 Energy Conversion Path of Conventional Systems

Furthermore, the fuel cells retain the best attributes of both batteries and internal combustion (IC) engines making it a versatile energy conversion system [3]. It is known that fuel cells are the only static energy systems that are adaptable to a wide range of power levels, e.g., microwatt (implantable devices), kilowatt (transportation) and megawatt (industrial) applications. However, the types of fuel cell systems to be used for specific applications will depend on the functional requirement, compatibility and economic constraints. Among the various fuel cell types, polymer electrolyte membrane (PEM) fuel cells are anticipated to be optimum for future technology applications due to

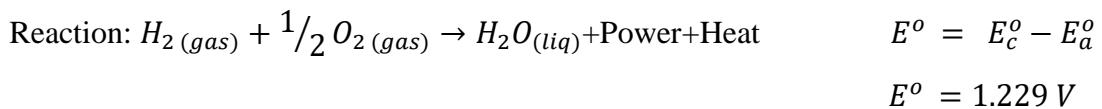
their versatile characteristics such as high power density (compatible for transportation), low operating temperature (60-90°C) and dynamic response [4].

1.3 Fuel Cell Reaction

The basic concept of the fuel cell (irrespective of type) is that it produces electricity with hydrogen (or hydrogen-rich fuel) and oxygen (air) as fuel in the electro chemical process, producing water and heat as the by-product. The anode, cathode and the net reaction of a PEM fuel cell are as follows:



Net



The ideal standard potential (E^o) at 298 K for a fuel cell in which H₂ and O₂ react is 1.229 V with the liquid water as product or 1.18 V with the gaseous water as product [5].

Each case assumes gaseous products as its basis. The open circuit potential of a fuel cell is influenced by the reactant concentrations and the maximum ideal potential occurs when the reactants at the anode and cathode are pure. In an air-fed system or if the feed to the anode is other than pure hydrogen, the cell potential will be reduced.

1.4 Fuel Cell Classification

Fuel cells are generally classified based on the electrolyte and characteristics of widely used fuel cells namely Alkaline Fuel Cell (AFC), Phosphoric Acid Fuel Cell (PAFC), Molten Carbonate Fuel Cell (MCFC), Solid Oxide Fuel Cell (SOFC), and Polymer Electrolyte Membrane Fuel Cell (PEMFC). Table 1.1 summarises the properties of the

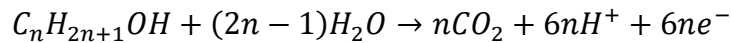
most widely used fuel cells, their characteristics, and applications based on their temperature.

Table 1.1 Classification of Fuel cells [Organised from high to low temperature]

Fuel Cell Type	Electrolyte/ Charge Carrier	System Efficiency	Advantages
Solid Oxide Fuel Cell (SOFC)	Ytria-stabilized zirconia, or more recently, lanthanide doped ceria O^{2-}	50-60%	High operating temperature. Therefore, nonnoble catalysts and can operate on cheap fuels.
Molten Carbonate Fuel Cell (MCFC)	Immobilized Carbonate solution CO_3^{2-}	50-60%	High operating temperature. Therefore, non-expensive catalysts and can operate on cheap fuels.
Phosphoric Acid Fuel Cell (PAFC)	Immobilized Phosphoric acid soaked in a matrix H^+	40-45%	Can use impure H_2 as fuel and can tolerate up to 1.5% CO (carbon monoxide).
Alkaline Fuel Cell (AFC)	Potassium hydroxide, soaked in a matrix OH^-	60%	Aqueous electrolyte promotes fast cathode reaction and high performance.
Polymer Electrolyte Membrane Fuel Cell (PEMFC)	Perfluoro- sulfonic acid (Nafion) H^+	60%	High power density, Low temperature and quick startup (excellent for vehicle applications).

Direct Alcohol Fuel Cell (DAFC)

Direct Alcohol Fuel Cell is a subset of PEM fuel cells that incorporates similar proton exchange membranes where the alcohol is fed directly into the anode of the stack instead of hydrogen gas. In these systems, the anode catalyst draws the hydrogen from liquid fuels (Hydrogen carrier). The empirical equation that governs the oxidation of alcohols is given by [6] as:



The limitation in hydrogen storage, low operating temperatures, and high energy density makes this DAFC an appropriate candidate for low power applications to energize mobile and other portable electronic kits [6].

Regenerative Fuel Cell (RFC)

The Regenerative Fuel Cell (RFC) is also usually a subset of PEM fuel cells capable of operating in both the fuel cell and electrolyser mode. While operating in fuel cell mode, it produces electricity from the hydrogen and oxygen/air. In the reverse mode, it acts as an electrolyser for generating hydrogen (which can be stored and used in fuel cell operational mode) and oxygen. The most significant advantage of RFC is that it can be bi-functional and can be used to deliver power ON demand.

1.5 Polarisation Curve and its Significance

The significance of the polarisation curve is that it is used to analyse the fuel cell performance and losses. The polarisation curve is the basic kinetic law for any electrochemical reaction and is a plot of current density (I) versus potential (V) for a specific electrode-electrolyte combination. The losses in a fuel cell that produces voltage drops are: a) Activation losses, b) Ohmic losses, c) Mass transport/Concentration losses. A typical fuel cell has a polarisation characteristic as shown in Figure 1.2.

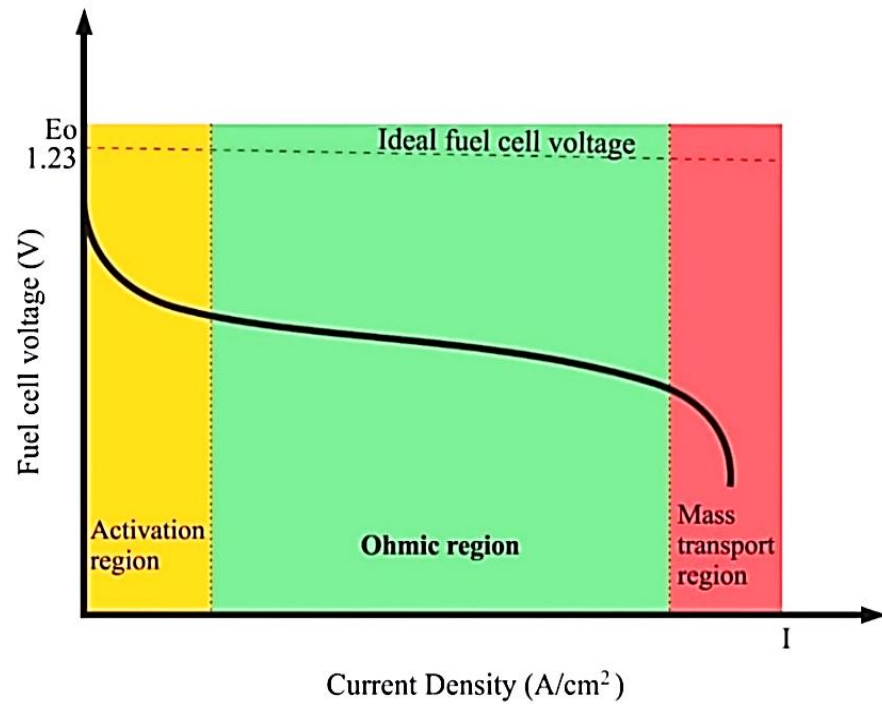


Figure 1.2 V-I Characteristics of Fuel Cells

The output voltage of the single PEM fuel cell is defined by the following equation [10].

$$V_{Fc} = E_0 - V_{act} - V_{Ohmic} - V_{Con}$$

V_{act} represents the activation losses that are caused by sluggish electrode kinetics, the electrocatalyst material, and reactant activities. V_{Ohmic} represents the Ohmic losses, which arise due to the resistance to the flow of ions in the electrolyte and resistance to flow of electrons through the electrode. In addition, the contact resistance at the cell terminals contributes to Ohmic losses. As a rule of thumb, PEM fuel cells are predominantly operated in the Ohmic region. V_{Con} represents the concentration or mass transportation loss, which is due to a decrease in the gas concentration at the surface of the electrode-electrolyte interface. In a PEM fuel cell, the GDL plays a significant part in reducing not only the mass transport related losses but also Ohmic losses. Thus, the function of the GDL is directly correlated to the performance of PEM fuel cell.

1.6 Fuel Cell Efficiency

For a fuel cell, the useful energy output is the electrical energy produced, and energy input is the enthalpy (energy content) of the fuel (hydrogen). Assuming that all of the Gibbs free energy can be converted into electrical energy, the maximum possible theoretical efficiency (η_{th}) of a fuel cell operating at 25°C by using the hydrogen higher heating value [7]:

$$\begin{aligned}\eta_{th} &= \frac{\Delta G_f^o}{\Delta H^o} = \frac{237.1 \frac{kJ}{mol}}{286 \frac{kJ}{mol}} \\ &= 83\%\end{aligned}$$

Where;

ΔG_f^o = Gibbs free energy of fuel

ΔH^o = Enthalpy (or heating value of fuel)

The theoretical efficiency also termed the thermodynamic efficiency. As mentioned previously, the ideal voltage of a cell operating reversibly on pure hydrogen and oxygen at 1 atm pressure and 25°C is 1.229 V. Thus, the thermodynamic efficiency of an actual fuel cell operating at a voltage of V_{cell} is given by:

$$\begin{aligned}\eta_{act} &= 0.83 \times V_{cell}/E_{ideal} \\ &= 0.83 \times V_{cell}/1.229 \\ &= 0.675 \times V_{cell}\end{aligned}$$

However, in fuel cells, the fuel (hydrogen) is not entirely converted - unlike most types of heat engines. To attain the total stack efficiency of a fuel cell, the ideal thermodynamic and voltage efficiency should be multiplied by the utilization factor, which refers to the fraction of the total fuel or oxidant introduced into a fuel cell that reacts electrochemically.

1.7 PEM Fuel Cells: Principle and Integral Components

Amongst the various fuel cell types, PEM fuel cells are intensively studied due to their distinctive characteristics such as high-power density, low-operating temperatures (60-80°C), rapid start-up and dynamic response.

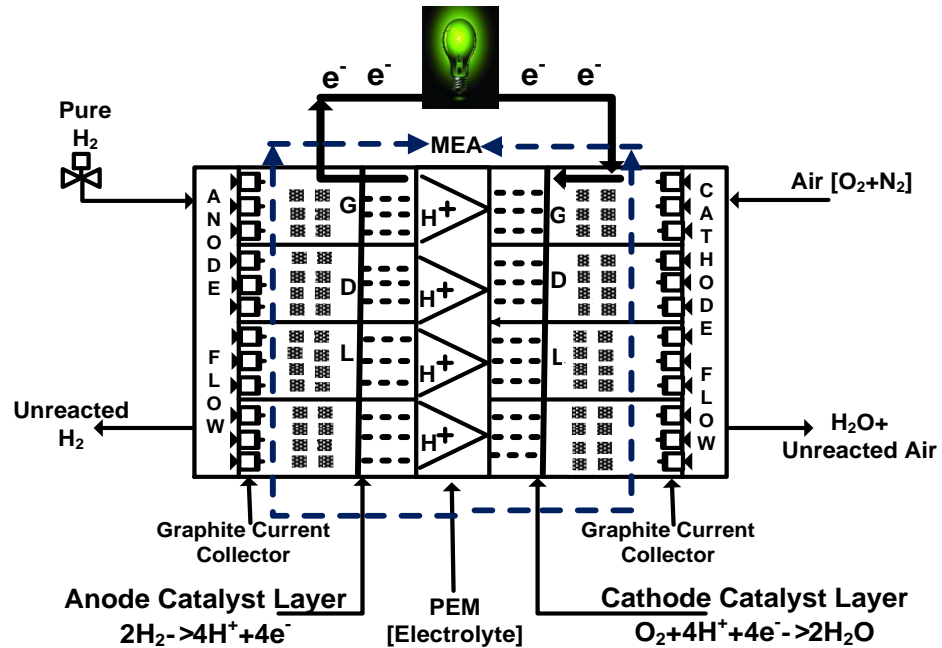


Figure 1.3 PEM fuel cell Stack Component and Ion transfer.

Figure 1.3 [8] is a schematic representation of a typical PEM fuel cell revealing the membrane and electrode components (MEA), flow field plates, gas diffusion layer (GDL) components and ion transport.

1.7.1 Membrane and Electrode Assembly (MEA)

For a PEM fuel cell, the Membrane and Electrode Assembly (MEA) is the core structure entailing an electrolyte (proton-exchange membrane) with surfaces coated with catalyst/carbon/binder layers and sandwiched by gas diffusion layers and current collectors. The components of a typical MEA and their functions are elaborated in Table 1.2.

Table 1.2 Integral Membrane and Electrode Components and their Function

Components	Functions
Proton Exchange or Polymer Electrolyte Membrane (PEM) e.g., Nafion	<ul style="list-style-type: none"> i. Conducts protons and impedes the flow of electrons. ii. Must be thin (to reduce ohmic loss) and should have high protonic conductivity (to pass protons)
Catalyst Layers (CL) e.g., Pt., Ru.	<ul style="list-style-type: none"> i. The active site, where the reaction takes place. ii. Must have optimal mass transport characteristics.
Gas Diffusion Layers (GDL). e.g., C-Paper and Cloth	<ul style="list-style-type: none"> i. Facilitates diffusion of reactant gases across the catalyst layer. ii. Aids the transportation of electricity, heat and product water from MEA. iii. Prevents the water flooding in the electrode, by consistently removing the by-product water. iv. Optimally maintains temperature distribution.

1.7.2 Flow Field (Graphite) Plate

The flow field or bipolar plate is usually made of graphite, and it functions to transfer electrons between adjacent cells. It can be made of either metal (stainless steel, titanium, aluminium, and several metal alloys) or conductive carbon polymer (high-density graphite made of polymer resin-impregnated graphite). These conductive plates act as an anode for one half-cell and as the cathode for the adjacent half-cell. A variety of bipolar plate designs are known, and the conventional designs typically comprise either pin, integrated cooling flow fields, interdigitated flow field, parallel or serpentine designs [9]. The bipolar plates provide a structural support and path for the products of the reaction to be evacuated from the cell [9]. In addition, the bipolar plates also assist in an efficient thermal management.

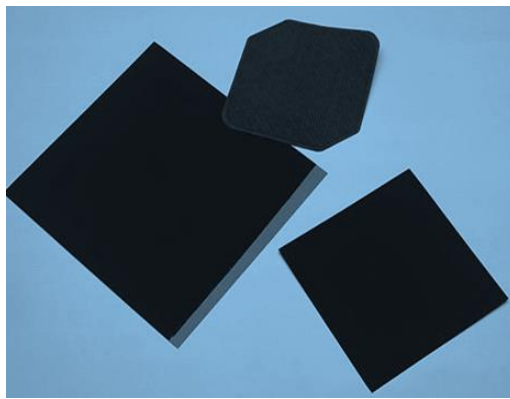
1.7.3 Electro-catalysts Layer and its Characteristics

Conventional PEM fuel cells use platinum on porous carbon as catalysts and nano platinum particles under certain conditions as they have a higher surface area. Physically, the catalyst layer is in direct contact with the membrane and the gas diffusion layer.

Platinum-Ruthenium (Pt/Ru) based alloys may be used where ‘impure’ hydrogen is used [10]. The catalyst layers need to be designed to generate high rates of the desired reactions and minimize the amount of catalyst necessary for attaining the required power output. The catalyst either covers the surface of the GDL or directly coats the surface of the membrane (catalyst-coated membrane).

1.7.4 Gas Diffusion Layer (GDL)

The GDL electrically interconnects the catalyst and current collector. The GDL acts as a pathway to the catalyst layer from the flow channels. It anatomically comprises of two layers, a hydrophobic agent (Poly Tetra Fluoro Ethylene) and a microporous layer made of Toray carbon paper or a carbon cloth that is covered with a microporous layer. GDL also aids to remove the product water or else flooding can occur where water blocks the GDL site and this limits the reactants ability to access the catalyst, and this significantly decreases performance. Several GDL microscopic variables such as porosity, tortuosity, and permeability impact the behaviour of the fuel cells [11]. The functions of an ideal GDL have been previously elaborated in Table 1.2. Figure 1.4 represents examples of commercial gas diffusion layers: a) carbon paper and b) carbon cloth.



a) Carbon paper



b) Carbon cloth.

Figure 1.4 Conventional gas diffusion layer a) Carbon paper b) Carbon cloth.

1.8 Outline of the Thesis

A gas diffusion layer (GDL) is one of the critical components in PEM fuel cells, and hence it has been given more emphasis due to its multifunctional characteristics of transporting the reactant gases, electric current, heat and product water. The general

objective of the thesis is to fabricate a durable and economical GDL, which can contribute to the commercialisation of the PEM fuel cell stack. The thesis is organised as follows:

- I. Chapter 1 provides a snapshot of the fundamentals of PEM fuel cells, their performance, efficiency, operating principles and key components.
- II. Chapter 2 comprehends the role of the currently available gas diffusion layer in PEM fuel cell stacks and establishes the characteristics of them including the geometry, porosity, conductivity and fabrication techniques. These characteristics influence the performance of the PEM fuel cell stack, and consequently, they were methodically reviewed. The chapter also envisages the research question as well as the contributions to the knowledge made.
- III. Chapter 3 deals with the methodology to perform the experiment, as well as the complete list of materials required systematically. The chapter also briefly illustrates the SLS principle of operation. In addition, the chapter provides a snapshot of the rationale for choosing the various materials as well as their characterisation.
- IV. Chapter 4 presents an initial trial executed through the two-independent processes namely, selective laser sintering (SLS) and micro fabrication technique. Chapter 4 also comprehensively deals with the characterisations studies that are performed to the GDL specimen, i.e. graphene-coated alumide specimen.
- V. Chapter 5 describes an experimental process using an iterative technique, which provides us with the feasibility to attain faster and flexible GDL product development. The investigation is performed with Alumide/Polyamide as base polymer and Titanium (micron and nano) as a functional powder. The various combinations of the base powder and the metallic powders in the composition is critically considered for analysis. Various characterisation studies such as thickness, surface morphology, electrical conductivity, tensile strength, hydrophobicity, porosity and thermal conductivity are performed and the

observations from these characterisation studies are comprehensively discussed. Chapter 5 also deals with the real-time evaluation of the proposed GDL through an experiment in the PEM fuel cell environment. A polarisation study is performed to find out the appropriate material.

- VI. Chapter 6 critically analyses the results and envisages the holistic assessment of the experiment based on the characterisation studies involved. The chapter also correlates the functional relationship of thermal conductivity, electrical conductivity and hydraulic conductivity for the proposed gas diffusion layer. This kind of interdisciplinary investigation is also a first of its kind for a PEM fuel cell application and can provide a more holistic insight into the material property from the various perspectives of Engineering. The chapter also analyses the various limitations of the present work holistically. The chapter also provides critical assessment and recommendations required in the proposed proof of concept.
- VII. Chapter 7 concludes with the significant contributions made by this thesis and demonstrates the various key findings. Apparently, future work is also discussed in the chapter.

Chapter 2: Literature Review

“If I was given 6 hours to cut a Tree, I would spend the first 4 hours in Sharpening the Axe.”

Abraham Lincoln

2.1 Introduction

PEM fuel cell is a reliable power system due to its characteristics such as dynamic response, high power density and operating efficiency [12]. The membrane and electrode assembly (MEA) is the integral component of a PEM fuel cell stack and is sometimes acknowledged as the “*heart of the PEM fuel cell stack*”. Gas diffusion medium is a critical component of a MEA that not only influences the characteristics such as dynamic response and power density, but also durability as well. Fundamentally, gas (hydrogen and air) being the reactants in PEM fuel cell is converted to electrical energy and heat. Therefore, the amount of gas passing through the diffusion layer is proportional to the current and heat produced in the stack.

Consequently, there are numerous engineering phenomena involved in its design, and there are numerous literatures about it. The present chapter provides a comprehensive review of the gas diffusion mechanism as well as the structural characteristics of the conventional GDL. The various characteristics involved in the GDL and the characteristics that govern the transport of reactant and product gas, transports of electric current, heat and product water. The chapter also deals with a snapshot of the advancement in modern GDL and novel manufacturing techniques involved in GDL fabrication.

2.2 Gas Diffusion and Structural Characteristics of GDL

Gas diffusion is a transport process involved in fuel cell stack, and Fick’s law [13] predicts how diffusion causes the concentration to change with time, and the equation is governed as follows:

$$\frac{\partial C_i}{\partial t} = D_i^{eq} \frac{\partial^2 C_i}{\partial z^2}$$

Where;

C_i is the concentration.

D_i^{eq} is the diffusion coefficient.

z is the position [length].

Fick's law is insufficient in approximating the mass diffusion process due to its fine pore sizes and, as a result, the effective diffusion coefficient is modified by Bruggeman's correction. This alteration is employed in species transport of oxidants and fuels in the porous media of the PEM fuel cells. However, the texture of porous media is very complex and, the relative influence of ordinary diffusion or Knudsen diffusion on species transport is governed by the pore geometry [14].

Mass transfer can take place by Knudsen or Fickian diffusion if the pores are sufficiently small [15] as well as the diffusion characteristics of the macroporous layer can be examined by Fick's laws, while the microporous layer exhibits Knudsen diffusion. The Knudsen number, K_n used to characterize the regime of diffusion is defined as:

$$K_n = \lambda_g/d_p$$

Where;

λ_g is the mean molecular free path.

d_p is the pore diameter.

An estimate of K_n under practical cell operating conditions shows that this usually occurs for the gases in a PEM fuel cell when the permeability is in the range of 10^{-16} to 10^{-17} m² and for $\lambda_g/d_p \ll 1$ the Knudsen diffusion effect is neglected [16]. The effective diffusion coefficient (D_{eff}) is related to the bulk diffusion coefficient (D) through the MacMullin number and is governed by the equation:

$$N_M = \frac{D}{D_{eff}}$$

The MacMullin number is determined only by the morphology of the GDL and can be expressed as a generalized relationship with tortuosity (τ) and porosity (ε):

$$N_M = f(\tau, \varepsilon) = \tau^n / \varepsilon^m$$

Where n and m are constants that depend on the geometrical model of the porous media, under some conditions of an operating fuel cell, pores in the GDL can be filled with liquid water, which effectively decreases the porosity for the gas stream. Porosity quantifies the reduction in a cross-sectional area available for gaseous transport, while tortuosity characterizes the convoluted nature of the porous pathways followed by diffusing species. The tortuosity (τ) of each sample was estimated using the Bruggeman equation [17]:

$$\tau = \frac{1}{\varepsilon^{1/2}}$$

The theoretical determination of tortuosity is model dependent and extremely cumbersome. A study by Springer et al. [18] reveals that the effective tortuous path length for gas diffusion in the cathode backing is about 2.6 times the thickness.

Observations by Fishman et al. [19] revealed that the GDL had been shown to be an anisotropic and heterogeneous material with transport properties varying significantly between the in-plane and through-plane directions. Ironically, Gostick et al. [20] claimed that most of the GDL materials were found to display higher in-plane than through-plane permeability. Measurement of relative permeability of GDL has received little attention; however, some early attempts to measure air relative permeability were reported by Koido et al. [21]. Properties of the GDL such as permeability, porosity, tortuosity, and the hydrophobic treatment can affect the degree of flooding, thus impacting the fuel cell performance [22]. The absolute gas permeability of PEM fuel cells using various gas diffusion layer (GDL) materials were analysed in three perpendicular directions to inspect the anisotropic properties, and it is observed that most materials were found to display higher in-plane permeability than through plane. Hussaini et al. [23] measured the absolute permeability and air-water relative permeability functions for typical GDL materials such as Toray carbon paper and E-Tek carbon cloth and concluded absolute permeability of the carbon paper materials, in the in-plane directions, are found to be higher than their through-plane values by about 18%, whereas for carbon cloth, through-plane permeability is found to be higher by about 75%. PEM fuel cell performance may

be strongly influenced by the in-plane permeability of the GDL [24], and liquid water saturation is found to be a linear function of a capillary number. At a given capillary number, carbon papers show similar saturation in both directions whereas carbon cloth shows higher saturation in the through-plane than in-plane. Physical characterization studies on diffusion mediums by Benziger et al. [25] provided details about the pore sizes of different gas diffusion media. Rofaiel et al. [26] presented a novel method for measuring heterogeneous through-plane PTFE distributions within the bulk of the GDL using energy dispersive X-ray spectrometry (EDX) imaging. Table 2.1 provides the physical characterization of diffusion medium.

Table 2.1 Physical characteristics of diffusion medium [25, 26]

Media	Dry areal mass (kg/m²)	Areal mass after liquid water contact (kg/m²)	Void fraction	Advancing/Receding contact angle
Carbon paper (Toray)	0.259±0.007	0.469±0.052	0.72±0.05	115° /30°
Carbon paper + 20% Teflon	0.374±0.007	0.423±0.035	0.69±0.05	170° /120°
Carbon paper + 40% Teflon	0.456±0.010	0.525±0.047	0.59±0.05	170° /120°
Carbon paper + 60% Teflon	0.476±0.009	0.526±0.044	0.50±0.05	170° /120°
Carbon cloth	0.355±0.009	0.484±0.027	0.75±0.05	95° /30°
Carbon cloth + 20% Teflon	0.476±0.012	0.551±0.047	0.73±0.05	170° /120°
Carbon cloth + 40% Teflon	0.595±0.011	0.648±0.041	0.68±0.05	170° /120°
Carbon cloth + 60% Teflon	0.697±0.017	0.839±0.055	0.52±0.05	170° /120°
E-TEK/ELAT electrode	0.435±0.011	0.620±0.036	0.74±0.05	170° /120°

2.3 Electrochemical Characteristics of GDL

Electrochemical impedance spectroscopy is, perhaps, the most reliable tool for in-situ fuel cell characterization [27]. The process of gas diffusion creates impedance called Warburg impedance, which depends on the frequency of the potential perturbation at high

frequencies, the Warburg impedance is small since diffusing reactants do not have to move very far, and at low frequencies, the reactants have to diffuse farther, increasing the impedance.

2.4 Conventional Gas Diffusion Medium (Carbon Paper vs. Carbon Cloth)

A GDL typically consists of a macro porous layer and a microporous layer (MPL). Carbon cloth or non-woven carbon paper is widely used as a GDL due to its high gas permeability, electronic and heat conductivity. The appropriate candidates for diffusion of reactant gases in PEM fuel cells are the carbon fibre-based products such as non-woven papers and woven cloths due to their high porosity (>70 %) and electrical conductivity. The typical properties of these two materials are specified in Table 2.2

Table 2.2 Comparison of features of carbon paper and carbon cloth [28].

Properties	Method	Carbon paper ^a	Carbon cloth ^b
Thickness (μm)	Callipers at 7 kPa	0.19	0.38
Areal weight(gm ⁻²)	Gravimetric	85	118
Density (gcm ⁻³)	At 7kPa Calculated	0.45	0.31
Resistance (Through-plane, Ωcm ²)	Two flat graphite blocks at 1.3 MPa	0.009 ^c	0.005 ^c
Bulk Resistivity (Through-plane Ωcm)	Mercury contacts	0.08	NA
Bulk Resistivity (In plane Ωcm)	Four probe	0.0055 ^d	0.0091 ^d
Gas permeability (through plane, Darcy)	Gurley permeometer	8 ^e	55 ^e
Material description	4301	Toray	Avcarb 1071

^a Reported by Toray (unless indicated otherwise)

^b Reported by Ballard Material Systems (unless indicated otherwise)

^c Measured at General Motors (GM), includes diffusion-media bulk resistance and two contact resistances (plate to diffusion media)

^d Measured at GM, uncompressed, average of resistivity in the machine and cross-machine direction.

^e Measured at GM, uncompressed, 1 Darcy =10⁻¹² m²

Gallo Stampino et al. [29] studied the electrical performance of PEM fuel cells with GDL made of carbon paper/cloth and demonstrated that a carbon paper-based specimen has superior performance in a wide range of current densities starting from OCP to 0.8 A/cm². Sasikumar et al. [30] investigated the performance of gas diffusion electrodes fabricated using carbon paper and carbon cloth and observed better performance with carbon paper. Their studies showed that the limitation of mass transport was a concern with carbon cloth under non-pressurized operating conditions, especially at higher current densities, due to the higher thickness and density. Yuan-Kai Liao et al. [31] compared the performance of conventional carbon cloth and Polyacrylonitrile based cloth that uses phenolic resin to improve the characteristics of the gas diffusion layer (GDL). Yun Wang et al. studied the structure-performance relationship of carbon cloth and paper as GDL [28] and revealed that under dry conditions, the carbon paper was found to be better due to its higher tortuous pore structure, which retained product water in the MEA and enhanced the membrane conductivity by reducing ohmic loss. However, they have observed that carbon cloth gives a better performance under humidified conditions. The experiment conducted by Williams et al. [32] was also in line with that of Yun Wang et al. Park and Popov [33] have analysed the influence of a GDL based on carbon paper and cloth through various techniques like mercury porosimetry, surface morphology analysis, polarisation techniques, ac-impedance spectroscopy, contact angle and water permeation measurement and observed that the MEA fabricated using carbon paper exhibited better performance compared to the carbon cloth, because of high water flow resistance owing to less permeable macro porous specimen, and more hydrophobic and compact microporous layer. The ac-impedance technique reveals that a micro porous layer that has a high volume of micropores and more hydrophobic property allows oxygen to diffuse freely towards the catalyst layer due to the active removal of water from the catalyst layer to the flow channels. Xie Zhi-Yong et al. [34] compared the performance of PEM fuel cells with pyrocarbon and conventional carbon paper composites as a gas diffusion layer. The carbon paper was fabricated using a conventional precursor and coating with pyrocarbon by pyrolyzing propylene via a chemical vapour deposition (CVD) method. For comparison, conventional carbon paper composites were prepared using polyacrylonitrile based carbon felt as the precursor followed by impregnation with resin, moulding and thermal treatment. Chunyu Du et al. [35] proposed a scheme of fabricating

a hierarchy of carbon paper with carbon nano tubes uniformly grown on carbon fibres and observed it to be good for the self-humidifying PEM fuel cells. They claimed that carbon paper facilitated the self-humidifying characteristics and can be attributed to its higher hydrophobic nature.

2.5 Significance of Micro-Porous layer (MPL) and its Fabrication

A Micro Porous Layer (MPL) is a sub-component, and is usually sandwiched between the GDL and the CL to reduce the ohmic resistance. It usually comprises of carbon black, Teflon as a hydrophobic binder and pore forming agents. The binders such as Teflon or PTFE serve two functions namely: (i) Binding the high surface area carbon particles into a cohesive layer (ii) Imparting hydrophobicity to the layer to facilitate the removal of water [36]. The MPL also provides a non-permeable support during catalyst deposition and manages liquid water flow during fuel cell operation [37-40]. Studies on the effect of varying carbon loadings in MPL fabrication were carried out to achieve higher performance in PEM fuel cell operation, and there are numerous publications discussing various types of carbon for MPLs [41]. Table 2.3 shows the physical properties of various carbon blacks used to fabricate MPL [42-45].

Table 2.3 Physical properties of various carbon blacks used to fabricate MPL [42-45]

Type of carbon	Particle size (nm)	Surface area (m ² /g)	Pore Volume(cm ³ /g)	Averaged pore radius (μm)
Shawinigan acetylene black (SAB)	40 –50	70	0.594	1.7
Vulcan XC-72	30	250	0.489	1.8
Black Pearl 2000 carbon	15	1501.8	2.67	--
Asbury graphite 850	--	13	0.346	3.5
Mogul L	--	140	0.276	6.0

The results acquired by various researchers by varying PTFE loading in MPL are summarized in Table 2.4. The literature [46][68][47, 48] shows that the superior

performances are obtained with the lowest PTFE loading, but it is not possible to totally eliminate it. Yan et al. [49] used fluorinated ethylene propylene (FEP) as a hydrophobic agent in GDL preparation and achieved the best performance with 20 % FEP content in MPL.

Table 2.4 Effect of PTFE content in MPL on PEMFC Performance [48, 50-52]

Gas Diffusion Medium	Reactants	PTFE (%)		Membrane	Power Density (W/cm ²)
		Range	Optimum		
Carbon Paper	H ₂ /Air	25-45	35	Nafion-112	0.360
Carbon Paper	H ₂ /Air	10-60	30-40	Nafion-112	0.493
Carbon Paper	H ₂ /O ₂	10-40	30	Nafion-115	0.250
Carbon Paper	H ₂ /Air	10-60	20	Nafion-117	0.360

2.6 Novel Gas Diffusion Medium

Limited exploration with other GDL apart from carbon cloth and carbon paper is available in the open literature. Few attempts have been made using metallic thin film as GDL by Fushinobu et al. [53], with micro-machined titanium film as GDL due to its high endurance property. A similar sort of experiment was also performed by Hottinen et al. [54] using titanium sinter material, and their investigation illustrated the applicability of titanium sinter as a GDL in free-breathing PEM fuel cells. Micromachined silicon has also been used as gas diffusion layer for micro PEM fuel cell applications tested with hydrogen/air [41]. The technique of incorporating sintered stainless steel fibre felt was implemented by Yi et al. [55] and they inferred that the compressive modulus and ductility of GDL were improved. In addition, they observed that the characteristics of treated stainless steel fibre felt were comparable to carbon paper. Glora et al. 2001 [56] and Long et al. [57] tried using aerogels to replace conventional gas diffusion layers and observed several advantages with aerogels over traditional carbon supports for fuel-cell catalysis including large surface areas (typically > 500 m²/g), high-fractional mesoporous pore volumes for gas transport, synthetic control over structural properties, and

availability in monolithic forms [57]. Glora et al. [56] employed a resorcinol-formaldehyde aerogel with the thickness of less than 500 μm and the highest achieved electronic conductivity was about 28 Scm^{-1} in an 80% porous GDL structure. Wang et al. [51] experiment were also in line with that of Glora et al. [56], and the carbon aerogel is prepared from a resorcinol-formaldehyde mix by a pyrolysis technique in an inert gas atmosphere, and their properties are elaborated in Table 2.5.

Table 2.5 Properties of Carbon Aerogels [51].

Parameters	Values
Density(gcm^{-2})	0.1 - 0.6
Surface Area (m^2/g)	400-1000
Average pore size (nm)	4 – 30
Electrical conductivity (Scm^{-1})	1– 10

Feng-Yuan Zhang et al. [58] developed a novel porous gas diffusion medium with improved thermal and electrical conductivity and controllable porosity using MEMS technology. The gas diffusion medium had a dimension with 12.5 μm thick copper foil and by applying a Micro Porous Layer (MPL) on it to enhance the in-plane transport.

2.7 Durability of GDL

Durability is one of the most significant issues impeding successful commercialization of PEM fuel cell stack. Studies on GDL components of PEM fuel cells degrade in different protocols, and the mechanisms involved in the degradation are not entirely implicit, because there are, different techniques employed to prepare functional components at various operating conditions which are not well quantified by the researchers. Specifically, the GDL plays an important role concerning the durability of the MEAs, which is a critical concern [59] as well as an abnormally high current density which significantly accelerates the deterioration of the GDL. In addition, corrosion on the GDL will increase resistance and decrease electrical conductivity. The snapshot on the vital degradation factors for GDL is revealed in Figure 2.1.

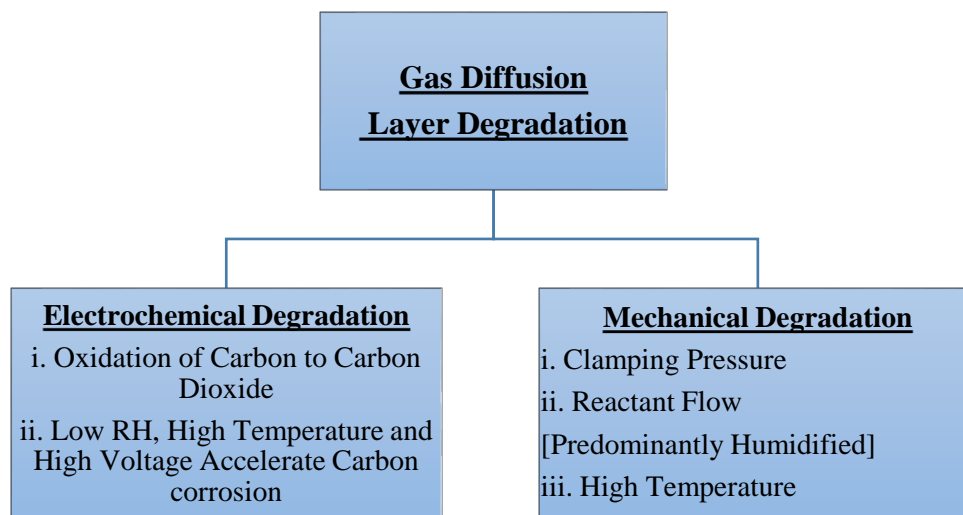


Figure 2.1 Key Degradation factors for Gas Diffusion Layer

The potential chemical causes for the GDL degradation may be due to carbon erosion, carbon corrosion, as well as changes in the characteristics such as porosity, hydrophobicity, microstructure, etc., which principally leads to mass transport problems. Hydrophobicity of GDL accomplishes water management in a fuel cell, and polytetrafluoroethylene (PTFE) is used as a hydrophobic agent. Changes in hydrophobicity lead to excess water accumulation (flooding problem), which can block the gas pathways to the catalyst sites, and accelerate the degradation [60, 61].

Thus, the various mechanisms in PEM fuel cell are interrelated, and one degradation mechanism may essentially trigger or exacerbate another. For instance, when the applied stress of GDL increases, it significantly decreases not only the electrical conductivity but also the porosity. Another such example is that water build-up at the cathode catalyst layer arises not only due to the product water but also due to the electro-osmotic drag, which can also drastically decline the cell performance by hindering the gas diffusion [62]. Wu et al. compared the physical characteristics of the GDLs before and after corrosion tests and validated that GDLs are susceptible to electrochemical oxidation [63]. Chen et al. [64] performed an effective ex-situ method for characterizing electrochemical durability of a gas diffusion layer (GDL).

In addition to the electrochemical degradation issues, a multifaceted manufacturing process that is followed to fabricate conventional GDL material severely increases the manufacturing cost.

2.8 Conventional Manufacturing Technique of GDL

Though, there are numerous GDLs in the literature whose manufacturing techniques are parallel; the proposed thesis considers SIGRACET[®] grade GDL 39 BC (325- μm thickness) as a baseline material. The unique characteristics of SGL 39 BC to consider is that it is denser and has a thicker microporous layer than its precursors (SGL 10 BC), and has a better water-retaining capability [9]. The manufacturing steps involved in the conventional GDL (SGL 39 BC) are illustrated in Figure 2.2, and more technical informations about it are provided in Appendix A.

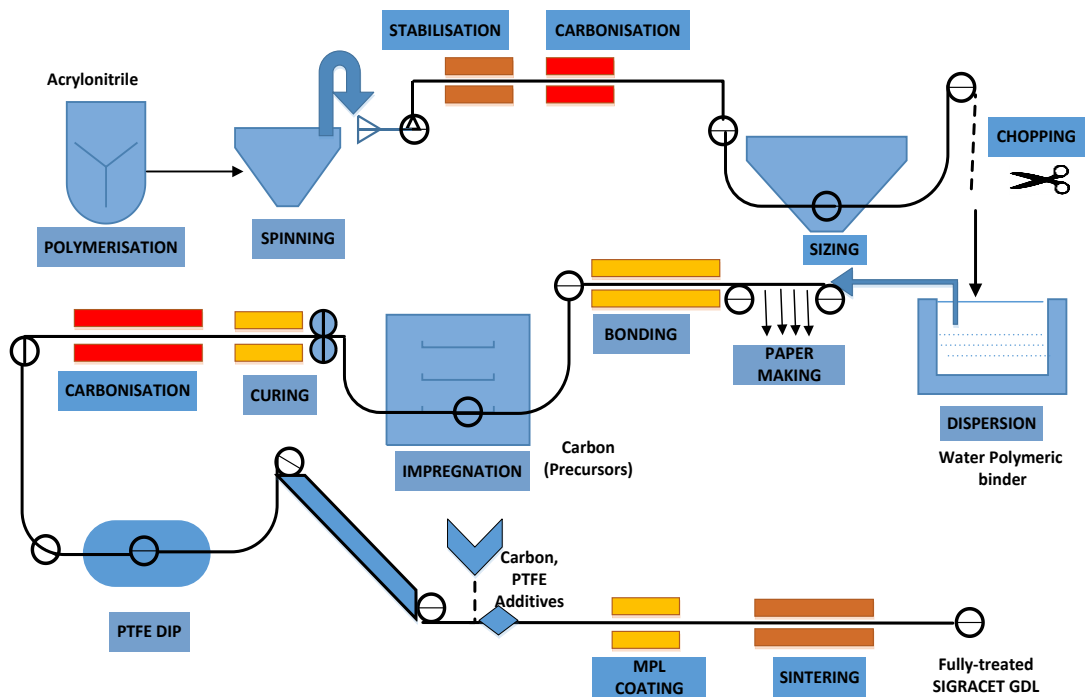


Figure 2.2 Manufacturing steps involved in the conventional GDL-SGL 39 BC [9]

The manufacturing step is that of the well-known wet laying technology where the chopped carbon fibres are processed to a primary carbon fibre. The raw paper is then

impregnated with carbonizable resins (carbonizable resins with the optional addition of carbon fillers), cured and recarbonized/graphitized [9]. The characteristics of the SGL 39 BC are demonstrated in Table 2.6.

Table 2.6 Properties of SGL 39 BC [Baseline-GDL]

Integral Properties	Units	Sigracet-SGL 39 BC
Thickness	μm	325
Area Weight	g/m^2	105
Open Porosity	%	50-52
Through-Plane Gas permeability (Gurley)	$\text{cm}^3\text{cm}^{-2}\text{s}^{-1}$	1.0-1.5
Hydrophobicity (Water Contact Angle)	(θ)	118.2 ± 10.98
In-Plane Conductivity**	Scm^{-1}	2.0-2.2
Through-Plane Conductivity**	Scm^{-1}	170/145
Thermal Conductivity	$\text{Wm}^{-1}\text{K}^{-1}$	0.25

** compressed with 1 MPa

The conventional manufacturing technique is an integral reason for the GDLs expensiveness.

2.9 Research Questions

Understanding the technical challenge (concerning to electrochemical oxidation) and manufacturing challenge of the conventional GDL. There arise two fundamental questions (issues) contributing to the specific research questions namely:

- I. Can we develop a carbon-free gas diffusion layer (GDL) for PEM fuel cell application?
- II. Can we streamline the GDL manufacturing technique and achieve the department of energy (US-DoE) target?

2.10 Contributions to knowledge

The thesis aims to be bi-functional in addressing the issues. Figure 2.3 answers the aforementioned research questions functionally through a Venn representation.

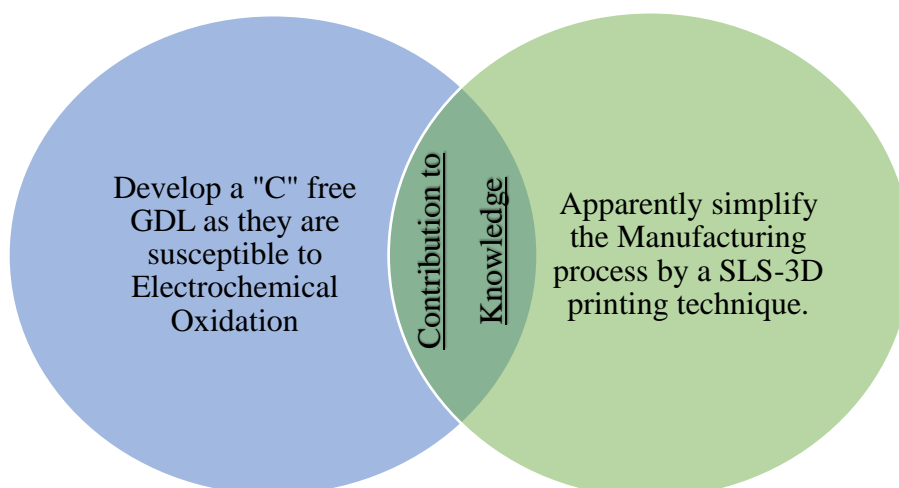
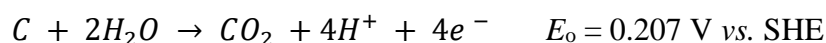


Figure 2.3 Functional chart on the contribution to Knowledge

The contribution to the knowledge of the present work is that the durability, manufacturing complexity, and cost can be significantly improved in a positive manner by the SLS (3D printing) manufacturing technique. Therefore, the contribution to knowledge in the proposed work is to:

- I. Improve the durability of GDL as they are susceptible to electrochemical oxidation [63, 65]. The electrochemical degradation is due to the oxidation of carbon (present in the carbon paper) to-carbon dioxide and is illustrated in equation:



- II. Apparently, simplify the manufacturing process by an additive manufacturing technique namely the Selective Laser Sintering (SLS). SLS is an additive manufacturing technique for fabricating specimen in precise geometry using computer-aided design (CAD) and computer-aided manufacturing (CAM). In particular, SLS scores the best regarding processing polymers in powder form. A CO₂ laser is commonly used considering the laser absorptivity of polymeric materials, and the powder material is converted into solid state thin films based on the raster path data generated from CAD files. The interconnected porosity of the sintered part can be controlled through material selection, physical design, and processing parameters.

- III. The US-DoE target of \$5.45/m² for a mass GDL production of 500,000 [66] can be easily accomplished through this manufacturing technique, because the process is predominantly single-stage unlike multiple stages for the conventional GDL production. In addition, the lead-time can also be reduced radically, thereby, leading to an improved productivity.

- IV. The thesis also correlates the structural and functional relationship of the GDL material fabricated through the SLS process. This analysis can provide an in-depth understanding of the change in the materials' functional property with regard to its structural modification.

Chapter 3: Methodology and Materials

“Methodology Should Not be a Fixed Track to a Fixed Destination”

J.C Jones

3.1 Introduction

The gas diffusion layer (GDL) is a multi-functional PEM fuel cell component, which functions to transport the reactant gases, product water, heat generated and the current diffusion. This chapter provides a brief discussion of the methodology and approach involved in the fabrication of a durable, cost-effective GDL by an additive manufacturing technique that incorporates the selective laser sintering (SLS) route. The rationale to select the SLS route in the present study is that it has the potential to fabricate a multi-functional component by scanning the base powder or composite powder multiple times using laser beam overlap. Thus, the desired attributes are acquired based on the functional requirement. The chapter also deals with the various base and filler materials involved in the present investigation. The chapter also envisages the characterisation technique involved in the present investigation along with the appropriate justification. A systematic design methodology is formulated and illustrated through the flowchart as shown in Figure 3.1 to attain the necessary characteristics. As illustrated in the flowchart, selective laser sintering processes were considered appropriate for the study due to its numerous advantages that are elaborated in the forthcoming section.

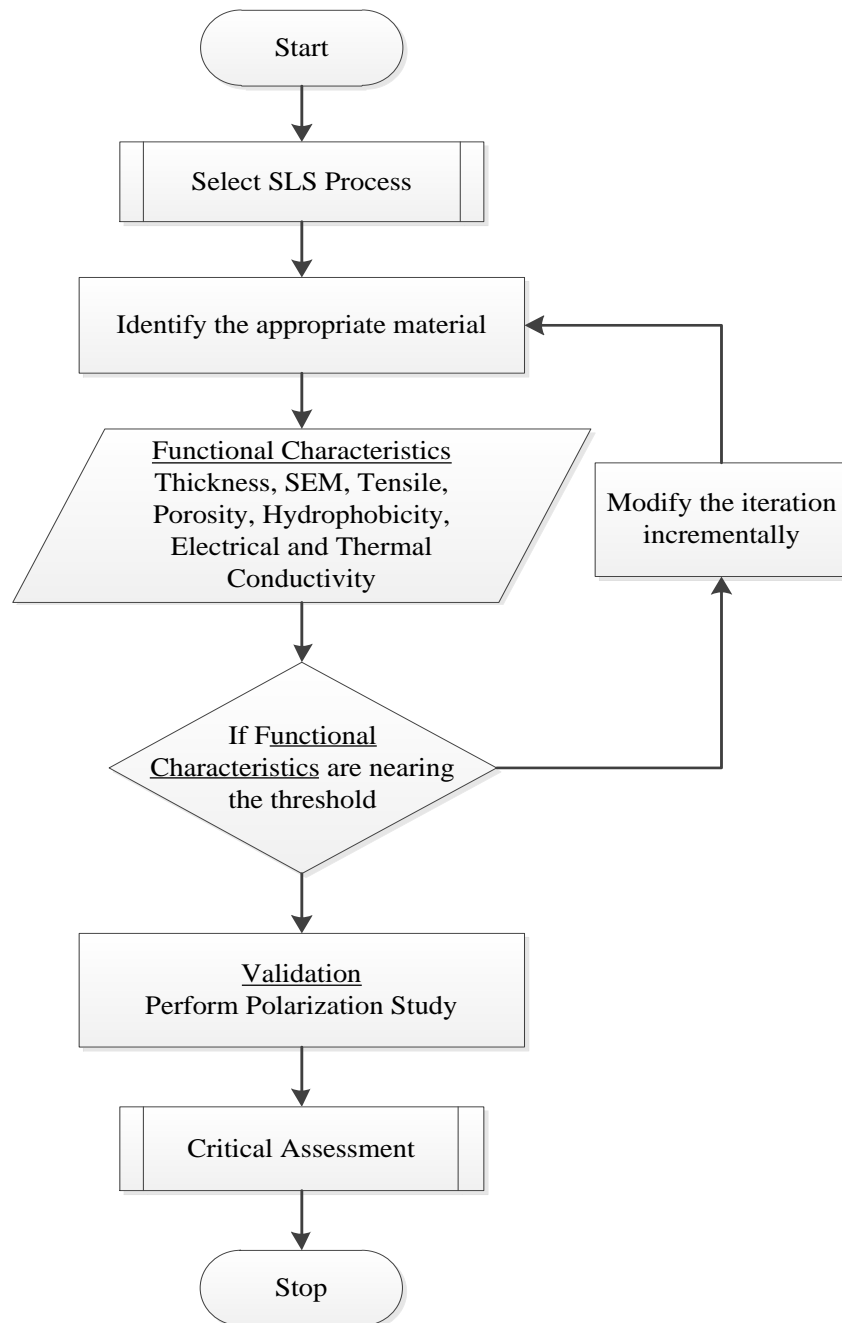


Figure 3.1 Flowchart illustrating the methodology and material selection

The initial step is the selection of appropriate materials for the SLS process, which is a crucial factor in the design of an end product. However, in the context of product design, the primary goal of material selection is to minimize the cost without any sacrifice in the performance [67]. In the successive step, the experiments are performed with the selected material with the objective to attain desired physical characteristics such as thickness,

surface morphology, tensile strength, porosity, hydrophobicity, electrical conductivity and thermal conductivity. Alterations are made in the material composition until the desired features are attained. Finally, the product is tested and validated against the baseline material. The list of various instruments used for the characterisation studies is also comprehensively assessed along with its specification.

3.2 Additive Manufacturing

Additive manufacturing refers to a 3D design process used to build up a multilayer component by stacking the appropriate material. The term "3D printing" is increasingly used as a synonym for additive manufacturing and has witnessed an extensive growth, since its induction by Charles Hull [68]. The unique feature of an additive manufacturing technique is that it manufactures parts in an additive manner (i.e. additive manufacturing) due to their complex shape production abilities, tool-less processing [69] and apart from that, multifunctional characteristics of a material can be easily attained.

3.2.1 Selective laser sintering

The SLS process, which is a subsection of additive manufacturing technique, was developed and patented in the 1980s by Carl Deckard from the University of Texas, USA. As an additive manufacturing layer technology, SLS involves the use of a high power laser (for example, a carbon dioxide laser) to fuse small particles of plastic, metal, ceramic or glass powders into a mass that has a desired three-dimensional shape. A vast variety of materials and characteristics of strength, durability, and functionality is possible with this cutting-edge technology. Nylon-based materials are predominant base materials for the present investigation and are illustrated in Table 3.1.

The laser selectively fuses powdered material by scanning cross-sections generated from a 3D digital description of the part (for example from a CAD file or scan data) on the surface of a powder bed. After each cross-section was scanned, the powder bed is lowered by one layer thickness, a new layer of material is applied on top, and the process is repeated until the desired component is fabricated. Figure 3.2 provides the general sketch of the SLS process.

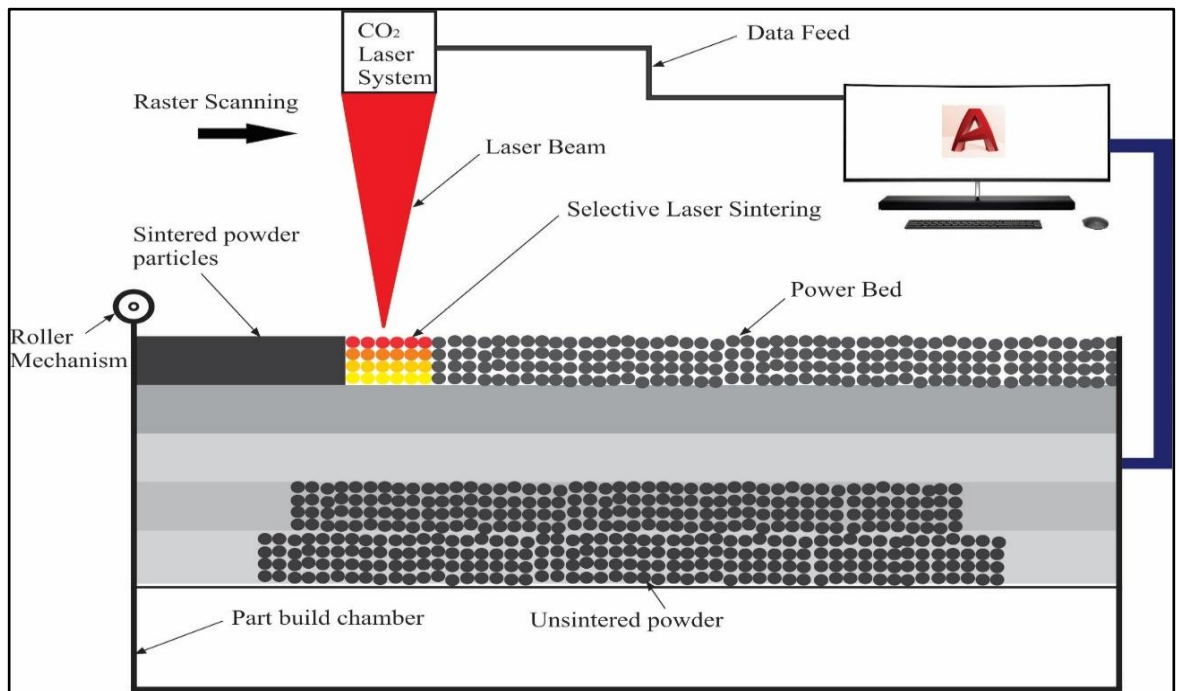


Figure 3.2 Selective laser sintering process

The distinct advantages of an SLS process is that:

- I. It is the fastest additive manufacturing technique and entirely self-supporting; it allows parts to be built within other parts in a process called nesting – with highly complex geometry that simply could not be constructed through any other approach.
- II. The components can be optimised to possess high strength, good conductivity, and good chemical resistance.
- III. Diverse finishing possibilities (e.g., metallization, stove enamelling, vibratory grinding, tub colouring, bonding, powder, coating, flocking) and functional possibilities (biocompatible) are possible.
- IV. Complex parts with interior components, channels, can be built without trapping the material inside and altering the surface from support removal.
- V. The fastest additive manufacturing process for printing functional, durable, prototypes or end-user parts.

The limitation of SLS process is that the printed parts have surface porosity. Incidentally, that limitation favours the GDL fabrication, as the GDL material must be porous to transport the reactant gases and eliminate the product water.

A series of experiments are performed by the SLS technique through an iteration technique to fabricate the gas diffusion material. The composite powder (combination of base and functional powder) is usually deposited in the powder bed to ensure the flatness of the surface. The initial temperature of the powder bed was maintained at above half the melting temperature. A manual powder dispersion method is used to produce the GDL test specimens.

3.3 SLS Process parameters

Laser Sintering is a complex process, which is impacted by materials structure and geometry. These factors are in turn correlated to the amount of energy delivered to the surface of the powder. The laser power and scanning speed can significantly determine the final properties of the specimen and have a substantial impact on the properties, like porosity and hardness of the end product layer [70]. Also, incorporating characteristics such as electrical conductivity can be easily accomplished. The energy density of the laser beam per unit area is defined as [71]:

$$E.D = P / (D \times v)$$

Where;

$E.D$ is the Energy Density (J/mm^2).

P is the laser power (W).

D the laser beam diameter (mm).

v is the laser scan velocity (mm/s).

3.4 Material Selection

Not all the materials that can be processed using the existing SLS infrastructure can be used to synthesise the gas diffusion material for the PEM fuel cells application. The desired material characteristics depend on a combination of properties, such as thickness, porosity, electrical conductivity, hydrophobicity and thermal conductivity. In addition, the material must be non-corrosive in the PEM fuel cell environment. The material

selection for GDL application depends on the selection of appropriate base materials and the filler material.

3.4.1 Selection of Base Material

The base material contributes to a significant percentage of the composite; therefore, it must be selected carefully knowing the application of end products. Table 3.1 provides the list of base materials that are compatible with the SLS process.

Table 3.1 List of base polymer materials.

Product class	Product name	Main properties	Typical applications
Polyamide 12	PA 2200	Multipurpose material Balanced property profile	Functional parts
	PrimePart® PLUS (PA 2221)	Economical multipurpose material Balanced property profile Variety of certificates available (Biocompatibility, Food contact)	Functional parts
	PA 2202 black	Balanced property profile Pigmented throughout	Functional parts in anthracite black colour
Polyamide 12, glass bead filled	PA 3200 GF	High stiffness Wear resistance Improved temperature performance	Stiff housings Parts with requirements on wear and abrasion Parts used under elevated thermal conditions

Table 3.2 List of base polymer materials (Contd...)

Product class	Product name	Main properties	Typical applications
Polyamide 12, aluminium filled	Alumide®	Easy post-processing, good machinability High-temperature performance Thermal conductivity (limited) High stiffness	Applications with metallic finish Parts requiring machining Parts with thermal loads
Polyamide 12, carbon fibre reinforced	CarbonMide®	Extreme strength and stiffness Thermal and limited electrical conductivity Best strength/weight ratio	Light and stiff functional parts Metal replacement
Polyamide 11	PA 1101	High ductility and impact resistance Otherwise balanced property profile (similar to PA 2200) From renewable sources	Functional parts requiring impact resistance Parts with functional elements like film hinges
	PA 1102 black	Similar to typical applications for PA 1101 Additionally: black, mass-colored applications, which remain black even under abrasive wear / scratching	Similar to typical applications for PA 1101 Additionally: black, integrated colour Through mass-colourisation suitable for scratch resistant parts

Among the various materials prescribed as a base powder for SLS, CarbonMide® features to be an appropriate choice due to its high electrical and thermal conductivity, which are the essential functional requirements of the GDL constraint. However, it is not selected

as the research objective is to develop a carbon-free GDL and consequently, alumide and polyamide were selected as the appropriate base materials. Thus, the base material used for this study is alumide and polyamide (PA). The SEM image of alumide and PA powder are shown in Figure 3.3 and Figure 3.4 respectively. Though the structural configuration of these two polymers is similar to their elemental composition (Figure 6.11 and Figure 6.12) reveals that they exhibit different functionality.

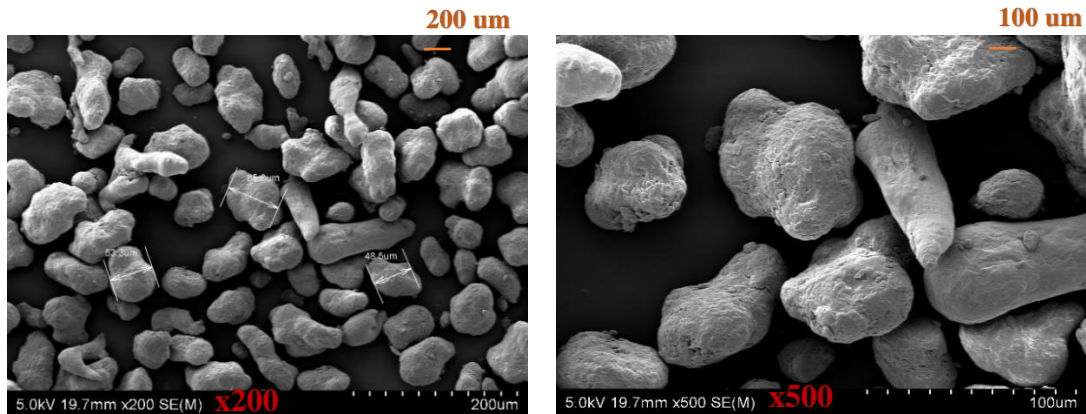


Figure 3.3 SEM image of alumide

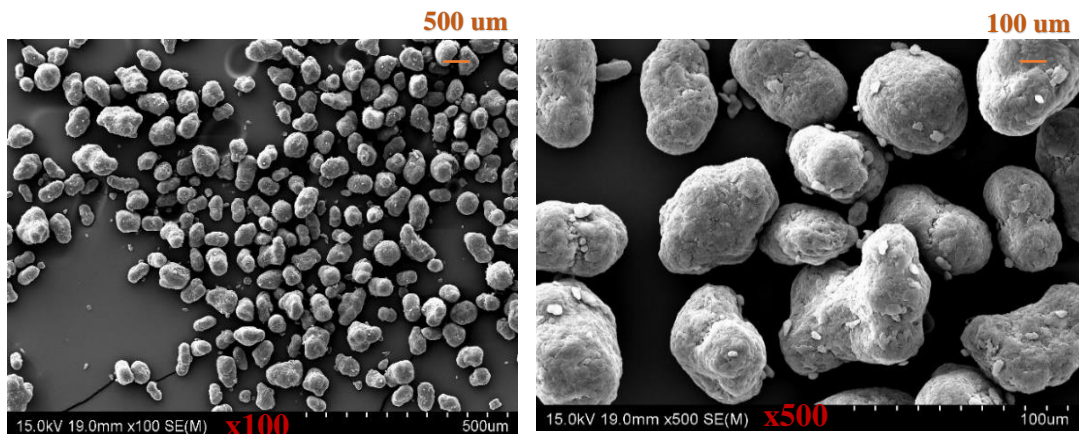


Figure 3.4 SEM image of polyamide

The advantage of alumide as the base material is it is relatively higher electrical conductivity and stiffness than many other materials used in 3D printing. In addition, inherently it possesses good flexural strength [72] and can also withstand much higher thermal loads, thus maintaining its desired shape. The experiment with PA as a base material is also performed because, as explained earlier, PA can serve as a promising

alternative to alumide specifically in a PEM fuel cell operating environment where metal ions (for instance, aluminium in the alumide) can potentially damage the membrane. The PA considered for the present investigation is PA2200.

3.4.2 Selection of Conductive Filler Material

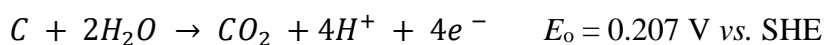
Conductive filler materials are added to the base materials to infuse electrical and thermal conductivity. However, they must be selected based on the corrosion resistance and its compatibility with PEM fuel cell working environment. As a consequence, a short assessment of the corrosion rate of various conductive materials was performed and are enumerated in Table 3.3 [73].

Table 3.3 Corrosion rates of materials [73]

Material	Corrosion rate (μm per year)
Aluminum	~250
Copper	>500
Gold	<15
Graphite	<15
Nickel	>1000
Silver	<15
Tin	>10000
Titanium	<100
Tungsten	<100
Zinc	>2000
Gold-nickel	~500
Phosphorous-nickel	<30
SS 316L	<100

However, it is eminent that these metallic material properties alone cannot be considered as a standard due to the diverse operating conditions in PEM fuel cell operating environments such as low pH, high power/high voltage, and high-temperature operation.

This operating condition while happening concurrently can potentially damage even low corrosive material like graphite (graphite is a carbon allotrope and can be oxidised to CO₂) specifically at a voltage greater than 0.207 V [63].



Despite being carbon graphene is still employed in the initial study, due to its two-dimensional structure, and has become a versatile candidate for the numerous scientific and engineering applications over the last decade. In addition, it also possesses unique property combinations which other composite materials do not, such as malleability, exceptional thermal and electrical conductivity, high strength, the ability to be rigid as well as lightweight [74]. In addition, its corrosion-protecting property has been well established [75], and as a consequence, it is considered for the initial investigation to have a general insight.

Metals like, Aluminium and Nickel can also be prone to oxidation in the PEM fuel cell environment and the metal ions formed could potentially damage the expensive membrane component. Few authors [76-78] reported that aluminium bipolar plates exposed to an operating environment similar to that of a PEM fuel cell are prone to corrosion. The corrosion rate of Titanium is higher than that of graphite as evident from Table 3.3. Paradoxically, in the PEM fuel cell operational environment, Titanium exhibits higher corrosion resistance and has been previously well established by various authors [54, 79-81] for GDL and bipolar plate fabrication respectively. Also, titanium is well recognized for its high strength-to-weight ratio, which rationalises that it is potentially a safe, durable and reliable filler material for GDL application and therefore considered commendable for this investigation.

The SEM image of Titanium (micron) and Titanium (nano) at various levels of magnification are shown in Figure 3.5 and Figure 3.6 respectively. The high surface area of the nano particles is revealed in Figure 3.6.

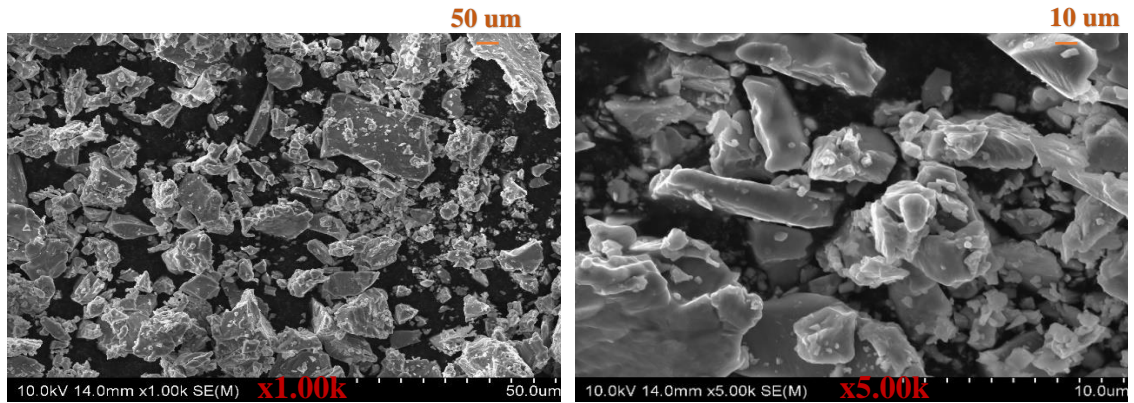


Figure 3.5 SEM image of Titanium (micron) Powder

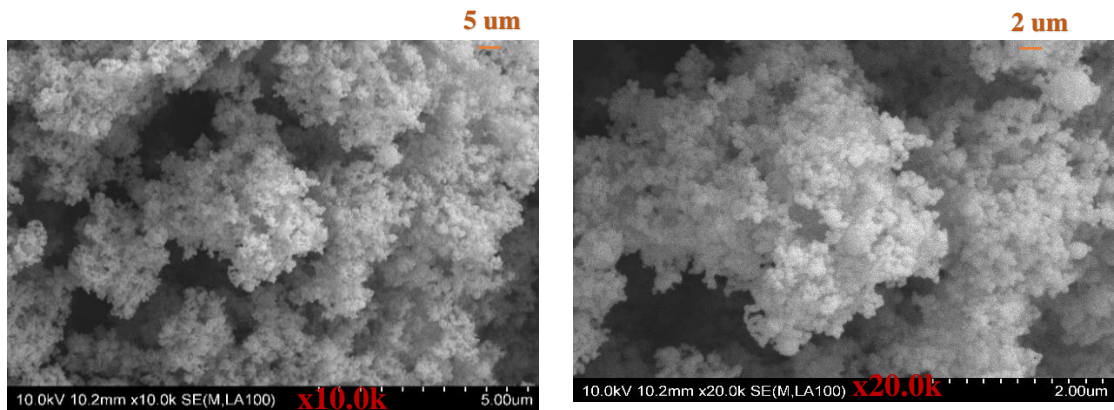


Figure 3.6 SEM image of Titanium (nano) Powder

Table 3.4 provides the general information on the base and conductive filler materials along with the supplier specifications.

Table 3.4 Base polymer and conductive filler materials

SLS Base Material	Filler Material
<u>Alumide</u> <u>Polyamide</u> (EOS Plastic Materials)	<u>Conductive Graphene</u> Ultra-high Concentration of Graphene Nanoplatelets purchased from graphene supermarket™ <u>Titanium Micron Powder</u> (US Research Nanomaterials, Houston, TX, USA) <u>Titanium Nano Powder</u> (US Research Nanomaterials, Houston, TX, USA)

3.5 Experimental methods and equipment

A comprehensive understanding of all the measurement instruments employed for the material (GDL) characterisation is a prerequisite and are specified in Table 3.5 along with the justification on its significance.

Table 3.5 Characterisation Techniques and the related Measuring Instruments

Characterisation	Measuring Instrument	Rationale
1a. Thickness	Vernier Calliper	Measure the thickness
1b. Surface Characterisation	SEM, EDX Hitachi SU-70, Tokyo, Japan	Measure the Surface Characterisation and Elemental composition
2. Tensile Characterisation	Texture analyser Stable Micro Systems Ltd. Godalming, UK	Measure the Tensile Strength of the GDL
3. Porosity and Permeability	Gurley Method	Measure the Air Porosity and Permeability through the GDL
4. Surface Contact angle/Hydrophobicity	Syringe 50 μ L –Hamilton HD Camera	Measure Surface Contact Angle
5. Electrical Characterisation	Tektronix, OR, USA	Measure In plane Electrical resistance
6. Thermal Characterisation	Laser Flash Analyser (NETZSCH, Bavaria, Germany)	Measure Thermal conductivity
7. Polarisation Curve	Electronic load Bank Amrel, USA. Graph (V Vs. I)	Measure the Performance

3.6 Characterisation Techniques

Characterisation techniques refer to the broad and general process by which a material's structure and properties are explored based on its configuration and measured values. It is an essential process in the field of material science, without which no scientific understanding of engineering materials could be validated or established. The present dissertation has a wide range of characterisation techniques, which are subsequently discussed in the following sections.

3.6.1 Thickness and Surface Characterisation

Thickness is a significant factor in achieving the desired PEM fuel cell performance and the GDL specimen. The morphology of the GDL structure was inspected using SEM images, which provides insight into the specimens' topography and composition. The scanning electron microscope (SEM) delivers both secondary electron and backscattered electron imaging, with a resolution of the order of μm at a high voltage of about 30 kV thereby establishing higher magnification of microstructure image.

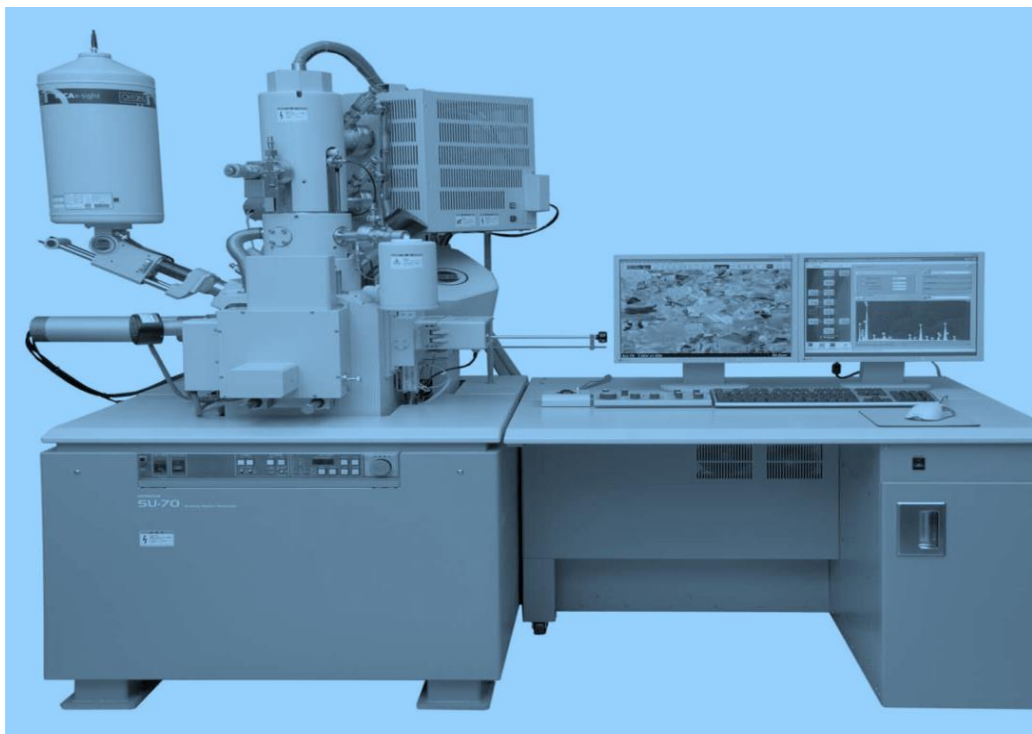


Figure 3.7 SEM with the integrated Energy Dispersive Spectrometer (EDX)

Figure 3.7 portrays the SEM facility that is integrated to Energy Dispersive Spectrometer (EDX) for fundamental chemical/elemental analysis via the Noran System 7 (NSS). The EDX characterisation capabilities are due in a large part to the fundamental principle that each element has a distinctive atomic structure allowing a unique set of peaks on its electromagnetic emission spectrum [84], which is the central principle of spectroscopy.

3.6.2 Tensile characterisation

The tensile test analyses the mechanical strength of the proposed GDL material to have minimal strength to be used for PEM fuel cell application, as it has to withstand the air/water flow and current/heat drift. ASTM D882 test method is used in the present work, to estimate the tensile properties of the thin films as the thickness is less than 1.0 mm. To avoid the tear and premature specimen failure, the tensile test was conducted at a speed of 0.5 mm/s along the machine direction (MD). The thin film GDL material is clamped between two fixtures and tested. For the present investigation, tensile strength is expressed in force per unit of length as it is the convention to measure tensile strength for a given paper or fabric [82]. As a consequence, N/cm is used as the unit of tensile strength throughout the course of the study. Figure 3.8 portrays the texture analyser used in the study.



Figure 3.8 Texture analyser to perform Tensile Test

3.6.3 Porosity/Air-Permeability Measurement (Gurley Method)

One of the features required of any gas diffusion layer is its access to the catalytic layer [83] and as a consequence porosity and permeability measurements are a prerequisite to analyse those characteristics. The Gurley method is considerably compatible to measure the air resistance of thin film material, and it adheres to ISO 5636 standard. It applies to thin film/papers, which have air permeance between 0.1 and 100 $\mu\text{m}/\text{Pa}\cdot\text{s}$. For the samples whose porous nature is high, an Image J technique is used to compute the porosity through the SEM image.

3.6.4 Surface contact angle measurement

An optimal hydrophobicity is an essential criterion for PEM fuel cell application. The GDL must be hydrophilic to maintain the good proton conduction of the Nafion membrane. Ironically, too much hydrophilic nature results in the flooding phenomenon of the electrodes by-product water as well as the humidified gas. Therefore, gas diffusion layers are usually coated with optimal hydrophobic materials. Thus, the measure of surface contact angle measurement becomes an integral component. The degree of hydrophobicity is determined by the simple concept that is proposed by Zamora et al. [83], in which a 20- μL drop was deposited on a sample and after stand-up for 1 hour, zoom shooting was conducted for the sample and then the contact angle was measured between the droplet and the surface. A higher contact angle means a higher hydrophobicity and a lower value signifies hydrophilic nature. This measurement, though not an ASTM or ISO standard, provided the measured values are close to an error of $\pm 15\%$.

3.6.5 Electrical Characterisation

Electrical Conductivity is a key property, which directly influences the fuel cell performance [39]. The figure of merit of the electrical characterisation signifies the ease with which electron transfer to facilitate the electrochemical reaction along the in-plane and the through plane. Electrical resistivity measurements of films are of significant concern in many applications, like solar cells [84] and PEM fuel cells. The In-plane electrical resistance was measured using the 4-wire Kelvin method as reported by

Williams et al. [32]. GDL samples of 2 mm width and 100 mm length were manually cut and the resistance was measured at 10 mm increments (10 points in total). The measured resistance (R) values were plotted against distances (l) and yielded a linear relationship whereby the slope of the line represented the in-plane resistance per unit of distance (R'). However, for the present GDL specimen since the dimension is 50 mm x 50 mm, the values for only 5 points were recorded. The slope of the curve that is plotted with the distance along the x-axis and the resistance across the y-axis provides the value of the measured in-plane resistance neglecting the effect of contact resistance. Figure 3.9 represent the digital multimeter to measure resistance (R).



Figure 3.9 Digital Multimeter to measure the in-plane resistance

3.6.6 Thermal Characterisation

PEM fuel cells under nominal operation produce an equivalent amount of thermal power comparable to their electrical power output [85]. The membrane is sensitive to excessive heat, and an active thermal management of the cell is mandatory. Removing the waste heat produced in an operating fuel cell is one of the significant functions of the GDL, and an optimal thermal conductivity of a GDL facilitates removing the waste heat and prevents large temperature gradients from forming within the cell [21]. The thermal conductivity of the GDL sample material was measured using three sets of instruments namely:

- i. The Armfield Linear Heat Conduction instrument that has been designed to demonstrate the application of the Fourier equation to simple steady-state conduction in one dimension.

$$k = -q / \nabla.T$$

k = Thermal Conductivity [$\text{Wm}^{-1}\text{K}^{-1}$]

q = Local heat flux density [Wm^{-2}]

$\nabla.T$ = Temperature gradient [Km^{-1}]

The units can be configured as a simple plane wall of uniform material and constant cross-sectional area or composite plane walls with different materials or changes in cross-sectional areas to allow the principles of heat flow by linear conduction to be investigated. Measurement of the heat flow and temperature gradient allows the thermal conductivity of the material to be calculated. The design allows the conductivity of thin samples of insulating material to be determined.

- ii. Thermtest TC-30. This is capable of measuring thermal conductivity in the range 0.033 to 9.58 $\text{Wm}^{-1}\text{K}^{-1}$. It is a guarded pulse technique and uses a pulse time of 0.5 seconds for the samples (regression from 0.2 to 0.5 seconds).
- iii. NETZSCH laser flash apparatus LFA 467 *HyperFlash*® (Figure 3.10) is also used in the study, which provided us with the most accurate values. The sample was tested at several temperatures according to their behaviour in the desired temperature range of 25°C to 160°C. The measurements are carried out in a foil sample holder (\varnothing 25.4 mm) and the values of 25°C, 80°C, and 140°C.



Figure 3.10 Laser flash apparatus NETZSCH

The formula to compute the thermal conductivity using the Laser flash apparatus is given as follow;

$$k = \alpha \rho C_p$$

k = Thermal Conductivity [$\text{Wm}^{-1}\text{K}^{-1}$]

α = Thermal Diffusivity [mm^2/s]

ρ = Bulk density [g/cm^3]

C_p = Specific heat J/(g.k)

As stated in the equation, the thermal conductivity is mathematically equal to the product of thermal diffusivity, bulk density and specific heat of the material (C_p). The incorporation of three independent instruments for the thermal conductivity provided us with more information and insight about the thermal conductivity measurement and the related challenges.

Apart from these characterisation studies, a general polarisation curve is performed for all the samples, which are elaborated in Chapter 5.

3.7 Closure

The present chapter deals with a broad-spectrum on the experimental design and methodology on how to selectively choose the base polymer and functional materials considering the PEM fuel cell operating environment and the SLS compatibility. The various measuring instruments involved in the characterisation are listed in the present chapter. The forthcoming chapter discourses a preliminary investigation and the related characterisation studies performed with those instruments discourses in the present chapter.

Chapter4: Preliminary Investigation and Measurement Techniques

“It is impossible to Control a variable if you cannot Measure it.”

Lord Kelvin

4.1 Introduction

To understand the figure of merit of a material and operating process an appropriate rationale is a prerequisite before the tangible experimentation. In the present chapter, an initial trial is executed to have a fundamental insight, as the proposed concept of incorporating the selective laser sintering (SLS) technique is first of its kind for GDL fabrication. This initial investigation provides a general understanding and integration of the SLS/microfabrication process and its compatibility for the gas diffusion layer fabrication. A snapshot of the measuring instrument involved in the characterisation studies is also executed apparently.

4.2 Initial Investigation

A smooth transition is always better for attaining the desired characteristics of new product development [86, 87] precisely when there is no adequate literature available. As a consequence, the initial experiment is performed with the well-established concept of using carbon (graphene) based conductive material, which has been used in PEM fuel cell application [88, 89] and alumide was used as a base material. As explained previously, alumide offers excellent flexibility for a 3D print and is cost effective.

The initial trial involves two independent phases with the first phase involving a) Fabrication of gas diffusion specimen (by SLS) and subsequent phase involves b) Micro fabrication coating applied to the specimen with the conductive graphene (by Spin coater). The selective laser sintering technique is used in the first phase of the initial trial, and Figure 4.1 illustrates the line sketch of the experimental set-up. As already discussed, during SLS, tiny particles or polymer powders are fused together by heat from a laser to form a solid, three-dimensional object. The laser heats the powder either below its boiling

point (sintering) or above its boiling point (melting), which fuses the particles in the powder together into a solid form. Like any other 3D printing technique, an object printed with an SLS machine starts as a computer-aided design (CAD) file. CAD files are converted to the .STL format, which can be interpreted by a 3D printing apparatus controlled by an appropriate processing unit. The operating parameters such as laser power and scanning speed are maintained at 15 W and 700 mm/s respectively. The powder was deposited on the powder bed and spread uniformly to ensure the flatness of the surface. The powder bed is sustained at around 60°C to maintain the solid-state sintering in the processed layers.

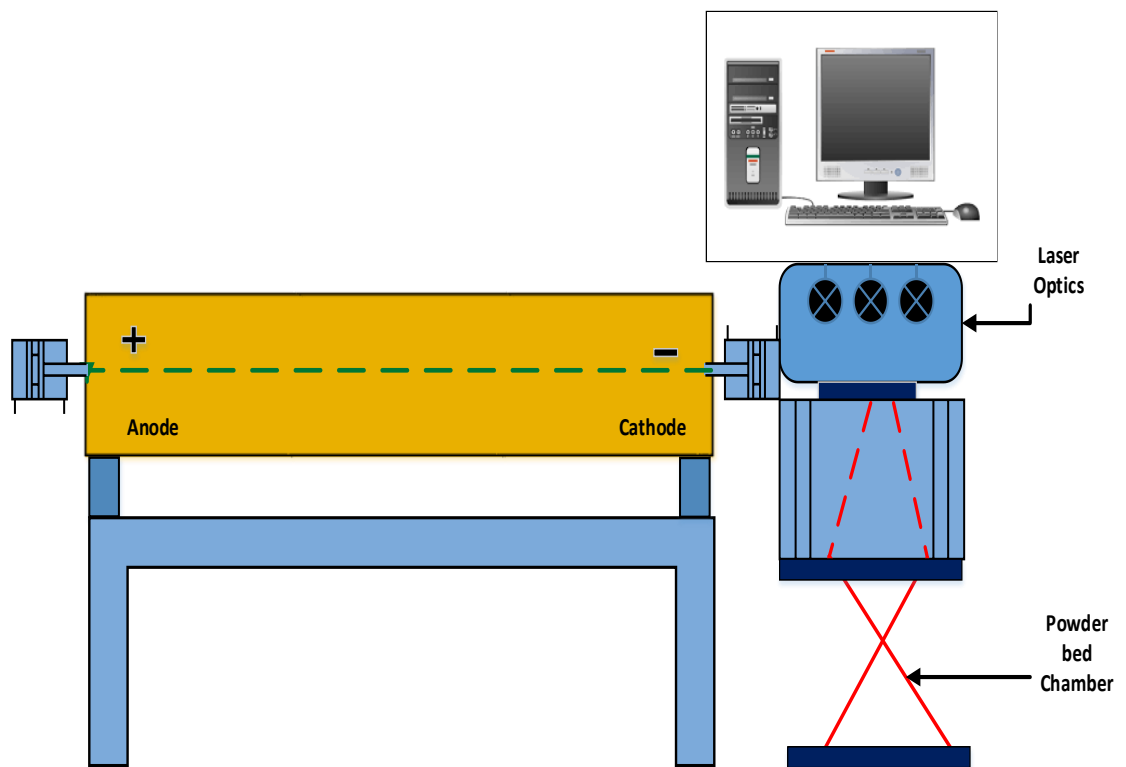


Figure 4.1 Line sketch of SLS experiment set-up [90]

Figure 4.2 is an actual photograph of the gas diffusion material synthesised by the selective laser sintering technique using just the alumide polymer. The fabricated specimen had most of the desired properties of the GDL, except the conductivity.



Figure 4.2 Actual Photograph of Alumide Thin film

Following the SLS process, in the second phase of the initial trial, a minor surface modification is performed by a spin coater, onto the specimen (fabricated from phase-I) to infuse electrical conductivity to the alumide specimen. Figure 4.3 portrays the spin coater used for microfabrication, which is operated in a well-ventilated space working under a chemical hood. The distinctive feature of the spin coater is that it provides a uniform surface coating to fabricate a defect-free GDL specimen.



Figure 4.3 Spin coater used for Microfabrication

Thus, the spin coating technique is used to deposit ultra-thin and uniform conductive (graphene) coating across the specimen (alumide film). The speed of the spin coater is varied from 5000-5500 RPM. Thus, the initial trial involves an integrated approach combining two independent processes namely SLS and spin coating.

4.3 Characterisation Techniques

Characterisation techniques refer to the broad and general process by which a material's structure and properties are explored based on its configuration and measured values. It is an essential process in the field of materials science, without which no scientific understanding of Engineering materials could be validated or established. The present dissertation has a wide range of characterisation techniques from micro to macro level. In the forthcoming section, the characterisation techniques for the gas diffusion material fabricated in the initial trial (graphene coated alumide material) are conversed.

4.3.1 Thickness and Surface Characterisation

Thickness is a significant factor in achieving the desired PEM fuel cell performance and the GDL specimen fabricated in the initial trial had a thickness of 595 μm . Though 290 μm was the thickness of just the alumide substrate, it almost doubled due to the micro-fabrication coating. The morphology of the GDL structure was inspected using SEM images, which provided insight into the specimens' topography and composition. Figure 4.4 illustrates the SEM that portrays the surface morphologies of the alumide specimen coated with conductive graphene at various levels of magnification.

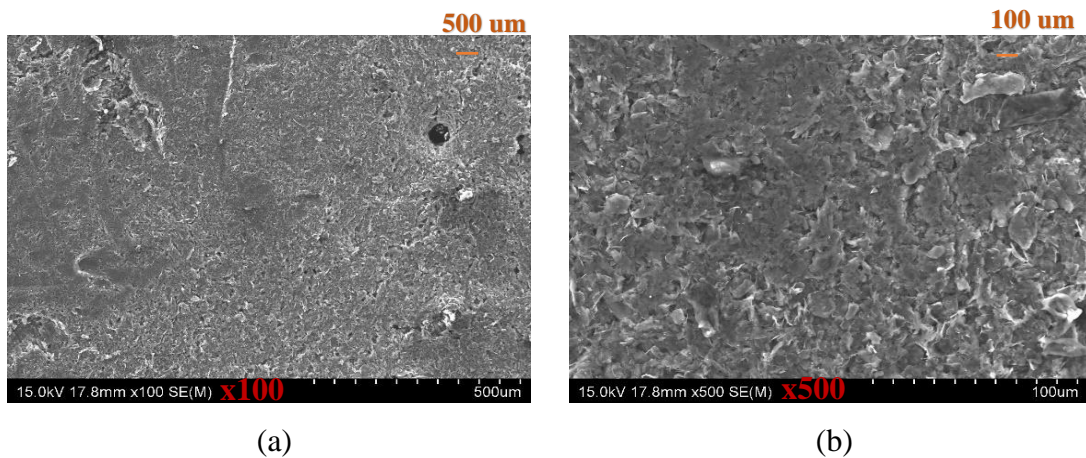


Figure 4.4 Surface morphology of graphene coated specimen at various levels of magnification

Though the surface of the graphene-coated thin film seemed to possess a smooth texture evident from high magnification SEM inspection; a small amount of roughness and is evident from the Figure 4.4.

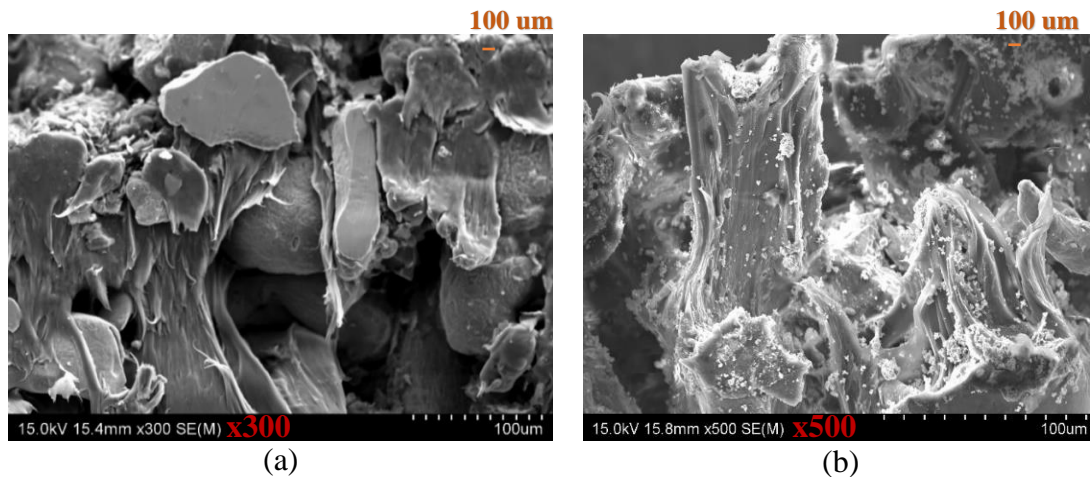


Figure 4.5 Cross-Sectional SEM of graphene coated on alumide specimen

The semi-fibrous nature of the graphene is also reasonably observed from the cross-sectional SEM image (Figure 4.5 (b)). A micro-thin coating fabricated through the spin-coater on the surface of alumide specimen with minimal defects and the corresponding elemental surface analysis is obvious from Figure 4.6. The EDX analysis also indicates that carbon (graphene) is the significant contributor with traces of aluminium, silicon, and zirconium. The insight into the fibre structure determines the porosity, permeability, and electrical properties of the GDL [25]. Though the porosity is marginally reduced through spin coating, the addition of graphene significantly escalated the in-plane electrical conductivity.

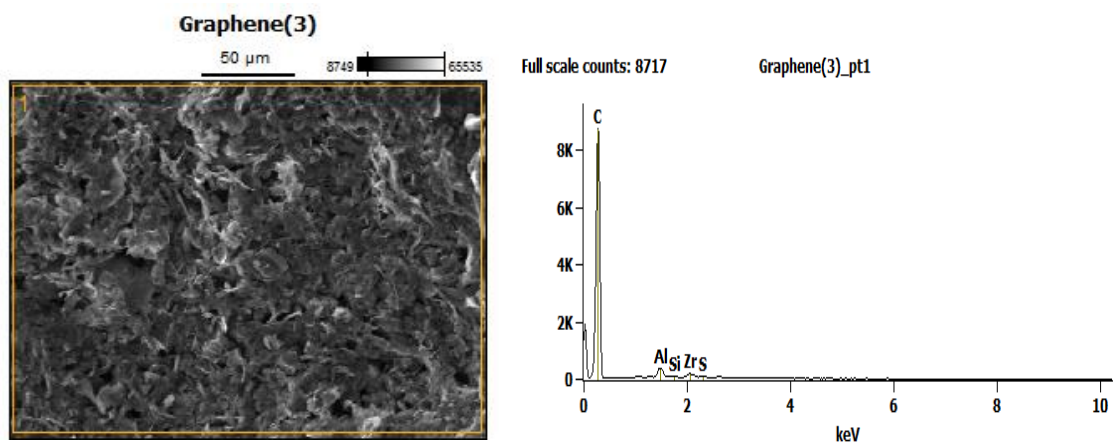


Figure 4.6 EDX of the graphene-coated alumide surface

4.3.2 Tensile Characterisation

The tensile test is employed to analyse the mechanical strength of the proposed GDL material to have minimal strength to be incorporated into PEM fuel cell application. ASTM D882 test method is followed in the present work to estimate the tensile properties of the thin films, as the thickness is less than 1.0 mm. To avoid the tear and premature specimen failure, the tensile test was conducted at a speed of 0.5 mm/s along the machine direction (MD).

The thin film GDL material is clamped between two fixtures and tested to measure its tensile strength in N/cm and its value is measured to be ca. 25 N/cm, which is higher than the tensile strength of the baseline material which had a tensile strength of ca. 20 N/cm. A higher thickness attributed due to the graphene coating is the predominant reason for such a high tensile strength.

4.3.3 Porosity/Air-Permeability Measurement (Gurley Method)

One of the features required for any GDL is its access to the catalytic layer [83]. Porosity and permeability measurements are conducted to analyse those characteristics. The Gurley method is considerably compatible to measure the air resistance of thin film material, and it adheres to ISO 5636 standard. It applies to thin film/papers, which have air permeance between 0.1 and 100 $\mu\text{m}/\text{Pa}\cdot\text{s}$. The specimen of the sintered composite GDL material microfabricated with the graphene possessed high porosity and air permeability. The integral reason for such a high porosity and air permeability is due to the SLS route, where the porosity is the default characteristics. Table 4.1 represents the porosity and air permeability value of the alumide and graphene specimen.

Table 4.1 Porosity/air permeability measurement of the alumide/graphene specimen

	Proposed 3D printed specimen Alumide/Graphene	Baseline material SGL-39 BC (Measured)
Porosity (mL/min)	24000	916
Permeance ($\mu\text{m}/\text{Pa}\cdot\text{s}$)	541.2	20.66

Despite the incorporation of the graphene particles by a spin coater, the proposed alumide graphene specimen exhibited a phenomenally good porosity and air permeability values based on the experimental observation from the Gurley method. With the development of digital images and computer software, image processing is a new and convenient method which can determine the pore size, pore size distribution, porosity and microstructure [91]. For the porosity measurement, Image J software technique is used where the porosity is computed from the SEM images.

4.3.4 Surface contact angle measurement

An optimal hydrophobicity is an essential criterion for PEM fuel cell application. The GDL must be hydrophilic to maintain the good proton conduction of the Nafion membrane. Ironically, too much hydrophilic nature results in the flooding phenomenon of the electrodes by-product water as well as the humidified gas. Therefore, gas diffusion layers are usually coated with optimal hydrophobic materials. Thus, surface contact angle measurement becomes an integral component.

The degree of hydrophobicity is determined by the simple concept that is proposed by Zamora et al. [83], in which a 20- μ L drop was deposited on a sample and after stand-up for 1 hour, zoom shooting was conducted for the sample and then the contact angle was measured between the droplet and the surface. A higher contact angle means a greater hydrophobicity and a lower value signifies hydrophilic nature and is expounded in Figure 4.7. This measurement, though not an ASTM or ISO standard, provided the measured values close to an error of $\pm 15\%$ by comparing it against baseline material.

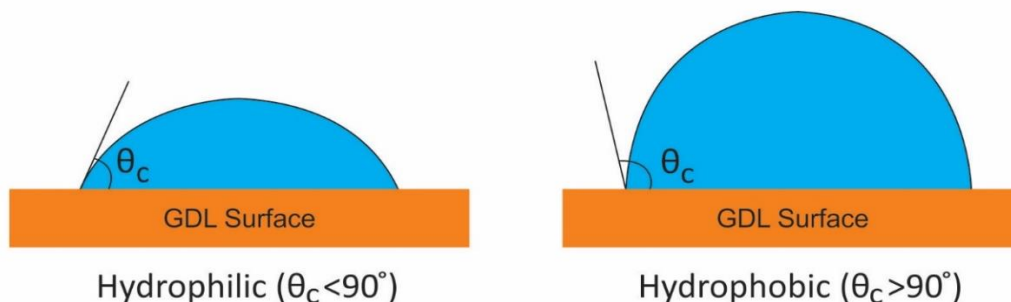


Figure 4.7 Surface Contact angle measurement a) Hydrophilic b) Hydrophobic

The graphene coated alumide material exhibited a surface contact angle of around 15° which validates that the specimen is exceptionally hydrophilic.

4.3.5 Electrical Characterisation

Electrical conductivity is a key property, which directly influences the fuel cell performance [39]. The figure of merit of the electrical characterisation signifies the ease with which electron transfer to facilitate the electrochemical reaction along the in-plane and the through plane. Electrical resistivity measurements of films are of major concern in many applications, like solar cells [84] and PEM fuel cells. In-plane electrical resistance was measured using the 4-wire Kelvin method as reported by Williams et al. [32]. GDL samples of 2 mm width and 100 mm length were manually cut and the resistance was measured at 10 mm increments (10 points in total). The measured resistance (R) values were plotted against distances (l) and yielded a linear relationship whereby the slope of the line represented the in-plane resistance per unit of distance (R'). However, for the present GDL specimen since the dimension is 50 mm x 50 mm, the values for only 5 points were recorded. The slope of the curve that is plotted with the distance along the x -axis and the resistance along the y -axis provides the value of the measured in-plane resistance neglecting the effect of contact resistance.

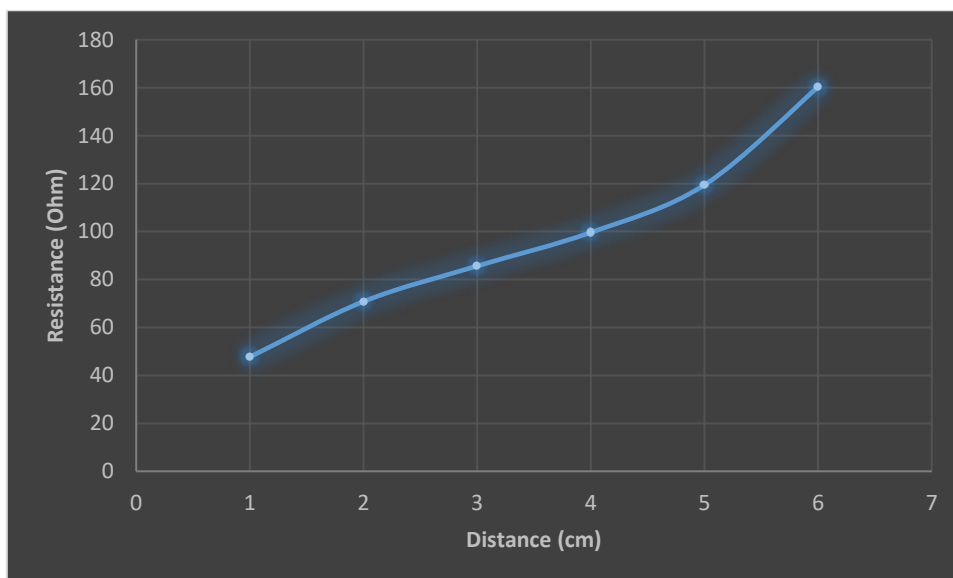


Figure 4.8 In-plane resistance measurement of graphene coated alumide specimen.

The slope of measured resistance as depicted in the graph (Figure 4.8) is $26.41 \Omega\text{cm}^{-1}$ for the graphene coated alumide specimen compared against the baseline material which exhibited a lower in-plane resistance of $0.313 \Omega\text{cm}^{-1}$.

4.3.6 Thermal Characterisation

The thermal conductivity of the graphene-coated GDL specimen is found to be $0.31 \text{ Wm}^{-1}\text{K}^{-1}$, which is higher than the baseline material, which had a thermal conductivity of $0.25 \text{ Wm}^{-1}\text{K}^{-1}$ (as per White paper attached-Appendix A) and $0.21 \text{ Wm}^{-1}\text{K}^{-1}$ as per measured value.

4.4 Summary Initial Trial

To re-establish the selection of graphene, it is perceived that the graphene-based materials are of specific interest in this study based on the promising literature results obtained in PEM fuel cell applications with graphene as a catalyst support [88] and as the catalyst [89]. Also, graphene's properties such as high electrical conductivity, high heat transfer rate, high specific area [92, 93] and corrosion resistance add value to the proposed requirement.

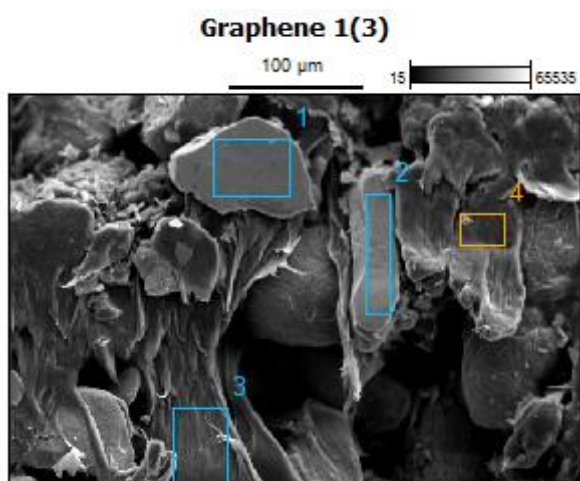


Figure 4.9 Cross-sectional image revealing graphene (point 3 and 4) and alumide (point 1 and 2)

Table 4.2 EDX cross-sectional analysis of the graphene coated alumide specimen

	<i>C</i>	<i>Al</i>	<i>Si</i>	<i>S</i>	<i>Ca</i>	<i>Zr</i>
<i>Graphene 1(3)_pt1</i>	2.36	94.12				3.52
<i>Graphene 1(3)_pt2</i>	3.00	93.50				3.50
<i>Graphene 1(3)_pt3</i>	91.24	1.07		0.26		7.43
<i>Graphene 1(3)_pt4</i>	89.93	0.40	1.29	0.34	0.35	7.70

The EDX analysis in Table 4.2 reveals that the cross-sectional regions 1 and 2 are the alumide particles along the axial and are evident from Figure 4.9 that the graphene particles in point 3 and 4 are semi-fibrous in nature and have a better malleability compared to the alumide particles, which are more rigid. These characteristics of graphene have been well established by various authors and are in line with the literature [74, 94]. However, the alumide powder does not have similar malleability and it still remains a bulky grain. The polarisation curve of the graphene-coated alumide specimen is provided in Chapter 5 along with other GDL materials fabricated by SLS route.

4.5 Closure

This chapter proposes an initial investigation that integrates an SLS and a microfabrication technique. Though microfabrication coating of graphene with alumide by spin coater is an inexpensive technique to induce electrical conductivity; it still remains quite complex due to two independent phases, which was the limitation of this trial. In addition, the microfabrication technique that was used to increase the electrical conductivity, incidentally also increases the thickness of the GDL material. Apart from that, technically, the hypothesis aims to fabricate a ‘C’ free GDL material (as graphene is carbon). Despite these challenges in the initial investigations, this chapter provides an opportunity to have an insight into the measurement techniques and the related instruments involved in the contemporary research through an initial investigation.

Chapter 5: Experimental and Characterisation Studies

“A Theory can be proved by Experiment, but no Path leads from Experiment to the birth of a Theory.”

Albert Einstein

5.1 Introduction

It is obvious that if experiments are executed randomly, reliable results might not be acquired. Therefore, it is essential to plan and organise the experiments in a systematic fashion so that trustworthy information is obtained [95]. Characterisation studies are performed after each set of experiments to evaluate the materials' structural and functional competence against the baseline material. The material analysis includes macroscopic techniques such as mechanical testing and thermal analysis [96] and the microscopic analysis such as SEM. The present work, however, has both the macroscopic and microscopic characterisations to substantially validate the materials' competence in the PEM fuel cell operating environment. There are totally seven characterisation techniques as discussed in Chapter 3. However, there have been few limitations involved in performing them due to the materials' nature and lack of standardised protocol. The final characterisation is an *in-situ* where the real time behaviour of the PEM fuel cell is assessed through a polarisation curve.

5.2 Experimental Design

The series of experiments in the present investigation is executed using an iterative technique, in which the incremental weight of optimizing the properties that aim to provide new product development flexibly. However, it is important to change one bottleneck at a time. Trying to do things in parallel without validating the impact of the specific parameter, will lose track on that specific parameter that assisted to attain the desired characteristics.

Due to lack of sufficient literature, a trial and error iterative process is used in the present study that involves selection of materials based on the PEM fuel cell, SLS operational

characteristics, the design of the experimental plan, measuring, analysis, optimization, and validation until the minimal level of fitness is attained. Figure 5.1 exemplifies the process involved in the proposed product development from stage A-E sequentially through an iteration process to attain faster, flexible and reliable convergence for a new gas diffusion medium that is immune to voltage oxidation and easy to be manufactured.

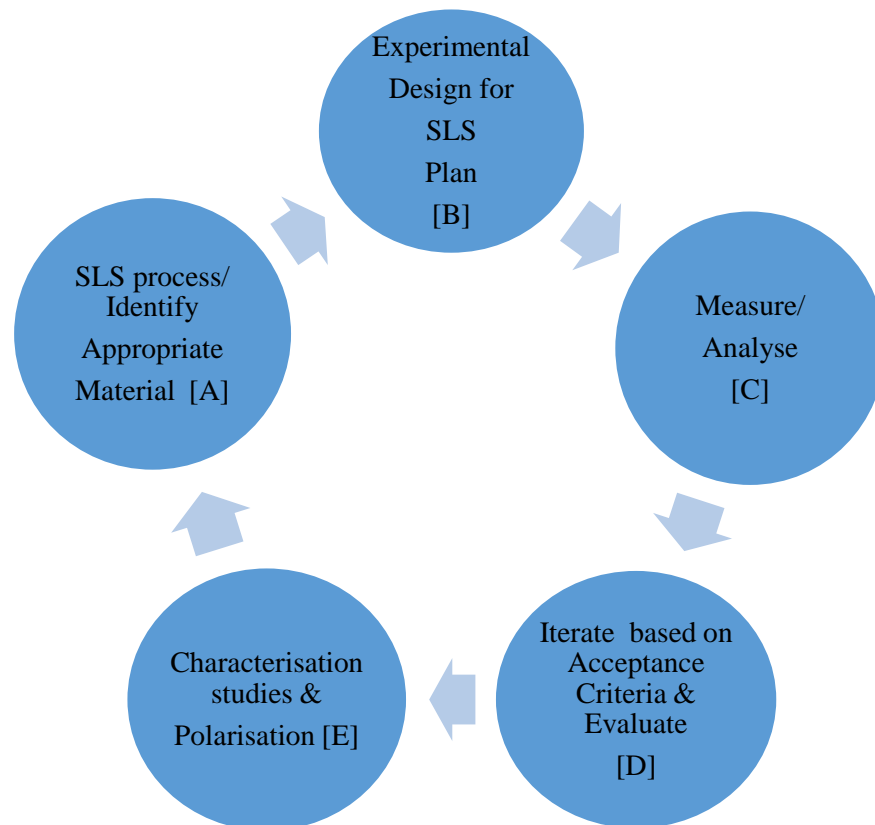


Figure 5.1 Systematic procedure of Experimental Process

A functional configuration was used to compute the minimal acceptance criterion based on the following properties: Thickness, Surface morphology (SEM), Tensile Strength, Porosity and permeability, Hydrophobicity, Electrical Conductivity, Thermal conductivity and Polarisation studies. Though porosity is one of the vital requirements for the GDLs functional requirement, it is learned from literature [97] that porosity is the default characteristics of any material processed through the selective laser sintering (SLS) method. Thus, inherently one of the essential

characteristics is accomplished through the SLS pathway. As explained in Chapter 3, alumide and polyamide are considered as the base material for this investigation. Conductive filler namely, titanium (micron and nano) powder is added to base powders to infuse appropriate electrical and thermal conductivity. Though the utilization of sintered titanium structures has already been proposed by Hottinen et al. [54] for GDL application, the proposed technique of 3D printing (SLS) is the first of its kind for GDL fabrication by a precise Laser beam. The composite powder (base polymer + conductive filler) is sintered in a precise mode (powder particles are fused together into a solid-state specimen) through this laser beam regulated by the computer through the CAD file to attain the desired functional characteristics.

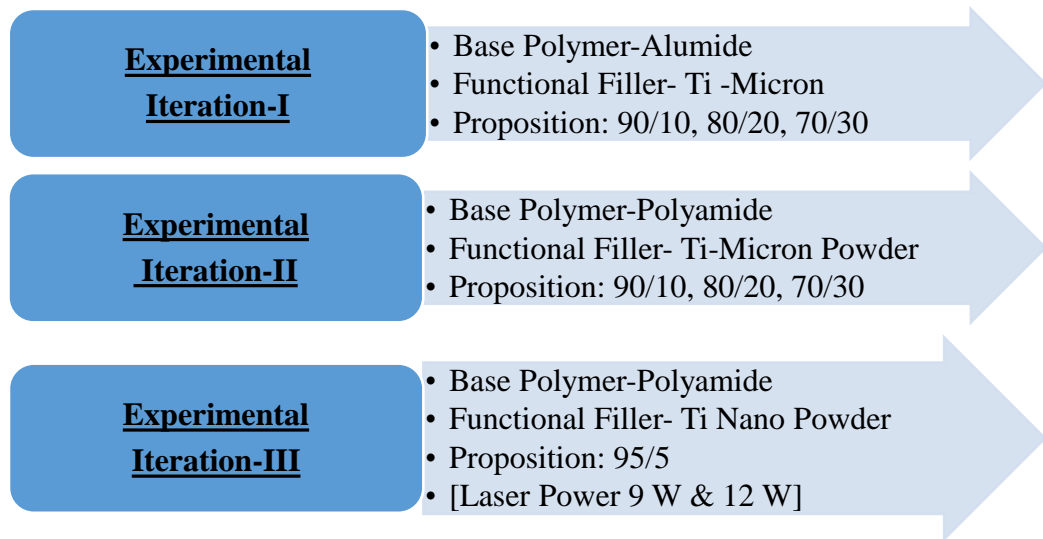


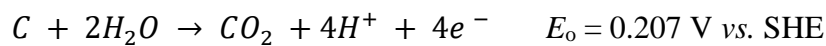
Figure 5.2 Functional chart of the experimental flow process

Figure 5.2 represents the functional chart of the experiment flow that is to be followed in the present thesis.

5.3 Experimental Iteration-I

The iteration-I is performed based on the feedback and the critical observation that is inferred from the initial trial. The potential limitations encountered in the initial trial are namely:

- i. The microfabrication technique incorporated to increase the electrical conductivity also causes an increase in the thickness of the gas diffusion layer. An increase in the thickness is non-favourable as it can lead to the corresponding increase in the Ohmic loss as well as an increase in the PEM fuel cell stack dimension (area and volume).
- ii. The overall production process involves two independent phases that can probably be reduced to a single phase.
- iii. Graphene, which is used in phase two of the initial trial, is also carbon, which can potentially be oxidised to CO₂ [63, 65].



It must be deliberated that the key research objective is to fabricate a carbon-free GDL. To circumvent these issues, in the present iteration a functional filler namely titanium micron powder in the appropriate percentage of 10%, 20%, and 30% is added directly into the base powder (alumide) and mixed mechanically using a mortar. For the 60% alumide/40% Ti composition there was a flammability due to the contact of laser heat with the high weight % Ti powder, and consequently, that composition was ignored for investigation.

The composite powder in the percentage of 10%, 20%, and 30% is fed into the powder bed of the SLS machine. To study the sintering, diffusion and subsequent bonding of the composite powder the experiments are executed by varying the power as illustrated in Table 5.1 for a fixed scanning speed of 450 mm/s.

Table 5.1 Laser power required to sinter various configuration of Alumide/Titanium

Laser Power (W)	Alumide/Titanium Composition (%)
15	90/10
12	80/20
9	70/30

Thus, the experiments of iteration I are performed on a trial and error basis sequentially and systematically. Subsequently, the characterisation studies are also executed to understand the SLS mechanism.

5.4 Characterisation for Iteration-I

5.4.1 Thickness and Surface Characterisation- Iteration-I

The thickness of the sample is measured to be around 550 μm for the Alumide/Titanium composition of 90/10, 445 μm for the Alumide/Titanium composition of 80/20 and 410 μm for the Alumide/Titanium composition of 70/30. The surface morphology characterisation of various combinations of alumide/titanium composites is performed and elaborated in the following section along with the SEM images for various magnification.

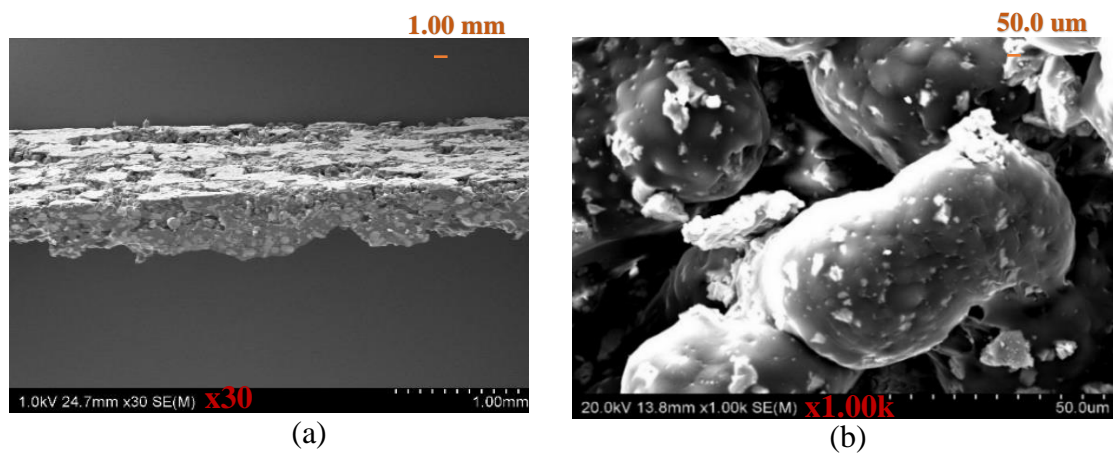


Figure 5.3 SEM of gas diffusion specimen fabricated with 90% Alumide and 10% Ti

The initial experiment with the iteration I was performed with the composition of 90% alumide/10% Ti powder and subsequently adding it to the powder bed and selectively sintering it layer by layer through the laser beam. The sintered gas diffusion layer exhibits non-uniform thickness with flakes (due to the non-effective sintering process) which is well observed in the SEM image. The specimen is highly disordered and exhibits a relatively higher anisotropic nature. The white shining flaky grains (inferred from the SEM – Figure 5.3 and Figure 5.4) are the titanium particles and are revealed by the EDX point analysis.

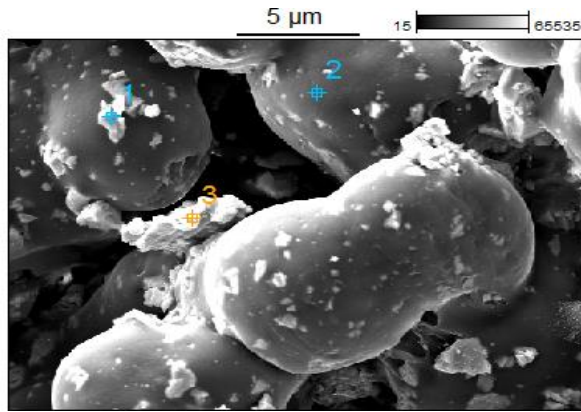


Figure 5.4 Point analysis SEM image of 90% alumide/10% Ti.

Figure 5.4 illustrates the SEM point analysis where there are white titanium rubbles (point 1 and 3) exposed. Though the particle size of the base powder and the conductive powder are in micron scale an inappropriate sintering has caused the alumide powder to swell considerably, however, the titanium powder sizes are relatively unaltered.

Table 5.2 also authenticates that the elemental composition corresponding to points 1 and 3 of Figure 5.4 are predominantly titanium particles compared to point 2.

Table 5.2 EDX analysis of GDL fabricated with 90% alumide and 10% Ti.

	C	N	Al	Ti
cs(3)_pt1	1.50	2.58	0.02	95.90
cs(3)_pt2	94.47		0.02	5.51
cs(3)_pt3	2.61	5.09	0.01	92.29

In the subsequent investigation, the SLS experiment is performed with 80% alumide/20% Ti and 70% alumide/30% Ti. Figure 5.5 shows the SEM image of 80% alumide/20% Ti and this combination is observed to be a relatively good blend with less anisotropic nature.

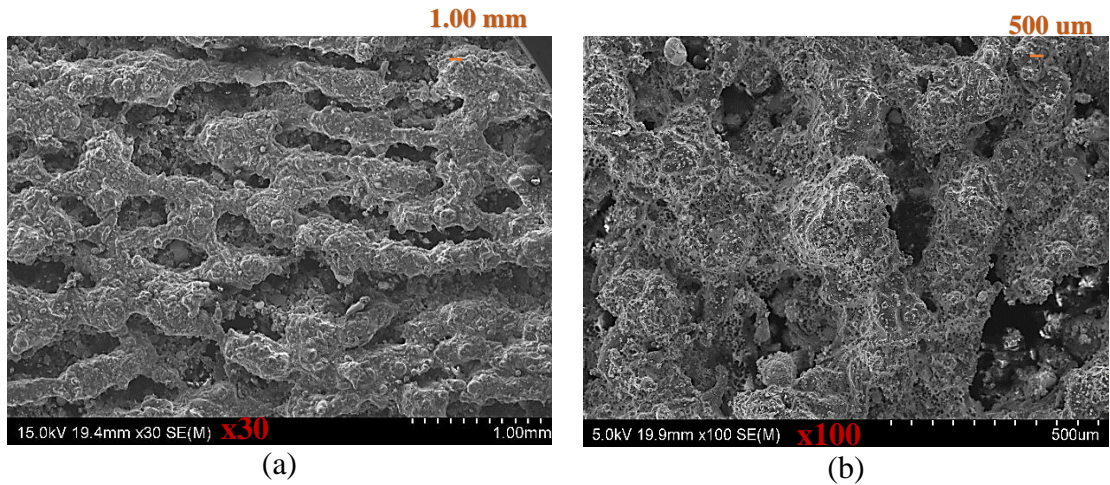


Figure 5.5 SEM image of 80% alumide/20% Ti at various levels of magnification
 In addition, the GDL composite fabricated with 20% Ti exhibited, relatively a better conductivity (among the three combinations), which might be attributed due to the equiaxed titanium distribution, and interconnected path, unlike the other combination. This phenomenon might have substantially aided the electron transport property.

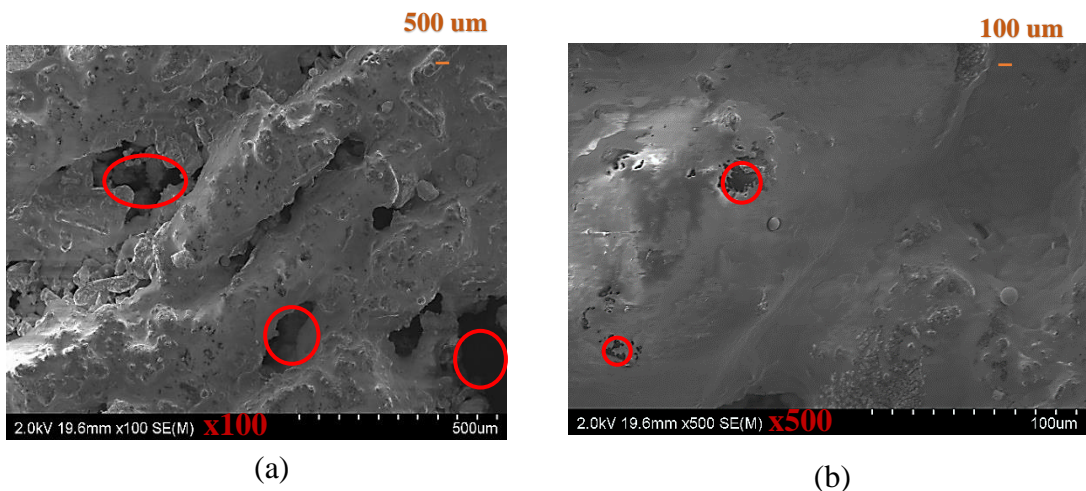


Figure 5.6 SEM image of the GDL fabricated with 70% alumide/30% Ti.

Figure 5.6 portrays the SEM image of a GDL with 30% Ti and this combination has a unique surface characteristic compared to the previous two combinations with 10 % Ti and 20% Ti composites. With the given energy densities, for the composition with 30% titanium and 70% alumide the particles are sufficiently fused since the higher quantity of titanium absorbs more energy which is transferred through the polymer, and the pore size

decreased considerably, indicating significant melting and subsequent inter-particle coalescence and bonding. However, large voids (Highlighted in the red colour of Figure 5.6) are randomly created probably due to the presence of Titanium particles increasing the viscosity of the melt pool as well as the resistance to the melt flow.

Table 5.3 reveals the elemental composition of the GDL specimen with 10%, 20% and 30% Titanium. Trace elements such as Zr is also present for all the combinations besides the oxide presence, which is one of the significant observation.

Table 5.3 Weight % elemental composition of entire GDL for Iteration-I

	C	N	O	Zr	Al	Ti
Ti_10% Al_90%	71.78	3.81	3.6	1.6	13.5	5.71
Ti_20% Al_80%	69.1	3.87	7.41	1.77	8.87	8.98
Ti_30% Al_70%	64.7	5.66	9.92	1.42	6.8	11.5

5.4.2 Tensile characterisation- Iteration-I

The measured values of all three specimens are detected to have a low tensile strength due to the materials' high porous and fragile nature. However, it was observed that the combination of 80% alumide and 20% Titanium had a relatively high tensile strength, which was measured to be 4 N/cm along the machine direction (MD). For the GDL of combinations with 90% alumide/10% Ti and 70% alumide/30% Ti, it is difficult to fix the specimen to the fixture due to their inherent brittle nature.

5.4.3 Porosity and Air permeability test- Iteration-I

Porosity is the default characteristics of the SLS process. The porosity and air permeability measurement using the Gurleys method was not competent to be performed due to the specimen's high porous nature as well low mechanical strength. Therefore, the non-invasive computational technique, namely Image J is incorporated, which validates that the GDL material is porous compared to the baseline material.

For the iteration II with 70% Alumide/30% Ti the material exhibited too high porosity and air permeability (evident from the SEM Figure 5.6). The material is too delicate to perform any of the characterisations except the SEM/EDX and hydrophobicity. However, few critical observations are derived from the analysis, which is illustrated in summary in the Section 5.4.7.

5.4.4 Surface contact angle - Iteration-I

It is evident from Table 5.4 that the surface contact angle of the GDL specimen for the composition with 80% alumide/20% Ti the material is more hydrophobic compared to the specimen fabricated with the composition of 90% alumide/10% Ti and 70% alumide/30% Ti.

Table 5.4 Surface contact angle measurement for Alumide/Titanium composition

Alumide/Titanium Composition (%)	Surface contact Angle (θ_c)
90/10	20° [Hydrophilic] \pm 3°
80/20	70° [Less Hydrophilic] \pm 10.5°
70/30	50°[Hydrophilic] \pm 7.5°

The surface contact angle for the baseline material is $118.2^\circ \pm 10.98^\circ$ and is hydrophobic in nature.

5.4.5 Electrical Characterisation- Iteration-I

The In-plane electrical resistance of the specimen was measured and varied from few hundreds (for 20 %Ti and 80% alumide) to thousands of Ωcm^{-1} for other combinations, and such a deviation might be attributed due to the anisotropic and porous nature of the material, improper sintering of the base powder and conductive filler especially at the backside of the specimen where the laser beam is not exposed.

5.4.6 Thermal Characterisation- Iteration-I

The thermal conductivity of the GDL specimen formed with 90% alumide/10% Ti, and 70% alumide/30% Ti is not able to be measured due to this porous nature and brittle nature, which might have affected the thermal conductivity. However, the thermal

conductivity values for this specimen is found to be $0.26 \text{ Wm}^{-1}\text{K}^{-1}$ for the composite with 80% alumide and 20% Ti which is marginally higher than the baseline material.

5.4.7 Summary- Iteration-I

- I. The general observation from the iteration I is that the thickness of the GDL specimen decreases when the titanium (% weight) increases. The composition of 80% Alumide/20% Ti exhibited relatively good overall characteristics including the microstructure characteristics and conductivity. It is also evident from the EDX that there is an oxide formation for all the composites with 10%, 20% and 30% Ti, which is one of the significant observations. The oxide formation might be either due to the presence of aluminium (in alumide) or titanium. However, during the EDX analysis of initial trial (refer Figure 4.6), there was no oxide formation while using alumide. Therefore, obviously, the oxide formation is due to the presence of titanium micron powder. The presence of oxide is crucial because the reason for a low electrical conductivity despite an increase in gravimetric titanium concentration might be attributed due to this phenomenon. Due to the non-uniform thickness, porosity and high anisotropic nature, the sample with 10% Titanium possessed low tensile strength and conductivity, whereas the sample with 30% Titanium had neither good electrical conductivity nor the tensile strength as the specimen is more smooth, porous and fragile.

- II. To summarize the critical observations, for the 30% titanium composition, it is inferred that, Laser converts the Titanium micron particles into metal oxides that is evident from the EDX and is well revealed in Table 5.3. Titanium oxides are non-conducting (semi-conductor) like materials, which might not have contributed to an increase in conductivity. In addition, these materials resembled the property of a ceramic material; which might have also been due to the presence of titanium oxide. The publications from Nature Letters [98], and Nature Materials [99] authenticate our observation where the titanium oxide (transition metal oxide) is used as the dielectric (insulator) for the ceramic capacitor.

III. In addition, the composition with 70% alumide/30% titanium, having more metallic powder might have absorbed more heat, might have melted the base material, liquidified it, and dispersed evenly along the surface of the specimen. This phenomenon is evident from the SEM of Figure 5.6 where the surface is smooth due to this effect. Though the polymer matrix is uniformly sintered due to the fusion and a smooth layer formation, there is also an increased agglomeration of the fused melt pool of polymer along the scan raster line. The SLS operational process is being solely driven by the reduction of surface energy of the base polymer, and it is unable to overcome the inter-agglomerate attractive forces and results in a mottled microstructure with alternating regions and random distribution of the polymer matrix. These observations are in line with the results of Velu et al. [90] for the selective laser sintering of polymer biocomposites.

The hydrophobic nature of the GDL specimen with 30% Ti and 70% alumide might also have been attributed due to this reason.

Either factor I or II or the combination of both I and II could have been the key cause of the reduced conductivity. In addition, the composite with 30% titanium exhibited a highly porous nature and a lower thickness, and consequently, the characterisations such as tensile and permeability analysis have not been able to be performed using the ASTM standard. Therefore, the Image J is used to perform the porosity measurement, which validates the proposed material to be more porous than the baseline material.

The fundamental concept that an increase in the electrical conductivity of the specimen proportionally increased with the Ti concentration (% weight) but is limited to the present investigation. The relatively high conductivity of the composite with 20% Titanium and 80% alumide might be because the titanium particles are equiaxially distributed along the specimen. The equiaxial titanium distribution must have aided the electron transport property due to its well-interconnected path.

With regard to the porosity and hydrophilic measurements, all three compositions have significantly different surface morphology. For instance, the composition with 10% and 30% Ti is predominantly hydrophilic. The composite with 20% Ti has the metallic particles uniformly dispersed and moderately hydrophobic. The other challenges that are

encountered in the iteration I are those pertaining to the measurement, which is elaborated in the next chapter.

5.5 Experimental Iteration-II

The necessity for iteration II is to overcome the potential limitation of iteration I namely:

1. Aluminium present in alumide can be converted to aluminium ions under PEM fuel cell operating environment and few researchers [76], [77, 78] have previously reported that aluminium bipolar plates exposed to such an environment are prone to corrosion.
2. In addition, the low tensile strength of the GDL specimen while using alumide/titanium composition is also a significant factor.

As a consequence, in the successive iterations, alumide is replaced by polyamide as the base material to fabricate the GDL film. The experiments of iteration II are performed parallel to iteration I with 10%, 20% and 30% titanium micron powder. Similar to the previous iteration for the Ti composition of 40% there was a flammability limiting us to perform the experiment. The Laser power required to sinter various configurations of Polyamide/Titanium is illustrated in Table 5.5.

Table 5.5 Laser power to sinter Polyamide/Titanium composite powder

Laser Power (W)	Polyamide/Titanium Composition (%)
15	90/10
12	80/20
9	70/30

It must be noted that when the titanium composition increases, the laser power is decreased because the energy absorption increases resulting in a wider sintered zone, in terms of higher energy absorption as the laser scans a given point and subsequent dissipation of the same, resulting in the augmented heating of the surrounding matrix phase.

5.6 Characterisation for Iteration-II

5.6.1 Thickness and Surface Characterisation - Iteration-II

The thickness of the GDL specimen is measured to be ca. 570 μm for the Polyamide/Titanium composition of 90/10 (measured through SEM instrument and is evident from Figure 5.7 b), ca. 440 μm for the Polyamide/Titanium composition of 80/20 and ca. 410 μm for the Polyamide/Titanium composition of 70/30. It is observed that the thickness of the specimen decreases when the titanium weight (%) increases analogous to the previous iteration. The more heat energy absorption by the titanium particle at the high concentration (% wt.) has potentially caused the reduction in the specimen thickness.

The surface and cross-sectional morphology of the specimen produced using SLS process is exemplified in Figure 5.7. The porous and non-homogeneous nature is well evident from the SEM image of the composition with 90% PA/10% Ti. The base powder and conductive fillers are loosely bound to each other and are not well sintered (evident from the cross-sectional SEM image) and this reason causes the specimen to be of high thickness and non-homogeneous nature (b).

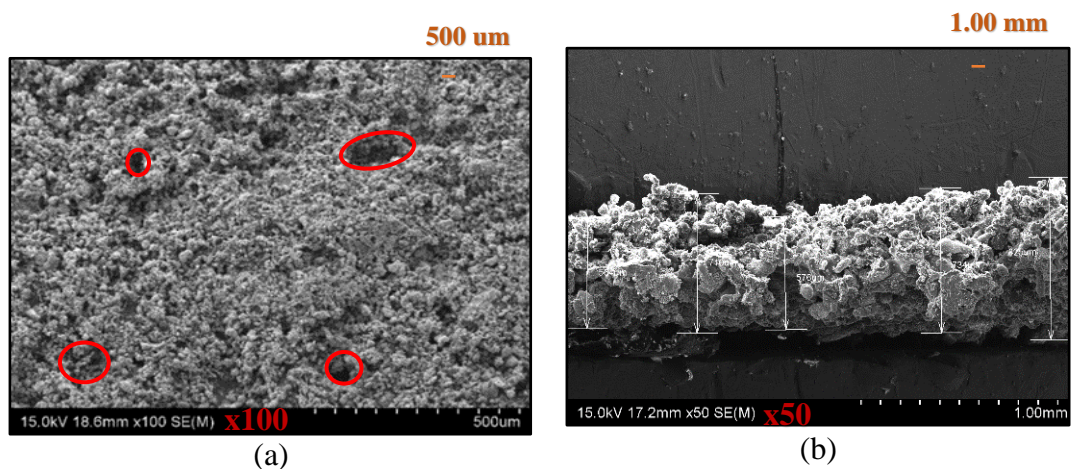


Figure 5.7 SEM image of the GDL with 90% PA/10% Ti (a) Surface View (b) Cross-sectional view

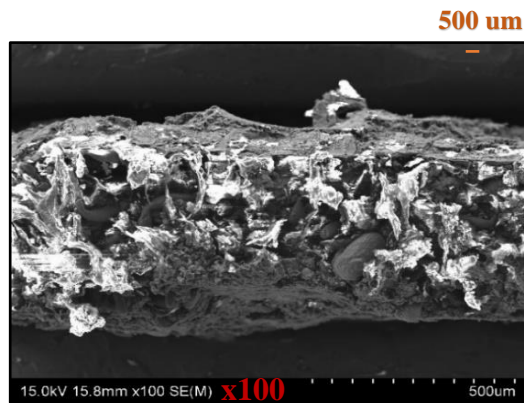


Figure 5.8 Cross-sectional view of the composite specimen with 80% PA/20% Ti.

The polymer matrix of the composite material is observed by the Cross-sectional view and is shown in Figure 5.8

5.6.2 Tensile Characterisation- Iteration-II

The tensile strength is measured to be around 5 N/cm along the MD of the composition with 80% PA/20% Titanium, which is higher than the previous iteration, however, lower than the baseline material. For, the composite with 30% Titanium the value is ca. 5 N/cm whereas for the composition with 10% Ti, the tensile strength is too low that it cannot even be clamped to the fixture. The in-effective sintering of the base and conductive powder has been attributed to its intrinsic nature and evident from the SEM Figure 5.7.

5.6.3 Porosity/Air permeability test Iteration-II

Though the conventional Gurley technique cannot measure the porosity and the air permeability measurements of the specimen, it is evident from Image J analysis of the SEM image that the material possessed a high porosity and pore size distribution compared to the baseline GDL.

5.6.4 Surface contact angle - Iteration-II

The material exhibited a predominantly hydrophilic nature with the surface contact angle measurement of $10^{\circ} \pm 1.5^{\circ}$ for the PA/Titanium composition of 90/10, $45^{\circ} \pm 6.75^{\circ}$ for the PA/Titanium composition of 80/20. The surface contact angle measurement for the

PA/Titanium composition of 70/30 is ca. $80^{\circ}\pm 12^{\circ}$ [region 1] and ca. $10^{\circ}\pm 1.5^{\circ}$ [region 2] where the region 1 and 2 are highlighted in Figure 5.9.

5.6.5 Electrical Characterisation- Iteration-II

The in-plane electrical resistance of the various composite materials (with the different proposition of PA/Titanium) is implemented along the surface of the GDL specimen, which is exposed to SLS. The in plane-electrical conductivity is relatively higher for the GDL specimen with the composition of 80% PA/20% Ti powder; compared to the composition with 90% PA/10% Ti powder and 70% PA/30% Ti powder. The values are in the range of ca. Ωcm^{-1} for the composition of 80% PA/20% Ti powder.

5.6.6 Thermal Characterisation- Iteration-II

The measured value of thermal conductivity of all the titanium/polyamide combinations is observed to be higher than the baseline material (carbon paper Sigracet 39 BC). Table 5.6 provides the thermal conductivity for the GDL specimen with PA/Titanium combination.

Table 5.6 Thermal conductivity of GDL specimen fabricated with PA/Titanium composite.

PA/Titanium Composition (%)	Thermal conductivity $\text{Wm}^{-1}\text{K}^{-1}$
90/10	0.37
80/20	0.54
70/30	0.59

5.6.7 Summary Iteration-II

The challenges in the measurement of the GDL specimens with 90% PA/10% Ti and 70% PA/30% Ti in the Iteration-II due to the materials non-linear and anisotropic nature, as well the non-uniform thickness of the material. Parenthetically, it was quite easy to measure the combination with 80% PA/20% Titanium, which had a reasonable tensile strength, electrical and thermal conductivity, and hydrophobicity that are reasonably close to the Baseline GDL material.

Though 20% titanium powder was the actual weight proportion contributed for the gas diffusion specimen preparation, it is sensed in the EDX (Table 5.7) that the weight as low as 14.8% has been used towards the specimen formation, the EDX analysis is contrary to the one performed in the initial trial as well the iteration III where the titanium particles are more than actually cast-off (By weight %).

Table 5.7 EDX analysis of the GDL specimen sintered with 80% PA/20% Ti

	<i>C</i>	<i>N</i>	<i>O</i>	<i>Ti</i>	<i>Zr</i>
<i>S7-PA</i>	66.1	8.3	9.1	14.8	1.7

The following possibilities (similar to the Iteration I) that might have happened in the SLS process are:

- i. An increase in the Ti alone doesn't provide a feasible solution to enhance the electrical conductivity because, with the present experimental set-up (non-inert atmospheric condition), the titanium present in the composite might be oxidised to titanium oxide.
- ii. Performing the experiment in argon condition can drastically enhance the electrical conductivity, and under such an operating condition, an increase in the Titanium can actually enhance the electrical conductivity of the gas diffusion material. If the SLS is operated under such an argon environment, a higher percentage of titanium such as 30% or 40% might be actually feasible.

Another critical observation of the iteration II is that for the GDL specimen with 70% PA/30% Ti the tensile strength along the sintered region 1, shown in Figure 5.9 has a much higher value compared to the non-sintered region. In addition, the in-plane electrical conductivity was also found to be higher in this region despite the region being brittle. Correlating these two phenomena, it is concluded that a GDL (thin film) polymer must be well sintered over the SLS process to have a reasonable tensile strength as well as the electrical conductivity. It also raises a query that if an increase in tensile strength, could contribute to the improved conductivity for this kind of material combinations.

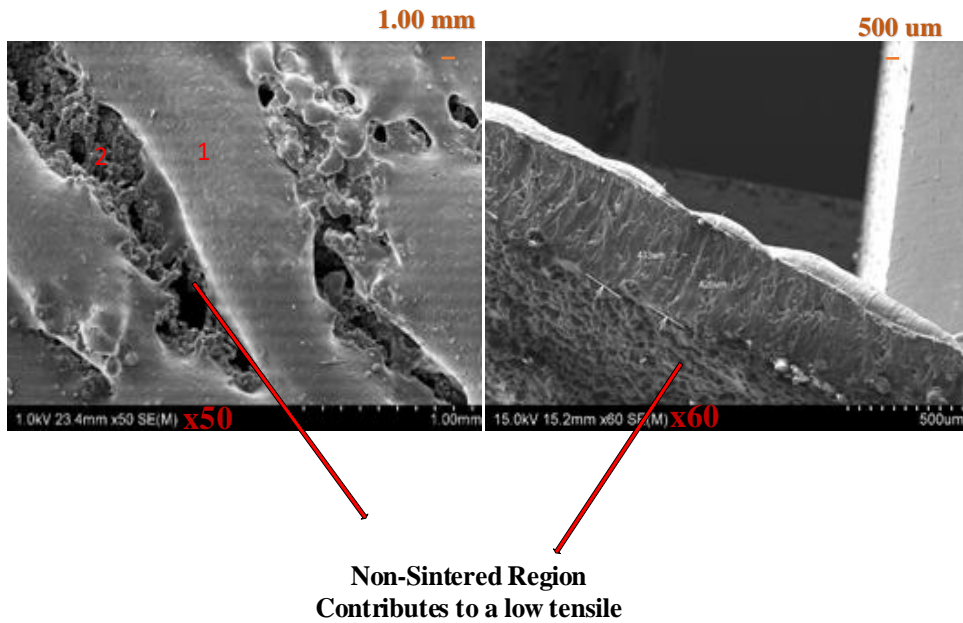


Figure 5.9 SEM of a GDL fabricated with 70% PA/30% Ti

5.7 Experimental Iteration-III

The change in the iteration III is the incorporation of titanium nanopowder as the conductive filler instead of titanium micron powder, which was used in the iteration I and II. The motivation to use titanium nano powder is that:

- i. Expected functional characteristics were not attained with the titanium micron powder.
- ii. Incidentally, titanium nano-particles have a wide range of electronic applications and metal-oxide nano-composites, microsensors [100]. In addition, they have high surface area, volume, and energy, which drives their utilization of them.

However, the percentage as low as 5% was used for the study because even with a quite higher percentage of 10% there was severe flammability and deformation due to the higher surface energy of the nano-powder, in augment to the laser energy.

Figure 5.10 exposes to the SEM image of the GDL specimen formed with 90% PA/10% Ti (Nano). There was a structural deformation of the specimen and crack formation, which was evidently revealed in the SEM image.

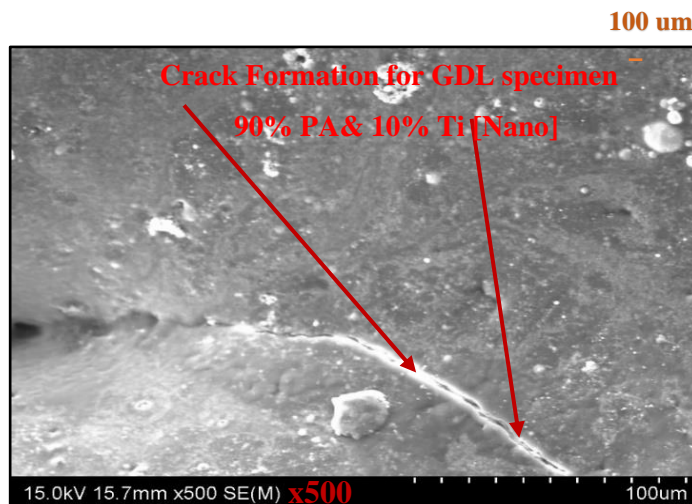


Figure 5.10 GDL specimen formed with 90% PA/10% Ti (Nano)

As a consequence, of this deformation and material's brittle nature, the investigations for composition with 90% PA/10% Ti have not been able to be performed, except the SEM.

5.8 Characterisation for Iteration-III

The characterisation studies were executed for the GDL composite formed with 5% titanium nano and 95% polyamide. However, for this iteration, the investigations were performed by varying the key operating parameter, namely laser power. The two different laser powers considered for the investigations were 9 W and 12 W respectively.

Though the percentage of titanium was relatively low, thought-provoking results were acquired which are discussed in the forthcoming sections.

5.8.1 Thickness and Surface Characterisation- Iteration-III

The minimal thickness of the GDL specimen is 417 μm for the 95% PA/5% titanium nano composition at 9 W laser power. However, the thickness of the GDL specimen is condensed to ca. 361 μm for the same composition at 12 W laser power. The thickness values were directly computed through the SEM instrument and are evident in Figure 5.15. The SEM image of the specimen at various magnifications is shown in the Figure 5.11 and Figure 5.12 respectively.

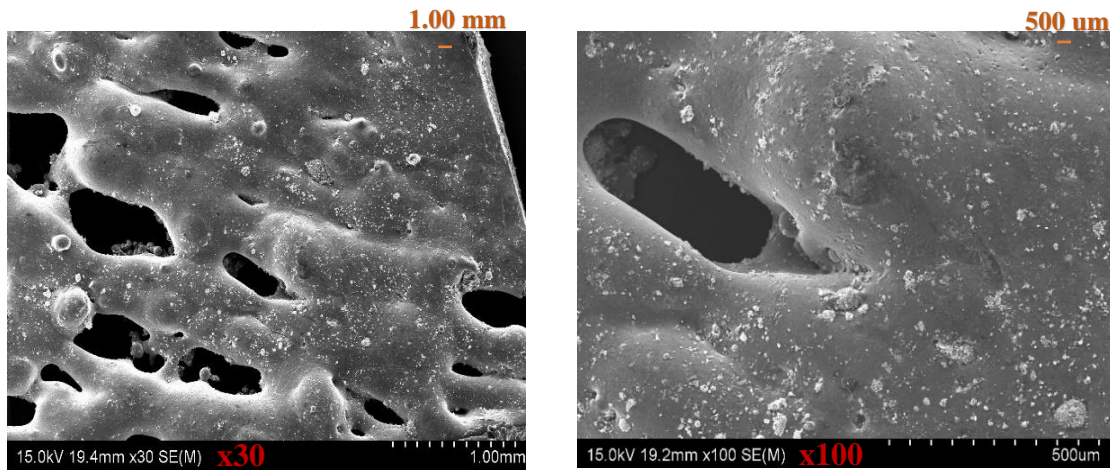


Figure 5.11 Low magnification SEM Images for 95% PA/5% Ti-Nano composites

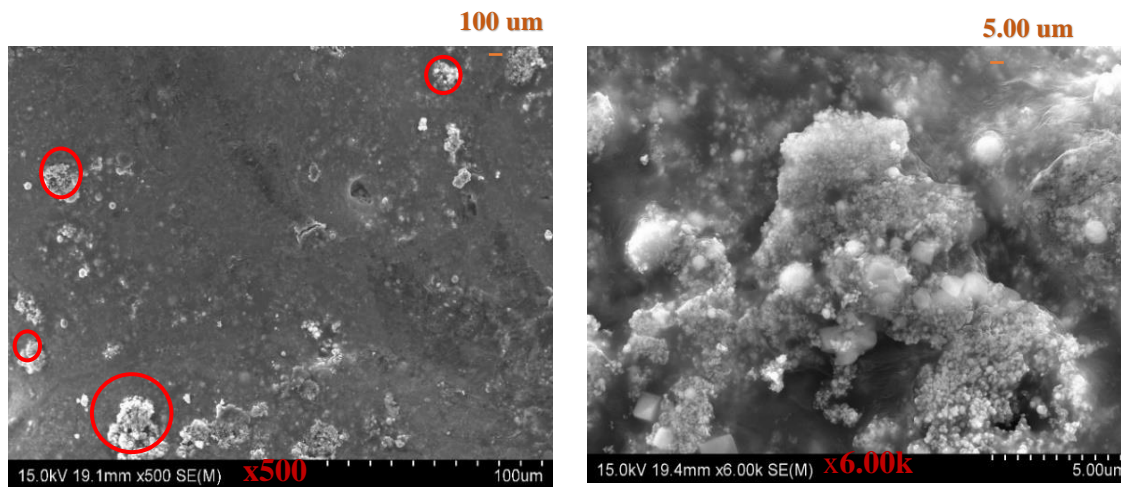


Figure 5.12 High magnification SEM of 95% PA/5% Ti-Nano composites

With the nano-sized powder, there was an agglomeration of the nano powder, unlike the micron particles, which are apparently visible with the high magnification SEM image in Figure 5.12. The heat energy absorbed by the nano-particles augmented with its high surface energy would have contributed to the phenomenon of agglomeration. Though 5% in weight is the actual composition, it is inferred from the SEM and the EDX point analysis that there are more Ti particles present, which is the unique feature of Nano particles attributed due to its intrinsically high surface-area.

5.8.2 Tensile Characterisation- Iteration-III

The tensile characterisations are observed to be high compared to iteration I and II. The values are measured to be around 20 N/cm for both the Laser power.

5.8.3 Porosity/Air permeability test- Iteration-III

The GDL material fabricated with Titanium nano powder possessed a high porosity and pore size distribution, which is evident from the SEM analysis through Image J.

5.8.4 Surface contact angle Iteration-III

The GDL specimen exhibited a reasonably a high surface contact angle of ca. $110^{\circ} \pm 16.5^{\circ}$ at the sintered surface. The value of hydrophobicity is the same for both the specimens fabricated at the laser speed of 9 W and 12 W. The surface contact angle authenticates that the material is predominantly hydrophobic. These values of hydrophobicity are higher than the iteration I and II and therefore Ti-nano particle would be the significant contributor.

5.8.5 Electrical Characterisation- Iteration-III

The electrical conductivity is observed to be as high as that of graphene coated alumide specimen; however, with a much lower thickness. The in-plane electrical resistance of the specimen fabricated with 95% PA/5% Ti-nano is ca. $35 \Omega\text{cm}^{-1}$ and ca. $21 \Omega\text{cm}^{-1}$ for the Laser power of 9 W and 12 W respectively.

5.8.6 Thermal Characterisation Iteration-III

The thermal conductivity is measured to be $0.43 \text{ Wm}^{-1}\text{K}^{-1}$ for the laser power of 9 W and $0.49 \text{ Wm}^{-1}\text{K}^{-1}$ for the laser power of 12 W. Though the values are quite a bit lower than the PA/ Ti (micron), combination, it is higher than the baseline material.

5.8.7 Summary- Iteration-III

The crucial inference in Iteration-III is that: though 5% is the gravimetric weight of titanium in the PA/titanium nanocomposite, it can be observed there are numerous active titanium particles spread throughout the specimen. In addition, there is also a Titanium

agglomeration that is revealed in Figure 5.13, which is more predominant than in the case of titanium micron powder that is used in the iteration I and II. Incorporation of nanoparticle would have been the substantial reason for the agglomeration effect. The GDL material also exhibited a substantial hydrophobicity compared to iteration I and II. The electrical conductivity is reasonably high for all the iterations, which is possibly due to the presence of nano titanium particles. The potential of nanoparticle surface energy augmented with the SLS energy (which had caused the base powder to melt and successively bond it along with the titanium nano particle) might be one of the possible reasons for the evenhanded characteristics of the mechanical, structural and electrical properties.

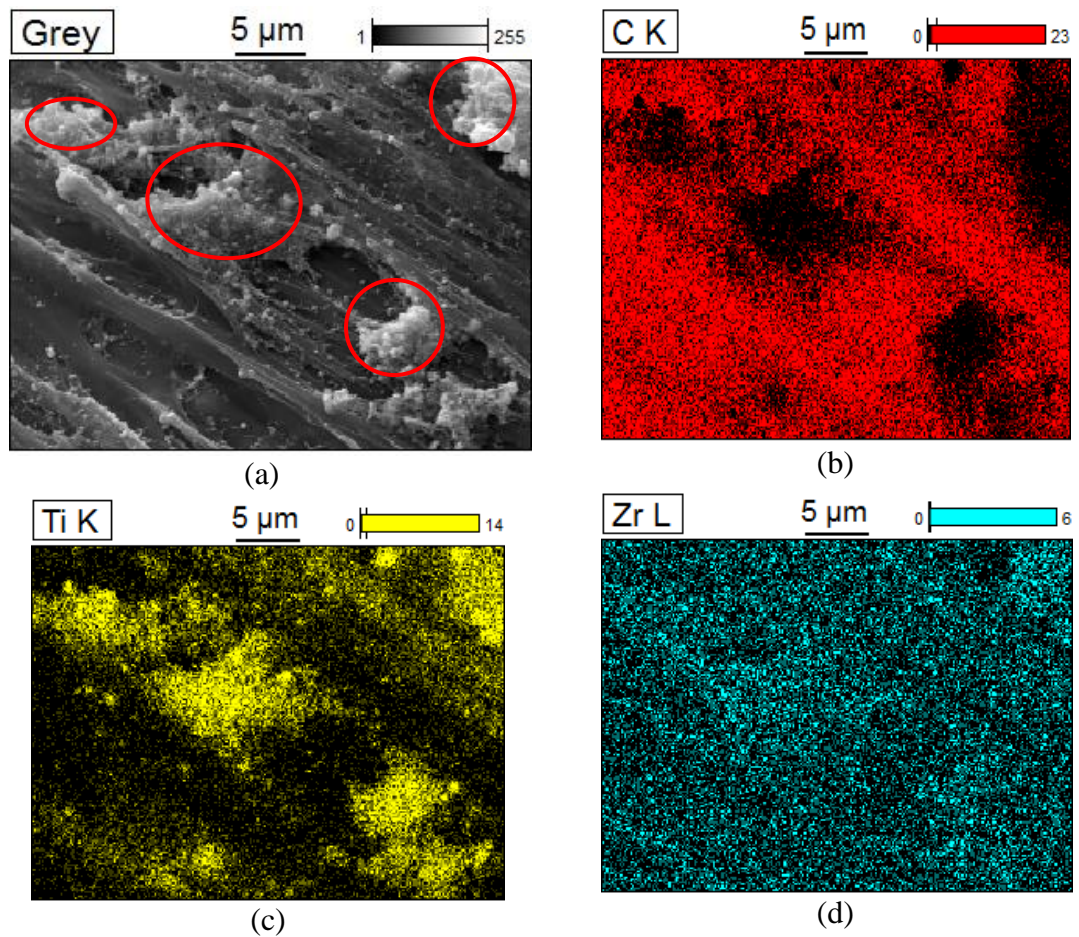


Figure 5.13 SEM point analysis/Mapping of Ti-Nano/PA composites

In line with the agreement in Figure 5.13, there is also an agglomeration of the nanoparticles, which are unique attributes of nanopowder [101]. The SEM mapping

comprehensively illuminates the titanium nano powder agglomeration effect as well the presence of titanium particle.

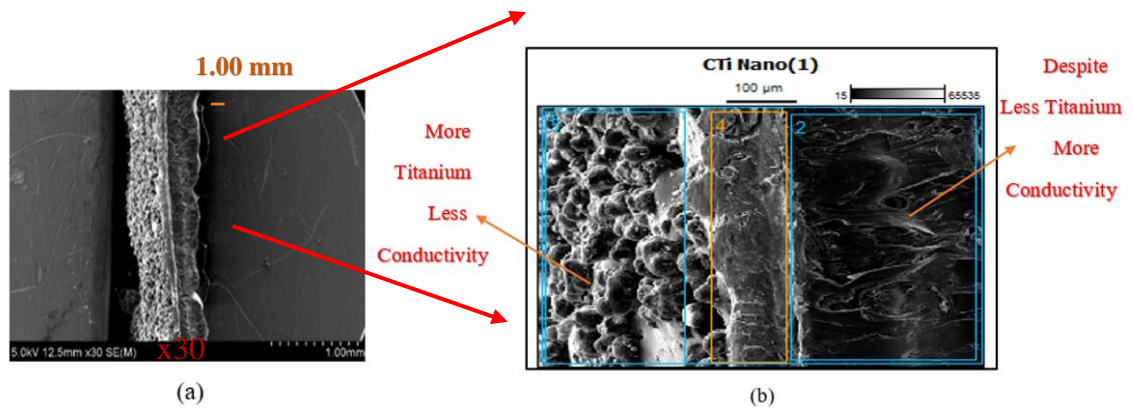


Figure 5.14 Cross-Sectional View of the GDL for 95% PA/5% Ti (Nano).

Figure 5.14 refers to the sintered specimen fabricated with 95% PA/5% Titanium Nano which provides the three regions of the specimen impacted by the laser power. The first region along the righthand side is the well-sintered region which is directly exposed to the SLS laser beam (direct contact), the lefthand side region is the one opposite to the SLS contact and consequently it is not sintered effectively; in between the two regions is an intermediate state which is moderately sintered. Table 5.8 correlates the data for the elemental composition for the points 1 (total area), 2 (right-hand side), 3 (left-hand side) and 4 (middle region). The well sintered region exhibited relatively high electrical conductivity and hydrophobicity compared to the other side.

Table 5.8 EDX analysis of various zones of the sintered GDL for the 95% PA/5% Ti (Nano) composition.

	<i>C</i>	<i>N</i>	<i>O</i>	<i>Ti</i>	<i>Zr</i>
<i>CTi Nano(1)_pt1</i>	53.00	2.26	5.26	23.25	13.35
<i>CTi Nano(1)_pt2</i>	75.04			11.03	13.94
<i>CTi Nano(1)_pt3</i>	29.63		4.19	39.10	14.44
<i>CTi Nano(1)_pt4</i>	39.98	1.43	4.83	37.11	15.23

The presence of titanium particles is relatively more along the moderately sintered and unsintered regions. Despite the high titanium concentration along point 3 (left-hand side), it is that region that exhibited poor electrical conductivity compared to point 2, which is

the well-sintered region. Thus, it is established, “The presence of titanium particle alone does not determine the electrical conductivity for the proposed GDL specimen,” which is a significant observation. It is also evident from the EDX Table 5.8 that provides the elemental composition. The oxide presence is low compared to the micron powder, and this might be a potential reason for the high electrical conductivity apart from the incorporation of nanopowder.

5.8.8 Significance of Laser Power

The final experimentation of the iteration III is performed with the laser power of 9 W and 12 W respectively to investigate the impact of the laser power on the structural and functional characteristics.

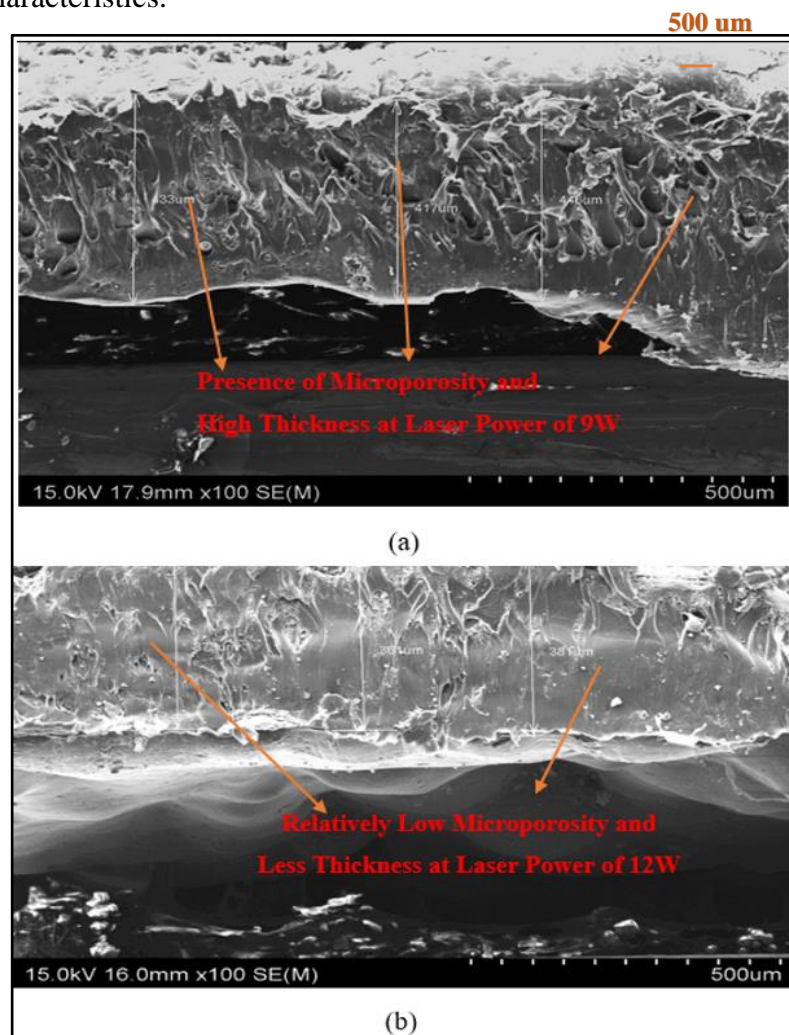


Figure 5.15 GDL Specimen of 95% PA/5% Ti-Nano a) Cross-sectional view at Laser Power of 9 W b) Cross-sectional view at Laser Power of 12 W

For both the cases, it was possible to fabricate a more homogeneous GDL material with a lower thickness, compared to the Iteration I and II, which is evident from the cross-sectional SEM. For an increased laser power (12 W), the thickness is still lower compared to the laser power of 9 W and this phenomenon is evident from Figure 5.15. Though the two GDL specimens (Figure 5.15 a & b) belong to the same material composition (95% PA/5% titanium), it is evident that the composite powder subjected to high laser power has relatively more strength. It was found that the sintered GDL thickness has a strong influence on microstructural effect. In addition, the level of micro porosity is reduced apparently with the thickness and also the surfaces become more hydrophobic when the laser speed is increased from 9 W to 12 W. These factors are also evident from the SEM analysis.

5.8.9 Balling Effect

The unique observation with regard to the incorporation of Titanium nano particles is the Balling effect, which is an unfavourable defect that occurred in the SLS-process and is shown in Figure 5.16. This phenomenon is due to localised irregularities resulting from cracks, heat affected zone, atmospheric conditions, and residual stress. Balling effect is fragmentation or droplets resulting from melt pool due to capillary instability [102, 103]. The predominant cause is that the stability of melt pool may be affected by increasing the scan speed as this can cause “balling effect” in the elongated liquid pool. Balling effect is an undesirable phenomenon related to laser-based processing and is a complex physical metallurgical process [104]. This phenomenon is significantly observed in the iteration where there is either high wt.% (Iteration I) of titanium or nano-titanium (Iteration III) and is evident from the high-resolution SEM image. It was initially considered that these balling effects are due to nano particle agglomeration but on meticulously evaluating the various literature [102, 103] of the laser processing technique, it is concluded that these effects are solely due to the laser sintering process which is absolutely a different phenomenon compared to agglomeration.

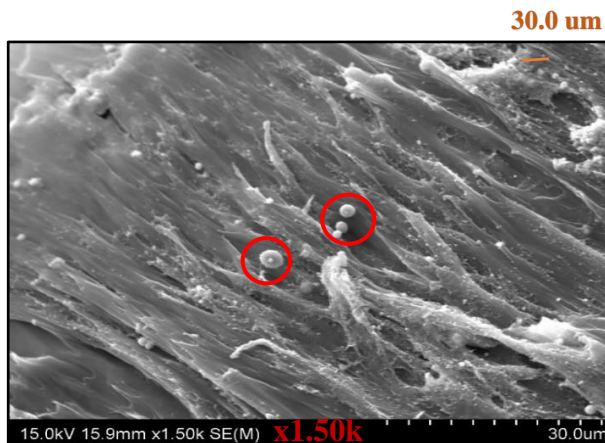


Figure 5.16 Balling effect in SEM image for 95% PA/5% Ti-Nano

The experiments of iteration III validate the following:

- a. Higher hydrophobicity is possible in the SLS processing, which can exhibit a high-water flow resistance for PEM fuel cell application.
- b. Oxide formation significantly reduced while using the Nano powder.
- c. The lower thickness and higher tensile strength can also be potentially possible by increasing the Laser power from 9 W to 12 W.
- d. The phenomenon of agglomeration (significance of Nano particles) and Balling Effects (significance of SLS process) are evident from the study.

5.9 PEM Fuel Cell Experimental Set-up

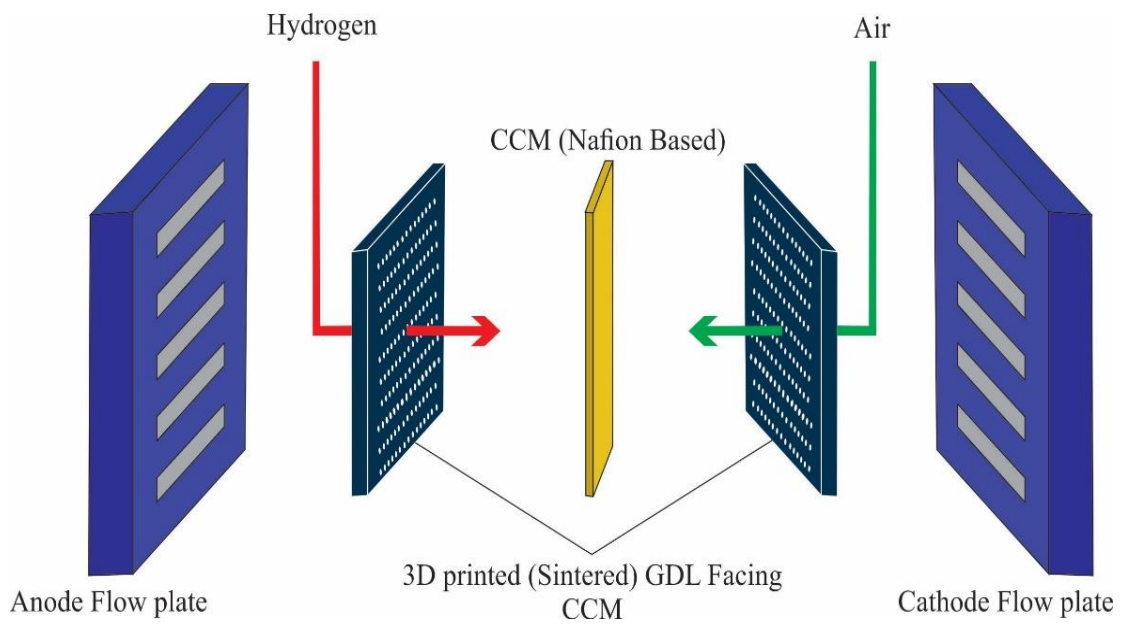
The MEA was prepared by coating Platinum (Pt) black catalyst on both sides of a Nafion membrane, by the screen printing method. Catalyst ink was first prepared by ultrasonically required quantity of Pt catalyst powder, Nafion 5 wt% solution in water (Dupont Inc, USA), propylene glycol, and isopropyl alcohol for 30 minutes. The catalyst ink was then coated on either side of Nafion membrane (DuPont, USA), by screen printing technique. The catalyst coated area (active area) was 5cm^2 , Pt loading in the catalyst layer was 0.25mgcm^{-2} on both sides, and the Nafion ionomer content was maintained at 40% in the catalyst layer for best performance [105]. The catalyst coated membrane was then dried at 50°C for 5 hours, washed, and humidified with demineralized water. The bonding of the catalyst layer to the membrane was good, no peeling of the catalyst layers was observed. Complete MEA was prepared by placing the GDL,

fabricated by SLS, on both sides of the catalyst coated membrane and was hot pressed at 130°C, for 1 minute at a low pressure of ca. 50 psi, so that the pressing does not adversely affect the GDL pore structure. The sintered region of the GDL faces the membrane coated with a thin layer of catalyst ink, before hot pressing, for better bonding and for reducing the contact resistance and to facilitate the electron transfer.

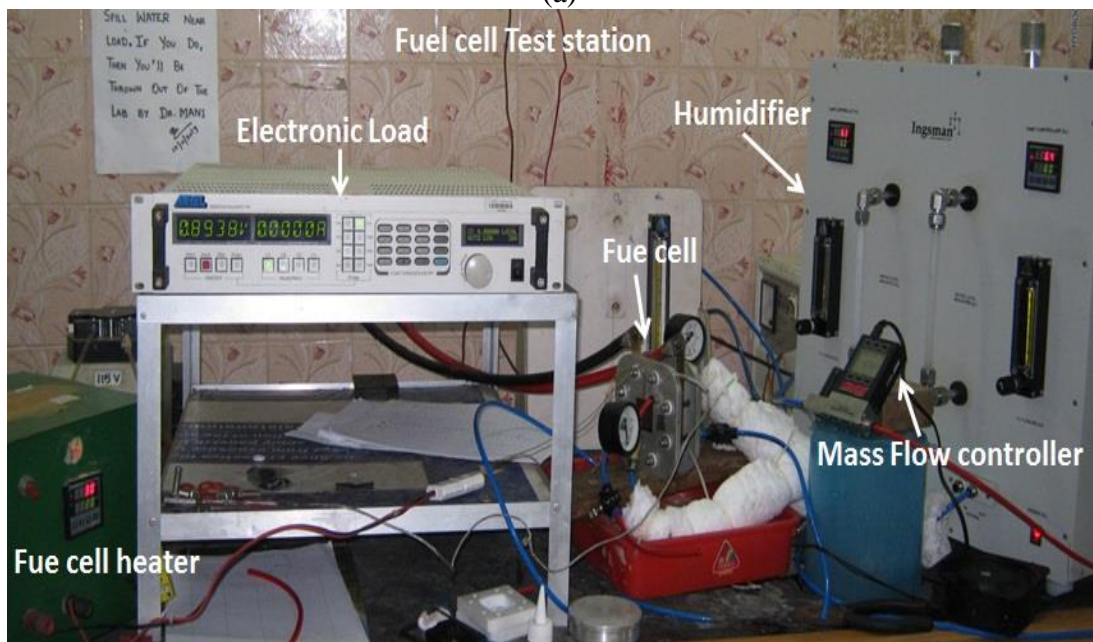
An MEA was also made for comparison purposes using a commercially available standard GDL, Sigracet-39BC, These MEAs were then used to assemble a Fuel cell and were characterised in a fuel cell test station.

The fuel cell was assembled by placing the MEA between two graphite plates, with parallel gas flow channels and silicone gaskets in a single cell test fixture. The graphite plates were provided with inlet and outlet ports for passing the reactants. Copper plates were placed on outer sides of both the graphite plates for current collection. The cell assembly was clamped between two end plates by applying a uniform torque of 75 kgf at the bolts.

The fuel cell was connected to the fuel cell test station, which was equipped with gas humidifier, gas flow meter, temperature indicator and controller, for testing the fuel cell at various environmental conditions. The fuel cell test station was also provided with an electronic load box (Amrel, USA) for operating the fuel cell under constant voltage or current conditions. The fuel cell terminals were connected to the two terminals of the electronic load box and are portrayed in the Figure 5.13 b. Hydrogen (99.99% purity) and oxidant canisters fitted with high pressure gas regulators were connected to the fuel cell test station and the gas outlet line from the fuel cell test station was connected to the inlet ports of fuel cell assembly. The gas pressure from the gas cylinder to the fuel cell test station was kept at 1 kg/cm². A line sketch set-up and the photograph of the experiment with fuel cell, fuel cell test station, and electronic load bank is shown in Figure 5.17 (a) and (b) for better understanding.



(a)



(b)

Figure 5.13 a) Line sketch of the Cell Assembly and b) Photograph of the Fuel cell experiment

5.10 Polarisation curve

In the previous ex-situ characterisation, the fabricated GDL specimen had been assessed based on its appropriateness of thickness, tensile strength, permeability (to percolate the gas and product water), electrical conductivity (to transport the electron), and thermal conductivity (to transport the heat). However, it provided a basic insight into the GDL specimens' fitness relative to the baseline material (Sigracet-SGL 39 BC), which is attached in the Appendix A.

Polarisation curve is the integral characterisation technique used to analyse the tangible PEM fuel cell performance of real-time operating environment. Polarisation characterisation provides a more comprehensive insight of the PEM fuel cell stack from the perspective. The load is applied to the cell using an electronic load bank and the voltage is measured. The graph is plotted with the current density along the x -axis and the cell voltage along the y -axis and is portrayed in Figure 5.18.

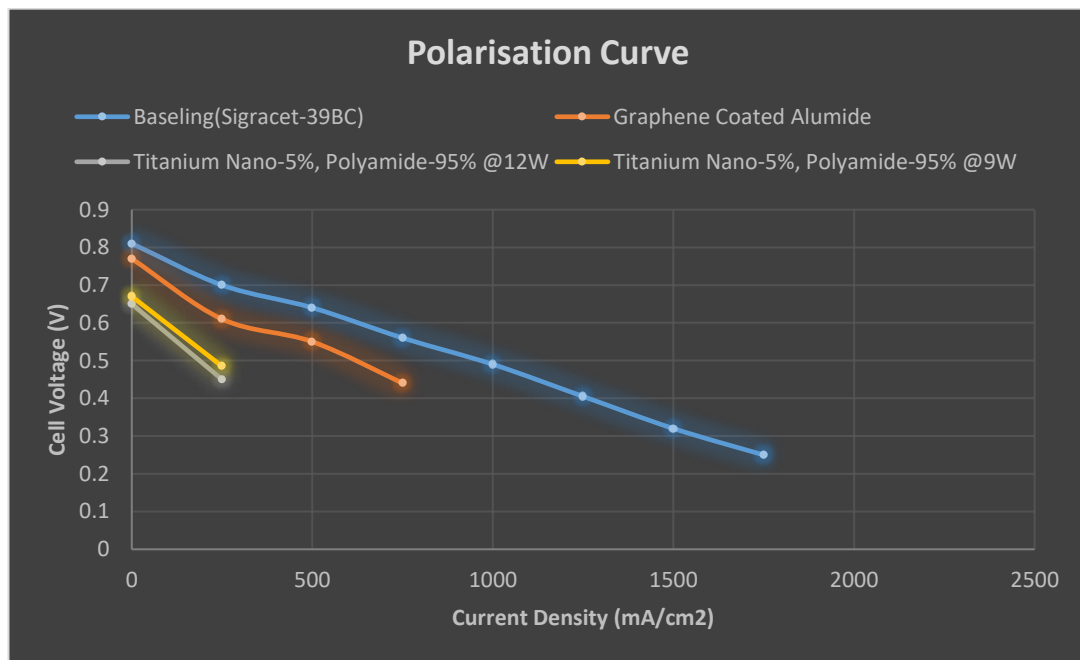


Figure 5.18 PEM Fuel cell Polarisation Curve

The factor to be considered while measuring the polarisation curves is that it should be determined only after the open-circuit electrode potential of the test material has attained a steady-state value. Though the general polarisation curve is performed for all the samples, the GDL films fabricated through iteration I and II are not competent enough to facilitate the electron transfer resulting in poor performance. However, the samples produced in the initial trial and those samples produced with the PA/titanium nano exhibited a better performance and are evident from the Figure 5.18.

5.11 Closure

In the present experiment, three iterations were performed to fabricate a GDL material and the appropriate characteristics were executed. Though these three iterations are too low to converge, it provided us with valuable information pertinent to the GDL fabrication by SLS route. At this stage, most of the characterisations that are required for the desired GDL fitness are verged with the buoyancy to attain the required feature. The experimental set-up of the fuel cell testing is also accomplished and the test values are evaluated based on the polarisation curve. From the polarisation curve, it is inferred that the GDL of the Iteration-III exhibit a reasonable performance among all the samples tested. Fine tuning SLS operational parameters and selection of appropriate materials are the key requirements to attain those attributes. This chapter comprehensively analyses the observations that are made in the characterisation study and validates that the proposed technique leads to an alternative and a simple manufacturing route for GDL fabrication. The forthcoming chapter deals with the in-depth interpretation of various limitations witnessed in the present investigation.

Chapter 6: Discussions and Recommendations

“The Aim of argument, or of Discussion, should not be Victory, but Progress”

Joseph Joubert

6.1 Introduction

The functional characteristics of the fabricated GDL specimen are assessed critically to derive valuable information. Although the functional characteristics, namely porosity/permeability, electrical conductivity and thermal conductivity belong to a different branch of engineering, it is inferred from the present investigation that there is a strong functional interrelationship amongst them. Insight into this correlation can also fine-tune the GDL characteristics. GDLs' functions to transport the reactant gases/product water, electrons and heat can be significantly impacted by this interrelationship and the present chapter comprehensively deals with it, grounded on the critical observation of the material fabricated. The unprecedented challenges encountered in the present study are the appropriate material selection, measurement system, and SLS process parameters, which have been discussed extensively.

6.2 Structural and Functional Relationship

The following observations have been made which are critically assessed:

6.2.1 Structural-Mechanical-Electrical Relation

- I. The gas diffusion material synthesised by SLS process has most of the desired properties but it lacked the appropriate electrical conductivity that is comparable to the reference material [82]. The addition of conductive filler materials to the base material that is intended to boost the electrical conductivity did not deliver a linear result. As per the literature, general characteristics of composite (polymer and metallic) materials must have their electrical properties close to the metals and the mechanical properties typical to that of plastics [106]. Ironically, as per

the present investigation, the GDL specimen fabricated with the proposed SLS process lacked an increase in the electrical conductivity despite an increase in titanium. However, a clear understanding of the various possible causes for such an eccentricity is systematically and comprehensively studied.

- II. From the SEM image of the GDL specimen with 90% Polyamide/10% Ti [micron], it is inferred that the ineffective sintering of base and conductive particles has resulted in the non-uniform thickness. This observation is detected for both the micron scale as well the nanoscale, which is evident from the SEM image of the GDL specimen Figure 6.1. However, the degree of variation is different for the micron and nano scales. The possible reason for this phenomenon might be due to the different degree of heat absorption due to the deviation in the geometry level, which caused a gradient in the surface energy absorption by the titanium nano particles.

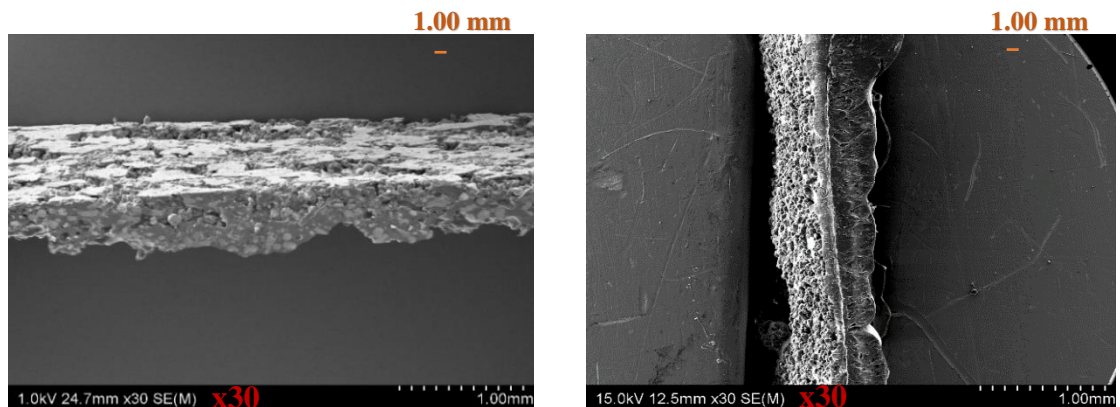


Figure 6.1 (a) SEM image of GDL with a) 90% Alumide/10% Ti [Micron] and
b) 95% PA/5% Ti [Nano]

Though the nature of non-uniform thickness and anisotropy is the resemblance in both cases, there is a dissimilarity with the level of tensile strength, electrical and thermal conductivity. The high tensile strength and conductivity of the GDL specimen fabricated with Ti Nano particles might be attributed to this reason. This raises a doubt regarding the functional interrelationship of tensile strength and electrical conductivity for this kind of thin film composites fabricated by the SLS process. From these experimental

observations, it is evident that a minimal level of tensile strength is a prerequisite for these thin film composite specimens (encompassed with metallic filler) fabricated by the SLS process so as to have an optimal electrical conductivity or vice versa. This tensile strength can also be proportional to the interconnected path that is highlighted in red is well observed for both the baseline material (a) as well as the graphene-coated alumide specimen (b) and are illuminated in Figure 6.2. The unique attributes of graphene are malleability, exceptional thermal and electrical conductivity and high strength to weight [94]. These characteristics of graphene have been well established by various authors and have been published in renowned literature [74, 94]. However, it must be noted that the interconnected path of the graphene-coated alumide specimen has thicker connectors and is malleable compared to the baseline material, which is thin and tubular.

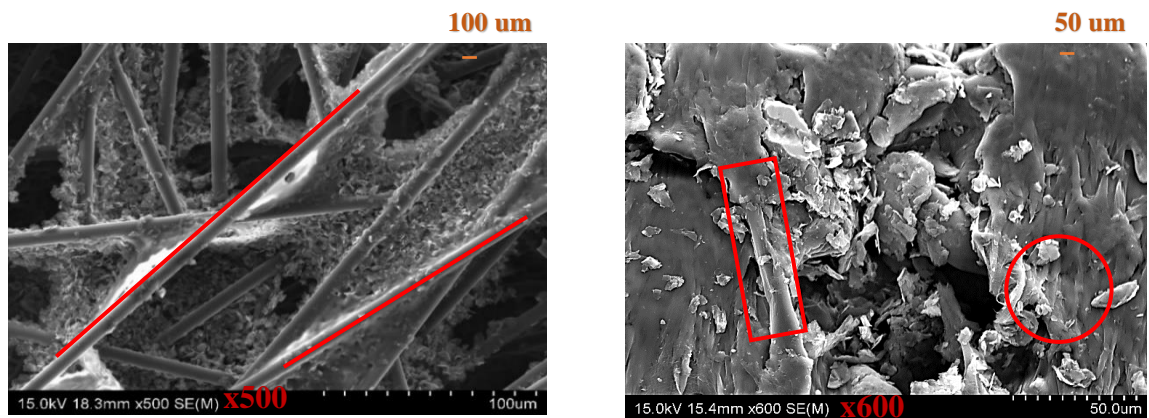


Figure 6.2 Role of Interconnector in Electrical Conductivity

The interconnected path for the Carbon paper (Baseline material) and the Graphene coated alumide are substantial contributors for the improved transport properties, which includes the electrical and thermal conductivity. Ironically, it must be noted that in the present investigation these interconnectors are visible only for the carbon-based specimen.

6.2.2 Hydrophobicity–Tensile Strength-Electrical Conductivity Relation

The unique observation with regard to the hydrophobicity for Iterations, II and III is that the polyamide composition with higher titanium (micron scale) content i.e. 70% PA/30% Ti (Micron) and the composition with 95% PA/5% Ti (Nano) exhibited similar surface morphology and hydrophobicity characteristics. The reason for the similarity is due to the fact that in the former case the titanium micron particles are in higher concentration, which has absorbed more laser heat and caused the melting of the base powder, thus instigating hydrophobicity. In the latter case, the higher hydrophobicity is attributed due to the higher surface energy/area of the titanium nano particles (though 5%) to liquefy the base polymer (polyamide) which flows throughout the specimen more effectively causing more hydrophobic nature to the specimen.

The positive aspect of these hydrophobic coatings is that there is no need for separate physical coating with a wet-proof agent like PTFE as in the case of the conventional techniques. Since the PTFE coating is attached to the specimen by means of weak Van der Waals forces, it could separate from the specimen surface due to physical changes like expansion and contraction, water penetration into the PTFE and carbon interface, and shear force by fluid flow during the operation of a fuel cell [107].

However, in the case of iteration III, the hydrophobicity is achieved through the laser heat that can provide more resistance to shear force (physical property) as well as resistance to voltage oxidation (chemical property) without the addition of any wet proof agent. It is also evident from the Figure 6.3 (SEM image) that the pore size was dwindled by this coating, which is hydrophobic and water-repellent.

The negative aspect of this hydrophobic covering is that it may possibly cover the metallic powder and be one of the potential reasons for the reduced electrical conductivity, which is overshadowing the active metallic (Ti) sites, and this phenomenon is well revealed in the Figure 6.3 (a) and (b) and is encircled; however, it must be noted that those regions of agglomeration (rectangle) have immunity to the hydrophobic coating.

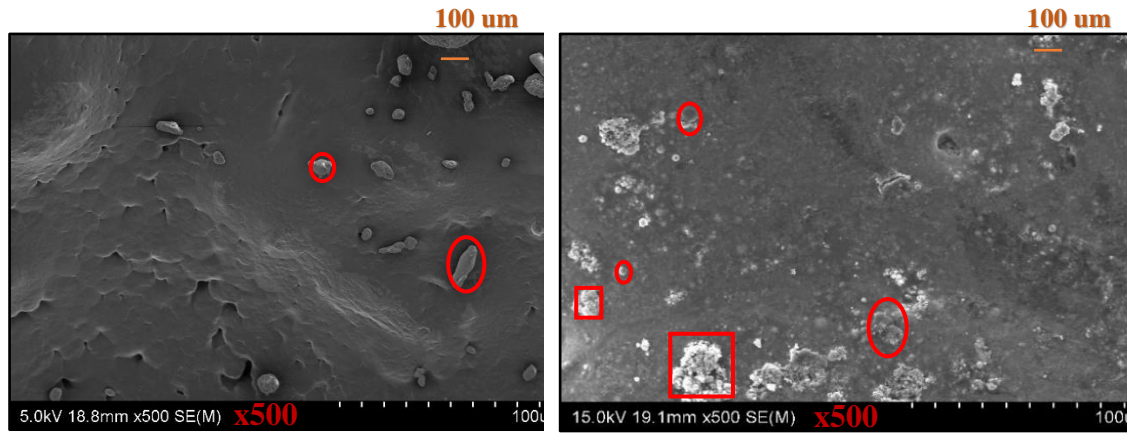


Figure 6.3 Hydrophobicity nature of GDL specimen fabricated with (a) 70% PA /30% Ti (Micron) and (b) 95% PA /5% Ti (Nano)

It has been well quantified in the literature of the SLS that the controlled porosity and mechanical property combinations are conceivable by optimizing the material composition and process parameters. However, in the present work, we would like to establish that in addition to the controlled porosity and mechanical property, the SLS technique has potential to achieve the electrical conductivity. Though the measured values of electrical conductivity are low, it provides a confidence that it can be boosted in future.

However, the constraint in the time frame is one of the severe limitation of the present study to selectively play with the material and the SLS operating parameters to improve the electrical conductivity.

6.2.3 Porosity-Electrical Conductivity-Thermal Conductivity Relation

The outcome of variation in GDL porosity is a non-uniform mass transportation and consequently, even a small change in the porosity may severely lower the overall cell current density. Thus, the porosity influences the electrical conductivity and the fuel cell performance [108]. It is also evident from the literature that [109] the thermal conductivity decreases steeply with increasing porosity for the nano materials.

6.3 Challenges in Measurement System

The proposed GDL specimen is a composite of base powder (alumide and polyamide) and conductive filler (Titanium micron and nanopowder). The combination of these two

materials possesses totally different characteristics that augmented with the non-optimised SLS process parameter condition results in a more heterogeneous, more non-linear and more anisotropic material. Therefore, the measurement approaches used for evaluating the characteristics are not appropriate due to this nature. In addition, there are no regulated measurement standards to compute the characteristics of this kind of hybrid materials. Nevertheless, the conventional measurement technique can provide an approximate and relative value that is followed in the present thesis. The unprecedented challenges involved in the measurement of these GDL specimens have been observed almost throughout the study specifically for the electrical and thermal conductivity, tensile characterisation, and porosity. Among these properties, the electrical and thermal measurement techniques were the most challenging ones.

6.3.1 Electrical and Thermal Measurements [Electrical Conductivity vs. Thermal Conductivity]

- I. One of the significant challenges pertaining to the electrical characterisation is the low resistance measurements using the conventional instruments, which are typically between tens to hundreds of Ω . At this level, it is important to use test equipment that minimises errors introduced by the test-lead resistance and/or contact resistance between the probe and the material being tested. In addition, the impact of contact resistance, which is the resistance to current flow through a closed pair of contacts, is also not considered. These limitations, due to contact resistance, is not only encountered in the electrical resistance but also for the thermal resistance measurement. The general characteristics of thin films are highly anisotropic with very different properties along the cross-plane and in-plane directions [110]. The proposed material is a more complex thin film due to its non-homogeneous and non-uniform thickness apart from the anisotropic nature.
- II. In addition, the through-plane electrical resistance measurement, which provides the information of current flow in direction perpendicular through the GDL, is not feasible due to these characteristics of heterogeneous and anisotropic nature. The

primary reason is due to the fact that electron flow across the GDL is severely limited where the composite powders are not well sintered.

III. The four-wire Kelvin method used to compute the in-plane electrical resistance (illustrated in Figure 6.4) to perform the test as stated by Williams et al. [32] is not a standardised method and highly depends on the materials intrinsic nature and linear operating range. As a consequence, applying Ohm's Law to this non-linear material is not the absolute measurement technique and can be erroneous in most of the conditions. The GDL samples in-plane electrical resistance per unit of distance (R') values are usually calculated using Ohm's Law as shown in Equations

$$R = \rho x l / A$$

$$\rho = [R/l] \times A$$

$$\rho = (R') \times A$$

R = in-plane electrical resistance of the GDL sample (Ω)

R' = in-plane electrical resistance per unit of distance of the GDL sample ($(\Omega)/\text{cm}$)

ρ = in-plane electrical resistivity of the GDL sample (Ωcm)

A = Area of cross-section of the GDL sample (cm^2)

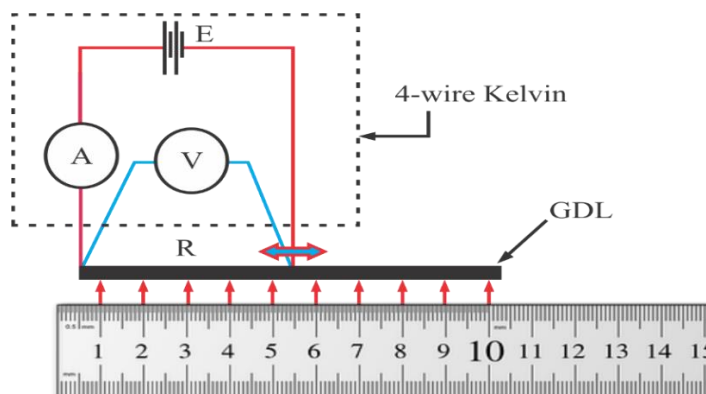


Figure 6.4 In-plane Electrical Resistance Measurement technique

IV It is observed that resistance of the baseline (carbon-based) and graphene coated alumide GDL had a linear relationship with respect to the distance. This phenomenon is evident from the graph illustrated in Figure 4.8. Conversely, such a linearity in sheet resistance (resistance per unit length) is not observed for the 3D printed GDLs which raises concerns about the applicability of Ohm's law to

these anisotropic polymeric materials (3D printed GDLs). In addition, while evaluating the thermal conductivity measurement using Fourier's law for these GDL materials it exhibited similar measurement challenges. Nevertheless, this critical observation in the present study causes the uncertainty about the applicability of Ohm's law measurement to the GDL specimen fabricated by SLS because of the following reasons pertaining to the electrical-thermal analogues: "Thermal conductivity measurement incorporating Fourier's law was also not able to be applied to compute the thermal conductivity of the proposed GDL specimen". This is observed due to the technical issues to measure the thermal conductivity of these thin films GDL samples with the linear heat conduction instrument namely Armfield HT11 that has been designed to demonstrate the application of the Fourier Rate equation to simple steady-state conduction. Figure 6.5 refers to the linear heat conduction instrument, which was attempted to analyse the thermal conductivity.



Figure 6.5 Armfield HT11 for Linear Heat Conductivity Measurement

This technique allows the measurement of the heat flow and temperature gradient allowing the thermal conductivity of the material to be calculated. However, the test was unable to be performed due to the inapplicability of Fourier's laws to compute the thermal conductivity, which raised severe concerns about the applicability of Ohm's law as well as to these materials. Thus, the Ohm's Law-Fourier's law comparison of the composite gas diffusion specimen is because, "In steady state conduction, all the laws of direct current electrical conduction can be applied to heat currents. In such cases, it is possible to take thermal resistances as the analogue to electrical resistances and temperature

functions the role of voltage, and heat transfer rate (heat power) is the analogue of electric current". To further reinforce our claim it is also stated in the literature that the heat transfer by Fourier heat conduction theory is generally thought [111] not necessarily to be applicable for thin films which further strengthens our hypothesis. The proposed GDL material, which is also a thin film, with more non-linear and anisotropic characteristics might follow a similar trend for the electrical behaviour as well. However, the specimen which is fabricated in the initial trial and the baseline material exhibited a linear characteristic.

6.3.2 Air porosity/permeability measurement

The porosity is the default characteristic of any material fabricated through the SLS. From the perspective of air porosity/permeability measurement, the Gurley permometer technique, which is used to measure the air porosity and permeability, is inappropriate for rough-surfaces (similar to the proposed material) due to the limitation in securely clamping to avoid significant edge leakage. The proposed composite GDL surface is rough which had limited its utilization for all the iterations except the initial trial. As a consequence, non-invasive computational measurement techniques namely Image J is used to have an insight on porosity through the SEM image. The limitation of this technique is that it is a non-ASTM standard and the porosity measurement is limited to those areas which are under the SEM.

6.3.3 Surface contact angle/Hydrophobicity measurement

The hydrophobic effect is an important phenomenon in PEM fuel cells, which represents the tendency to repel water, and can substantially improve the PEM fuel cell performance. Thus, the investigation of surface contact angle measurement becomes an integral concept in the present study. The degree of hydrophobicity is determined by the simple technique that is proposed by Zamora et al [83], in which a 20- μ L drop from the syringe was deposited in a sample and after stand-up for 1 hour, zoom shooting was conducted for the sample and then the contact angle was measured between the droplet and the surface. Although this technique is a non-ASTM standard, it provides a reasonable relative value while performing the calibration against the baseline material (Sigracet-39 BC) with a discrepancy of $\pm 15^\circ$.

6.3.4 Necessity for Real-Time Dynamic Measurement Technique

The circumstantial challenge with GDL layer measurement is the fact that it is subjected to multiple physical impacts due to the diverse operating environment, such as high clamping forces, substantial current transients, temperature gradients, high voltage and low pH conditions. The impact becomes more predominant when these conditions occur simultaneously. Therefore, a more advanced and explicit measurement technique considering all these dynamic operating constraints is a prerequisite to have a comprehensive understanding. Design of such a measurement system can provide more insight into the actual operating performance

6.3.5 Uncertainty Analysis

Experimental uncertainty estimates are needed to evaluate the confidence in the results and assessing them in a physical measurement unavoidably involves an element of subjective judgment [112]. However, in the proposed experiments uncertainty analysis had not been performed due to the materials non-homogeneous nature that provides us with a relative value rather than an absolute one. In addition, elemental analysis (EDX) is normally a semi-quantitative and consequently the results have significant uncertainty. Measuring the values against the baseline materials is rationale in the present investigation to assess the relative performance and this approach has been followed.

6.4 Materials Limitation and Operational Environment

Finding out appropriate conductive and base materials will contribute significantly to the present work on the development of this novel composite gas diffusion material.

It has been well established in the literature that the Sintering behaviour of titanium powder has not been well understood due to its high reactivity and complex diffusion behaviour and this phenomenon is in line with the present observation [113]. One of the potential limitations with the conductive filler is that the titanium used in the study is converted to titanium oxide. If we can use conducting titanium oxides (Magnéli phase) which is already in the oxide state the challenge pertaining to the oxide formation can be averted because these conducting metal oxides cannot be further oxidised during the SLS process. These substoichiometric titanium oxides, $[\text{Ti}_n \text{O}_{2n-1} (n = 4-9)]$, are often

referred to as Magnéli phase TiO_x and have attracted much attention recently because of the growing demand for conductive materials [114].

The complexity encountered in the synthesis as well as procurement of those conducting titanium oxides limited us to incorporate it in the present study; however, future experiments will be performed using these advanced solid-state materials.

In addition to the appropriate conductive filler selection, the appropriate base polymer material is also a mandatory factor. The commonly applied SLS base polymers powder to date are those of the polyamide family, which have poor conductivity [115] limiting us to play with the wide range of materials combination for the SLS manufacturing route. Performing the investigation in a non-argon environment is one of the limitations pertaining to the current SLS experimental set-up.

6.5 SLS Process Parameter Limitation

In addition, SLS process parameters play a key role in influencing the quality of the product. The key process parameters involved in the present SLS process are the energy density of the SLS instrument that is governed by the laser power, beam diameter and the laser scan velocity. In the present experiment, the laser power and the laser speed are kept constant (except for the iteration III where the Laser Power is marginally varied) throughout the course of the experiment, which can be one of the severe limitations to attain the desired functional characteristics.

In addition to the operating parameters, namely laser power and speed, there are also other independent operating parameters that govern the GDL specimen's geometry and functional characteristics. For instance, the energy input to the surface is a function of the pulsed flux, the duration of the pulse, and the delay between successive pulses. These three parameters are computed as a function of the independent operating parameters.

The flow diagram in Figure 6.6 shows how the energy to the surface of the composite powder is a function of the independent operating parameters. The calculation of the energy input is based on the assumption that the laser output has a Gaussian intensity distribution. However, this assumption is valid for the CO_2 laser that is most commonly used in the SLS process [116].

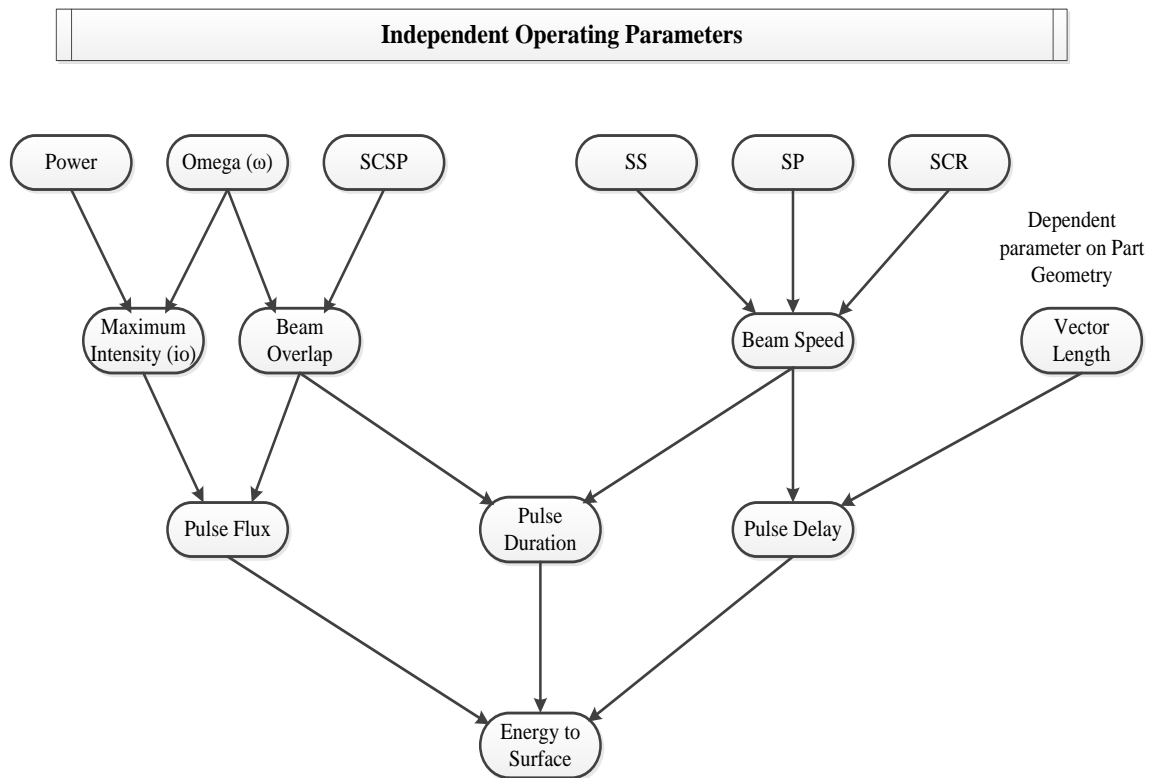


Figure 6.6 Effect of various operating parameters on the energy input to surface

The laser spot size can be represented by a characteristic radius, ω that can be measured using a beam profilometer. The beam profilometer measures the intensity profile across the laser spot at the surface of the powder bed using a knife edge method [117]. The maximum intensity is in the beam centre and decreases radially as governed by the equation:

$$I = I_0 \exp(-2r^2/\omega^2)$$

Where;

I is intensity of field

r is Radial coordinate

ω is Beam radius

This Gaussian equation is equivalent to the distribution of electro-magnetic field in the cavity that is reproduced itself during frequent propagation of light wave between resonator mirrors. However, the real divergence of laser radiation differs from that of ideal Gaussian beam [118].

The scan radius, SCR, is the distance from the fast axis-scanning mirror to the sintering plane. The scan radius determines the maximum scan width because the galvo mirrors only have a range of 40° over the surface of the powder bed [116]. The scanning speed is a function of the scan radius and the laser operating parameters as exposed in equation:

$$\text{Beam Speed} = 1.04378 \frac{SS \times SCR}{SP}$$

The laser power is often the preferred operating parameter to control due to the simplicity to regulate it. When the power is increased, the sintering energy at the surface also proportionally increases. The laser scanner parameters, SS (step size) and SP (step period), specify the speed at which the galvo mirrors turn and in conjunction with the scan radius define the beam speed. The scan spacing, SCSP, is the distance between adjacent scan vectors. The scan spacing can be adjusted to change the amount of beam overlap during a scan prior to sintering when the layer is divided into a series of parallel scan vectors [116]. All these independent parameters can significantly influence the process performance that in turn can influence the functionality and aspect ratio of the GDL specimen. In the future experiments, fine-tuning of these parameters will be implemented to fabricate the appropriate GDL specimen.

6.5.1 Causes of Improper Sintering

One unique observation that is witnessed throughout the course of all the iterations is an inappropriate sintering process especially on the backside of the specimen where the laser beam is not well exposed.

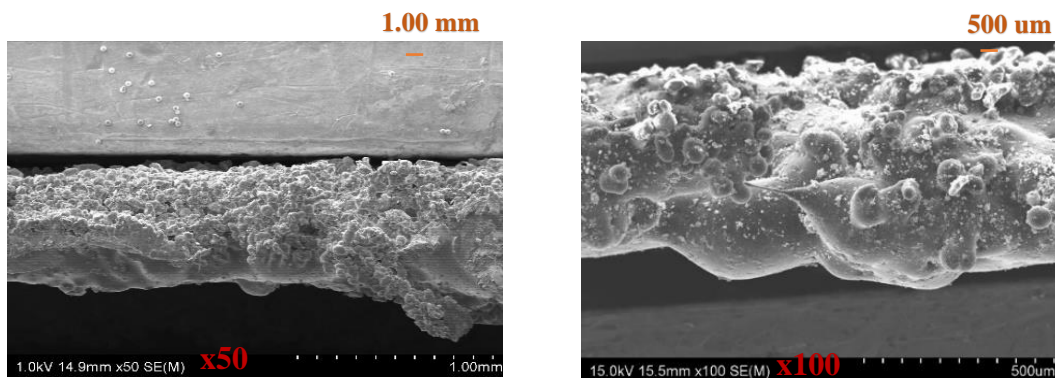


Figure 6.7 Improper SLS along the Bottom of the GDL specimen

Figure 6.7 reveals that the base powder is not sintered along the bottom region for the sample with 70% polyamide/30% Ti that ironically had a high level of sintering in the laser-exposed region. This phenomenon might be one of the potential limitation to attain the desired conductivity and tensile strength. In addition, weighing the impact of SLS operating parameters is not incorporated in the present investigation due to the limitation in the time frame and the lack of sufficient literature.

In the present experiment, the operating parameters considered are the Laser power and Laser speed and even that has been almost constant throughout, the course of the experiment for the fixed GDL composition (except the iteration III).

6.5.2 Balling effect Vs. Agglomeration

The unique observation with regard to the incorporation of Titanium nano particle as well the high % wt. of Titanium (micron) is the Balling effect, which is an unfavourable defect occurring due to irregularities from cracks, heat affected zone, atmospheric conditions, and residual stress. Balling effect is fragmentation resulting from melt pool due to capillary instability [102, 103] and is an undesirable phenomenon related to laser-based processing and is a complex physical metallurgical process [104]. This phenomenon is significant in the iteration where there is either high wt.% (Iteration II) of titanium and also for the nano-titanium (Iteration III) which is sintered at high laser power of 12 W. It was initially considered that these balling effects are due to agglomeration but on meticulously evaluating various literature [102, 103] of the laser processing technique, it is concluded that these effects are solely due to the laser sintering process which is absolutely a different phenomenon compared to agglomeration. Figure 6.8 refers to the balling and agglomeration effect in the present investigation. Nano crystalline powders have a large specific surface area and a high defect density which might have contributed to the agglomeration effect.

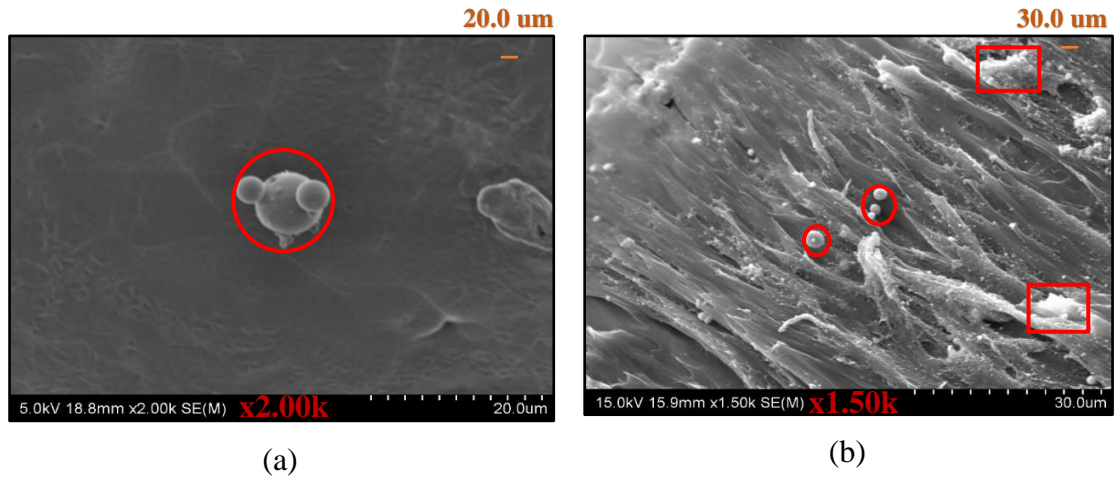


Figure 6.8 Balling and Agglomeration Phenomenon GDL composition

Last but not least, in the present investigation, a basic mortar and pestle arrangement is attempted for mixing the base and conductive powder to prepare the composite powder. However, this arrangement might be insufficient to achieve a homogeneous GDL specimen. Alternative tools such as the advanced ball can be more efficient to fabricate a homogeneous, conductive and more isotropic gas diffusion material.

6.6 Repercussion of Wiedemann–Franz law

It is very evident from the measurements that the presence of titanium metallic powder has actually contributed to an increase in the thermal conductivity. In fact, an increase in titanium powder (% wt.) is proportional to the increase in the thermal conductivity and is evident from iteration II. The composite powder having proportionate metallic titanium powder is correspondingly supposed to obey Wiedemann–Franz law, which states the thermal conductivity is proportional to the electrical conductivity at constant temperature and is given by [119].

$$\frac{K}{\sigma} = \frac{\pi^2}{3} \left[\frac{k_b}{e} \right]^2 T \quad (6.6)$$

K = Thermal Conductivity

σ = Electrical Conductivity

$(k_b/e)^2$ = Lorenz Number (constant)

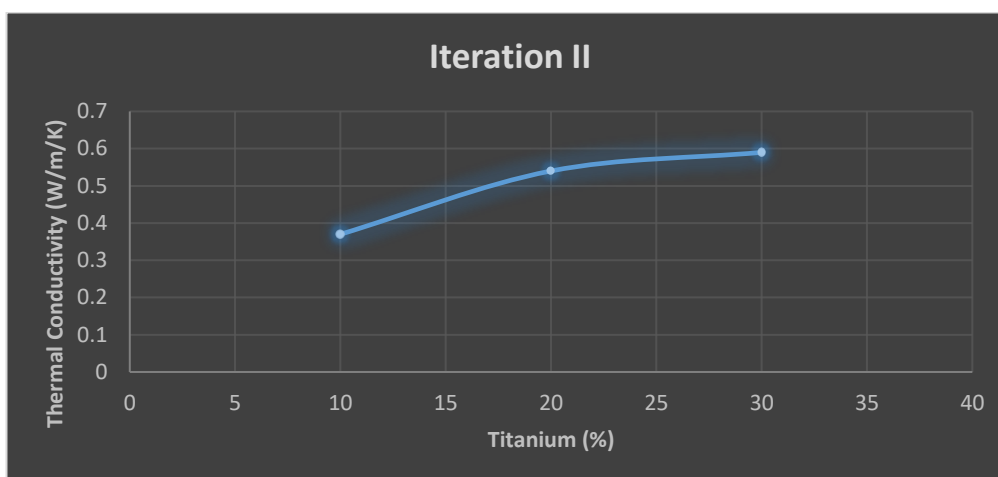


Figure 6.9 Linear increase in the Thermal conductivity with Ti [Iteration II]

Figure 6.9 validates an increase in thermal conductivity with an increase in the titanium wt% for the iteration II. The potential role for the electrical conductivity improvement is undoubtedly possible by the addition of titanium metallic powder analogous to the thermal conductivity [as the composite powder has a finite amount of metallic titanium powder] as well. Correlating the present finding to follow the Wiedemann–Franz law gives more confidence and it further rationalises our hypothesis through the findings from the fundamental Physics perspective.

The limitation for an increase in electrical conductivity such as conversion of titanium-to-titanium oxide and the lack of infrastructure to perform the experiment in argon conditions is already illustrated in the previous chapters and can be mitigated in future studies. Under that circumstance, an increase in electrical conductivity is finitely possible. Selecting appropriate base material and the conductive filler that is mutually compatible with the SLS manufacturing technique can accelerate the foundation of a state of the art GDL.

6.7 Critical Assessment

GDLs influence the performance of the PEM fuel cell stack not only on the ohmic region but also on the mass transport region. As illustrated in Figure 6.10 an ideal GDL can minimise the Ohmic and mass transport loss thereby significantly influencing the PEM fuel cell performance and enhancing the power density.

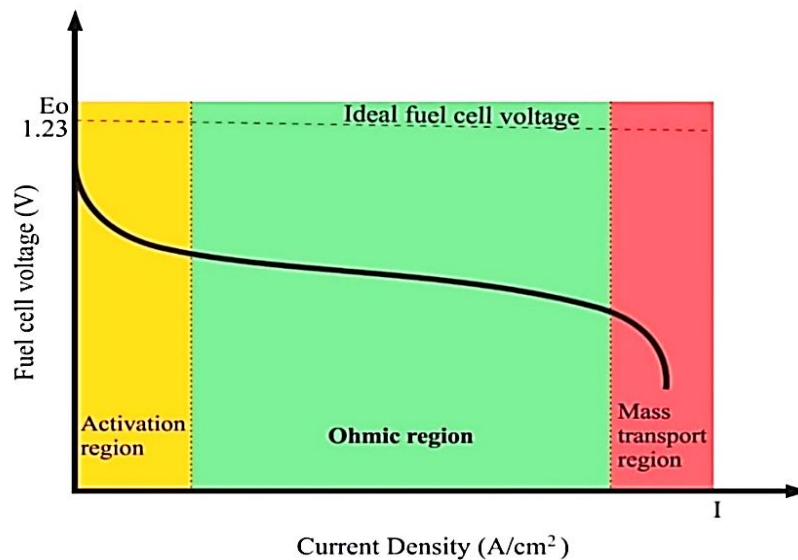


Figure 6.10 V-I Characteristics of Fuel Cells

However, this process is not exactly linear as the exothermic reaction augments to the heat in addition to the Ohmic heat. In addition to this non-linearity, the PEM fuel cell operational environment is also subjected to diverse operational conditions such as high voltage, high current, high temperature, high/low humidification and low pH, which increases the level of complexity. Similarly, the SLS process is also a complex process. Integrating the two complex processes (PEM fuel cell and SLS operation) involves a holistic understanding on both the subjects comprehensively to attain the desired attributes. A general thought on the SLS operational process and material selection is a pre-requisite to attaining the anticipated gas diffusion material characteristics.

The role of percolation model, which is an already matured concept, can be used to construct a GDL as well as optimize the volume/weight of GDL materials. The thickness of the GDL is about 90-200 μm for each electrode and it can increase along the stacking direction [120]; a similar level of thickness is also witnessed with the current 3D printed GDL. In addition, it must be noted that the percolation threshold is the critical loading of the filler leading to the conductive network formed in the matrix. The percolation threshold also depends on the particle size of the conductive filler, this observation is in agreement with the study by Jie Jin et al. [121] which can actually complement SLS. In future, this percolation threshold value can be fed to the SLS printer to get only the desired material with appropriate functional characteristics (thermal, electrical and hydraulic

conductivity) as a rule of thumb. This percolation threshold can possibly be added to the material datasheet, like the conductivity, porosity, hydrophobicity, etc., which might provide the users/researchers with an insight into the nature of the material. Such a progress is not only limited to GDL of PEM fuel cell application but also to the GDL used in the PEM electrolyzers and batteries.

6.8 Presence of Zirconium in the proposed GDL specimen

One of the unique observations in all the specimens of the GDL fabricated through the SLS process is that small traces of Zirconium are present throughout the study.

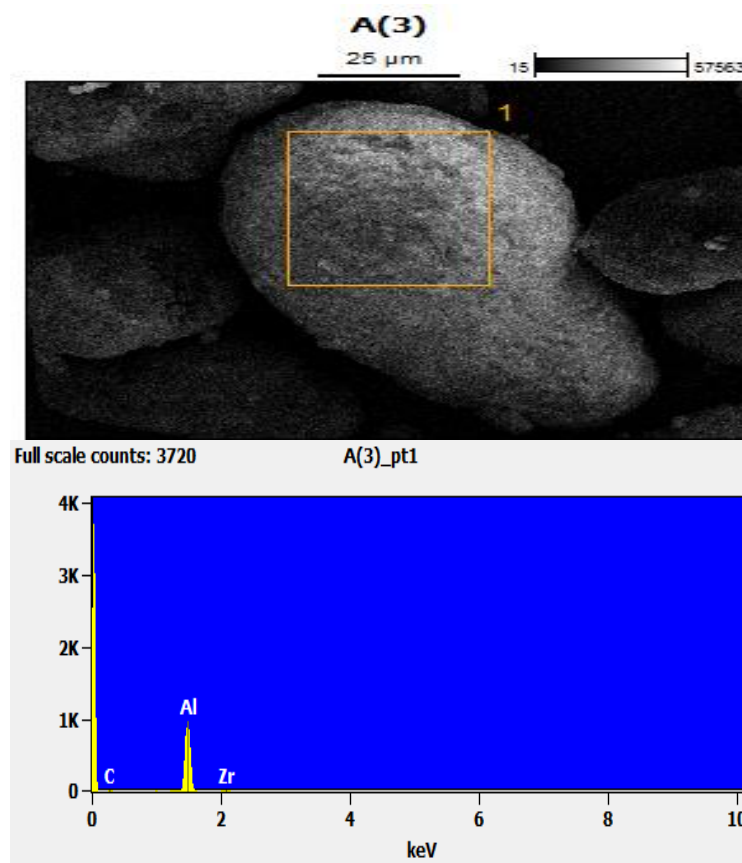


Figure 6.11 Zirconium presence in Alumide powder

The presence of Zirconium in the alumide and polyamide powder is evident from SEM and is revealed in Figure 6.11 and Figure 6.12 respectively.

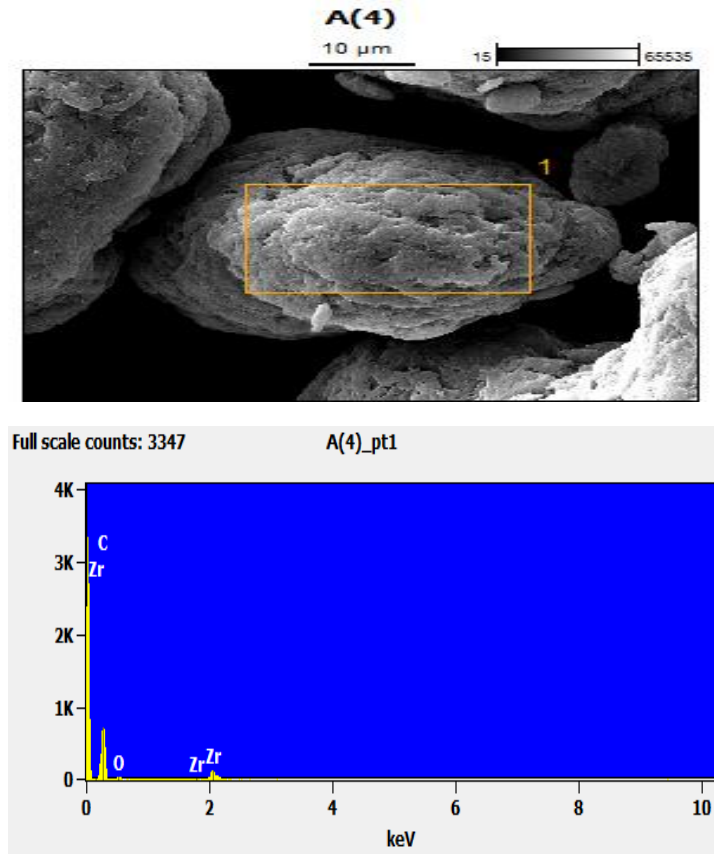


Figure 6.12 Zirconium presence in Polyamide powder.

However, Zirconium would have also been present in the Titanium micron and nano particles because Zirconium and Titanium have a similar crystal structure and atomic size [122] and have similar properties and are in the same group in the periodic table. As a consequence, Zirconium indication might also have been due to an X-ray interference effect and is observed to be scattered uniformly which is illuminated in the SEM Figure 5.13 (d).

Conversely, Zirconium is a conductive metal and has a strong resistance to corrosion. Also, it slightly adds a yield strength to titanium [122] which is actually an advantage for our requirement. Beyond all, Zirconium has not been observed to interfere with the PEM fuel cell operating environment in any of the previous literature.

6.9 Closure

The structural morphology of the GDL specimen is correlated to the material characteristics such as electrical conductivity, thermal conductivity, porosity and tensile strength. Though the aforementioned correlation requires further investigation in order to draw more quantitative results, it provided us with a basic understanding. A more comprehensive understanding of the SLS operational process and material selection that has a good compatibility and is a prerequisite to attain the anticipated gas diffusion material characteristic.

Chapter 7: Conclusion and Future Work

“The Conclusion of Good Research Leads to the Introduction of New Products”

Arunkumar Jayakumar

The gas diffusion layer is one of the integral components of a PEM fuel cell stack and in the present investigation, it has been attempted to fabricate a GDL that addresses the specific research questions that are formulated in Chapter 2. Table 7.1 addresses the research gaps that were identified in the course of this project, and the outcomes achieved, together with potential future developments.

Table 7.1 Research Questions, Outcomes and its Implications

Research Question	What/How was Done	Implications
Can we develop a carbon-free gas diffusion layer (GDL) for PEM fuel cell application?	Yes, an attempt to develop carbon free GDL incorporating SLS has been identified. An iterative approach is followed.	The characteristics of the specimen validate that the SLS technology can be a promising methodology for GDL fabrication. Selection of appropriate materials and fine-tuning of SLS operational parameters play a significant role to optimize the final GDL.
Can we streamline the GDL manufacturing technique to reduce the cost to achieve the target of US department of energy (DoE) target?	Yes, and apparently the reduction in the lead time can also be achieved by the SLS technique.	A standardised protocol has to be prepared for optimising the materials and SLS operational parameters for this manufacturing process.

The specific findings and the future direction of this research work are:

1. A novel approach to synthesise a carbon-free GDL for a PEM fuel cell stack by a selective laser sintering (3D printing) is attempted. The proposed GDL specimen is a composite of base polymer powder (alumide and polyamide) and conductive filler (Titanium micron and nanopowder) with the different composition. These two materials are of different physical and chemical properties (one being a

polymer and the other a metallic powder) which are fused together to fabricate a novel specimen with desirable hybrid characteristics. Table 7.2 provides the quantitative characteristics of the GDL specimens fabricated by SLS process which converges towards the conventional GDL material.

Table 7.2 Quantitative Results of the Proposed GDL Material

Properties	Iteration I			Iteration II			Iteration III	
	Base Polymer-Alumide Functional Filler- Ti -Micron			Base Polymer-Polyamide Functional Filler- Ti-Micron			Base Polymer- Polyamide Functional Filler- Ti Nano	
	90/10	80/20	70/30	90/10	80/20	70/30	95/5	
							Laser Power 9 W	Laser Power 12 W
Thickness (µm)	550	445	410	570	440	410	417	361
Tensile Strength (N/cm)	<< 4	4	<< 4	Not Measurable	5	5	20	20
Porosity and Air-Permeability *	More Porous	Porous	More Porous	More Porous	More Porous	More Porous	More Porous	More Porous
Surface contact angle	20° ± 3°	70° ± 10.5°	50° ± 7.5°	10° ± 1.5°	45° ± 6.75°	80° ± 12° and 10° ± 1.5°	110° ± 16.5°	110° ± 16.5°
In-plane electrical resistance Ωcm ⁻¹	Few thousands	Few hundreds	Few thousands	-	Few hundreds	-	35	21
Thermal Conductivity Wm ⁻¹ K ⁻¹	Not Measurable	0.26	Not Measurable	0.37	0.54	0.59	0.43	0.49

*Porosity is the default characteristics in SLS Process

- Porosity is the default characteristic, which is attained through the SLS process [97] and this attribute is observed for every GDL specimen fabricated throughout the course of the experiment.

3. The proposed gas diffusion material exhibited a highly anisotropic and non-linear nature. Though there were limitations involved in the application of Ohm's Law to compute the electrical conductivity and Fourier's Law to compute the thermal conductivity; it provided an opportunity to learn the nature of the gas diffusion materials. The drawback involved in performing the through-plane conductivity measurement is also due to this anisotropic and non-homogeneous nature of the material.
4. Most of the GDL materials fabricated in the present SLS process exhibited a hydrophilic nature. Ironically, the hydrophobic nature is observed for the composition with 5% Ti (Nano) and 95% Polyamide. Thus, the SLS experiment validates that incorporation of hydrophobicity is achievable through the present approach without the need of PTFE.
5. Laser power is often the preferred control parameter due to the simplicity of its regulation. However, there are also other independent SLS process parameters, such as scan speed, laser spot size, beam diameter, scan radius, step size and scan spacing. The size of the laser spot and the scan radius are both machine specific and may differ from one SLS machine to another. Fine-tuning these parameters can potentially yield a more desired material with better structural and functional characteristics. However, understanding the significance of these operational parameters is a prerequisite. There are also numerous combinations of the SLS operating parameters and understanding the integrated effect can provide a more holistic insight.
6. The predominant reason for not attaining the desired electrical conductivity is that the laser energy converts the titanium particles (at least a small amount) to the titanium oxides, which limits the improvement in the conductivity. However, performing the SLS experiment under inert conditions (Argon condition) can be a promising approach to circumvent this issue. There have been numerous

literatures [123-125] that validate better performance characteristics under argon environment.

7. On the other hand, it is observed from the successive experiments that there is a linear increase in the thermal conductivity of the GDL specimen with the increase in the titanium concentration (% Weight). Therefore, hypothetically, in accordance with the Wiedemann Franz law, since the GDL specimens have a finite amount of metallic titanium powder, the electrical conductivity can also be linearly increased. Performing the SLS experiment under inert conditions using a more advanced ball mill to blend the base and conductive powder can significantly improve the overall product fitness.
8. Selecting an appropriate base polymer and conductive filler material can accelerate the product development with more augmented fitness. However, it must be noted that not all the existing SLS base materials are compatible with the GDL fabrication and not all the materials appropriate for the GDL application are compatible with the SLS manufacturing technique.
9. An increase in metallic filler to the polymer alone cannot lead to the increase in the electrical conductivity and this phenomenon is observed in the present investigation. Another critical observation of the present thesis is the structural-functional relationship exhibited by the 3D printed GDL specimen. From the experimental investigation correlating all the functional characteristics, it is observed that the material with reasonable conductivity also exhibited a good tensile strength and vice versa. Thus, an effective sintering is an essential criterion to incorporate the SLS technique for GDL application. Selecting the appropriate material, size, geometry and aspect ratio can also significantly influence the final characteristics of the GDL specimen. More time, processing equipment and related infrastructure pertaining to materials and SLS operating parameters are required to perform the successive iterations with additional material combinations of varying geometry (micron to nano).

10. The SLS process parameters, and their fine-tuning enable the optimization of the GDL characteristics. For instance, in the iteration III, the two GDL specimens fabricated with the same material composition (95% polyamide/5% titanium nano); exhibited different functional characteristics. i.e. the composite powder subjected to laser power of 12W had high conductivity, high tensile strength and lower thickness compared to the one fabricated with 9 W. This clearly illustrates the significant effect of regulating only one operating parameter (Laser power). The combined synergistic effect of adjusting more operating parameters can contribute more significantly.

11. The US-DoE target of \$5.45 /m² [66] for a mass GDL production of 500,000 fuel cell stacks can be easily accomplished through this SLS practice. In addition, the manufacturing complexity can also be drastically reduced by the SLS technique. The proposed concept provided us with promising interpretations and can be fine-tuned with more qualitative research before going into mass-production.

REFERENCES

1. Kordesch, K.V. and G.R. Simader, *Fuel Cell Systems: Sections 4.6-4.8. Fuel Cells: and Their Applications*: p. 133-179.
2. Grove, W.R., XXIV. *On voltaic series and the combination of gases by platinum*. Philosophical Magazine Series 3, 1839. **14**(86-87): p. 127-130.
3. Jayakumar, A., A. Chalmers, and T.T. Lie, *A Review of Prospects for Adoption of Fuel Cell Electric Vehicles in New Zealand*. IET Electrical Systems in Transportation, 2017.
4. Kumar, J.A., P. Kalyani, and R. Saravanan, *Studies on PEM fuel cells using various alcohols for low power applications*. 2008.
5. Handbook, F.C., *EG&G technical services*. Inc., Albuquerque, NM, DOE/NETL-2004/1206, 2004.
6. kumar, J.A., P. Kalyani, and R. Saravanan, *Studies on PEM fuel cells using various alcohols for low power applications*. International Journal of Electrochemical Science, 2008. **3**(8): p. 961-969.
7. Zhang, J., *PEM fuel cell electrocatalysts and catalyst layers: fundamentals and applications*. 2008: Springer Science & Business Media.
8. Jayakumar, A., et al., *A technical review on gas diffusion, mechanism and medium of PEM fuel cell*. Ionics, 2015. **21**(1): p. 1-18.
9. Li, X. and I. Sabir, *Review of bipolar plates in PEM fuel cells: Flow-field designs*. International journal of hydrogen energy, 2005. **30**(4): p. 359-371.
10. Haile, S.M., *Fuel cell materials and components*. Acta Materialia, 2003. **51**(19): p. 5981-6000.
11. Espinoza, M., et al., *Compress effects on porosity, gas-phase tortuosity, and gas permeability in a simulated PEM gas diffusion layer*. International Journal of Energy Research, 2015. **39**(11): p. 1528-1536.
12. Radhakrishnan, A., *Thermal Conductivity Measurement of Gas Diffusion Layer Used in PEMFC*, in *Department of Mechanical Engineering 2009*, Kate Gleason College of Engineering Rochester Institute of Technology, Rochester, NY
13. Rohling, J., et al., *Determination of binary diffusion coefficients of gases using photothermal deflection technique*. Applied Physics B, 2007. **87**(2): p. 355-362.

14. Johnson, M.F. and W.E. Stewart, *Pore structure and gaseous diffusion in solid catalysts*. Journal of Catalysis, 1965. **4**(2): p. 248-252.
15. Kast, W. and C.-R. Hohenthanner, *Mass transfer within the gas-phase of porous media*. International Journal of Heat and Mass Transfer, 2000. **43**(5): p. 807-823.
16. Djilali, N. and D. Lu, *Influence of heat transfer on gas and water transport in fuel cells*. International Journal of Thermal Sciences, 2002. **41**(1): p. 29-40.
17. Van Brakel, J. and P. Heertjes, *Analysis of diffusion in macroporous media in terms of a porosity, a tortuosity and a constrictivity factor*. International Journal of Heat and Mass Transfer, 1974. **17**(9): p. 1093-1103.
18. Springer, T., et al., *Characterization of polymer electrolyte fuel cells using AC impedance spectroscopy*. Journal of the Electrochemical Society, 1996. **143**(2): p. 587-599.
19. Fishman, Z., J. Hinebaugh, and A. Bazylak, *Microscale tomography investigations of heterogeneous porosity distributions of PEMFC GDLs*. Journal of The Electrochemical Society, 2010. **157**(11): p. B1643-B1650.
20. Gostick, J.T., et al., *In-plane and through-plane gas permeability of carbon fiber electrode backing layers*. Journal of Power Sources, 2006. **162**(1): p. 228-238.
21. Koido, T., et al., *Two-phase transport properties and transport simulation of the gas diffusion layer of a PEFC*. ECS Transactions, 2006. **3**(1): p. 425-434.
22. Shimpalee, S., U. Beuscher, and J.W. Van Zee, *Analysis of GDL flooding effects on PEMFC performance*. Electrochimica Acta, 2007. **52**(24): p. 6748-6754.
23. Hussaini, I. and C. Wang, *Measurement of relative permeability of fuel cell diffusion media*. Journal of Power Sources, 2010. **195**(12): p. 3830-3840.
24. Feser, J., A. Prasad, and S. Advani, *Experimental characterization of in-plane permeability of gas diffusion layers*. Journal of Power Sources, 2006. **162**(2): p. 1226-1231.
25. Benziger, J., et al., *Water flow in the gas diffusion layer of PEM fuel cells*. Journal of Membrane Science, 2005. **261**(1): p. 98-106.
26. Rofaiel, A., et al., *Heterogeneous through-plane distributions of polytetrafluoroethylene in polymer electrolyte membrane fuel cell gas diffusion layers*. Journal of Power Sources, 2012. **201**: p. 219-225.

27. Hirschorn, B., B. Tribollet, and M.E. Orazem, *On Selection of the Perturbation Amplitude Required to Avoid Nonlinear Effects in Impedance Measurements*. Israel Journal of Chemistry, 2008. **48**(3-4): p. 133-142.
28. Wang, Y., C.-Y. Wang, and K. Chen, *Elucidating differences between carbon paper and carbon cloth in polymer electrolyte fuel cells*. Electrochimica Acta, 2007. **52**(12): p. 3965-3975.
29. Stampino, P.G., L. Omati, and G. Dotelli, *Electrical performance of PEM fuel cells with different gas diffusion layers*. Journal of Fuel Cell Science and Technology, 2011. **8**(4): p. 041005.
30. Sasikumar, G. and H. Ryu, *Comparison of Electrode Backing Materials for Polymer Electrolyte Membrane Fuel Cells*. Journal of the Korean Electrochemical Society, 2003. **6**, (No.3): p. 183-186.
31. Liao, Y.-K., T.-H. Ko, and C.-H. Liu, *Performance of a polymer electrolyte membrane fuel cell with fabricated carbon fiber cloth electrode*. Energy & Fuels, 2008. **22**(5): p. 3351-3354.
32. Williams, M.V., et al., *Characterization of gas diffusion layers for PEMFC*. Journal of the Electrochemical Society, 2004. **151**(8): p. A1173-A1180.
33. Park, S. and B.N. Popov, *Effect of a GDL based on carbon paper or carbon cloth on PEM fuel cell performance*. Fuel, 2011. **90**(1): p. 436-440.
34. Xie, Z.-Y., et al., *Improved properties of carbon fiber paper as electrode for fuel cell by coating pyrocarbon via CVD method*. Transactions of Nonferrous Metals Society of China, 2010. **20**(8): p. 1412-1417.
35. Du, C., B. Wang, and X. Cheng, *Hierarchy carbon paper for the gas diffusion layer of proton exchange membrane fuel cells*. Journal of Power Sources, 2009. **187**(2): p. 505-508.
36. Thoben, B. and A. Siebke, *INFLUENCE OF DIFFERENT GAS DIFFUSION LAYERS ON THE WATER MANAGEMENT OF THE PEFC CATHODE*. Journal of New Materials for Electrochemical Systems, 2004. **7**(1): p. 13-20.
37. Paganin, V., E. Ticianelli, and E. Gonzalez, *Development and electrochemical studies of gas diffusion electrodes for polymer electrolyte fuel cells*. Journal of Applied Electrochemistry, 1996. **26**(3): p. 297-304.

38. Lee, H.-K., et al., *A study on the characteristics of the diffusion layer thickness and porosity of the PEMFC*. Journal of Power Sources, 2004. **131**(1): p. 200-206.
39. Mathias, M., et al., *Diffusion media materials and characterisation*. Handbook of fuel cells, 2003.
40. Rajalakshmi, N., et al. *Characterisation and Optimisation of Low Cost Activated Carbon Fabric as a Substrate Layer for PEMFC Electrodes*. in *ASME 2005 3rd International Conference on Fuel Cell Science, Engineering and Technology*. 2005. American Society of Mechanical Engineers.
41. Modroukas, D., V. Modi, and L.G. Fr chet te, *Micromachined silicon structures for free-convection PEM fuel cells*. Journal of Micromechanics and Microengineering, 2005. **15**(9): p. S193.
42. Ong, A.L., et al., *Effect of preparative parameters on the characteristic of poly (vinylidene fluoride)-based microporous layer for proton exchange membrane fuel cells*. Journal of Power Sources, 2008. **183**(1): p. 62-68.
43. Chen, J., et al., *Facilitating mass transport in gas diffusion layer of PEMFC by fabricating micro-porous layer with dry layer preparation*. Journal of Power Sources, 2008. **182**(2): p. 531-539.
44. Hung, T., et al., *Highly efficient single-layer gas diffusion layers for the proton exchange membrane fuel cell*. Journal of Power Sources, 2008. **184**(1): p. 165-171.
45. Andersen, S.M., et al., *Durability of carbon nanofiber (CNF) & carbon nanotube (CNT) as catalyst support for Proton Exchange Membrane Fuel Cells*. Solid State Ionics, 2013. **231**: p. 94-101.
46. Han, M., S. Chan, and S. Jiang, *Development of carbon-filled gas diffusion layer for polymer electrolyte fuel cells*. Journal of power sources, 2006. **159**(2): p. 1005-1014.
47. Qi, Z. and A. Kaufman, *Improvement of water management by a microporous sublayer for PEM fuel cells*. Journal of Power Sources, 2002. **109**(1): p. 38-46.
48. Wang, X., et al., *A bi-functional micro-porous layer with composite carbon black for PEM fuel cells*. Journal of power sources, 2006. **162**(1): p. 474-479.

49. Yan, W.-M., et al., *Effects of fabrication processes and material parameters of GDL on cell performance of PEM fuel cell*. International Journal of Hydrogen Energy, 2007. **32**(17): p. 4452-4458.
50. Lim, C. and C. Wang, *Effects of hydrophobic polymer content in GDL on power performance of a PEM fuel cell*. Electrochimica Acta, 2004. **49**(24): p. 4149-4156.
51. Wang, J., et al., *Carbon cloth reinforced carbon aerogel films derived from resorcinol formaldehyde*. Journal of Porous Materials, 2001. **8**(2): p. 159-165.
52. Wang, X., et al., *Micro-porous layer with composite carbon black for PEM fuel cells*. Electrochimica Acta, 2006. **51**(23): p. 4909-4915.
53. Fushinobu, K., D. Takahashi, and K. Okazaki, *Micromachined metallic thin films for the gas diffusion layer of PEFCs*. Journal of power sources, 2006. **158**(2): p. 1240-1245.
54. Hottinen, T., et al., *Titanium sinter as gas diffusion backing in PEMFC*. Journal of power sources, 2003. **118**(1): p. 183-188.
55. Yi, P., et al., *Investigation of sintered stainless steel fiber felt as gas diffusion layer in proton exchange membrane fuel cells*. International Journal of Hydrogen Energy, 2012. **37**(15): p. 11334-11344.
56. Glora, M., et al., *Integration of carbon aerogels in PEM fuel cells*. Journal of non-crystalline solids, 2001. **285**(1): p. 283-287.
57. Long, J.W., et al., *Sulfur-functionalized carbon aerogel supports for noble-metal fuel-cell catalysts*.
58. Zhang, F.-Y., S.G. Advani, and A.K. Prasad, *Performance of a metallic gas diffusion layer for PEM fuel cells*. Journal of power sources, 2008. **176**(1): p. 293-298.
59. Escribano, S., et al., *Characterization of PEMFCs gas diffusion layers properties*. Journal of Power Sources, 2006. **156**(1): p. 8-13.
60. Borup, R., et al., *Scientific aspects of polymer electrolyte fuel cell durability and degradation*. Chemical reviews, 2007. **107**(10): p. 3904-3951.
61. Seidenberger, K., et al., *Estimation of water distribution and degradation mechanisms in polymer electrolyte membrane fuel cell gas diffusion layers using a 3D Monte Carlo model*. Journal of Power Sources, 2011. **196**(12): p. 5317-5324.

62. Pasaogullari, U. and C. Wang, *Liquid water transport in gas diffusion layer of polymer electrolyte fuel cells*. Journal of the Electrochemical Society, 2004. **151**(3): p. A399-A406.
63. Wu, J., et al., *A review of PEM fuel cell durability: Degradation mechanisms and mitigation strategies*. Journal of Power Sources, 2008. **184**(1): p. 104-119.
64. Chen, G., et al., *Electrochemical durability of gas diffusion layer under simulated proton exchange membrane fuel cell conditions*. international journal of hydrogen energy, 2009. **34**(19): p. 8185-8192.
65. Stevens, D. and J. Dahn, *Thermal degradation of the support in carbon-supported platinum electrocatalysts for PEM fuel cells*. Carbon, 2005. **43**(1): p. 179-188.
66. James, B.D. and A.B. Spisak, *Mass Production Cost Estimation of Direct H2 PEM Fuel Cell Systems for Transportation Applications: 2012 Update*. report by Strategic Analysis, Inc., under Award Number DEEE0005236 for the US Department of Energy, 2012. **18**.
67. Dieter, G.E., *Overview of the materials selection process*. ASM Handbook, 1997. **20**: p. 243-254.
68. Hull, C.W., *Apparatus for production of three-dimensional objects by stereolithography*. 1986, Google Patents.
69. Fahad, M. and N. Hopkinson, *Evaluation and comparison of geometrical accuracy of parts produced by sintering-based additive manufacturing processes*. The International Journal of Advanced Manufacturing Technology, 2017. **88**(9-12): p. 3389-3394.
70. Dahotre, N.B. and S. Harimkar, *Laser fabrication and machining of materials*. 2008: Springer Science & Business Media.
71. Nelson, J.C., *Selective laser sintering: a definition of the process and an empirical sintering model*. 1993, University of Texas at Austin.
72. Ju, H., H. Meng, and C.-Y. Wang, *A single-phase, non-isothermal model for PEM fuel cells*. International Journal of Heat and Mass Transfer, 2005. **48**(7): p. 1303-1315.
73. Lee, S.-J., C.-H. Huang, and Y.-P. Chen, *Investigation of PVD coating on corrosion resistance of metallic bipolar plates in PEM fuel cell*. Journal of materials processing technology, 2003. **140**(1): p. 688-693.

74. Geim, A.K. and K.S. Novoselov, *The rise of graphene*. Nature materials, 2007. **6**(3): p. 183-191.
75. Prasai, D., et al., *Graphene: corrosion-inhibiting coating*. ACS nano, 2012. **6**(2): p. 1102-1108.
76. Hermann, A., T. Chaudhuri, and P. Spagnol, *Bipolar plates for PEM fuel cells: a review*. International journal of hydrogen Energy, 2005. **30**(12): p. 1297-1302.
77. Hung, Y., K. El-Khatib, and H. Tawfik, *Testing and evaluation of aluminum coated bipolar plates of PEM fuel cells operating at 70 C*. Journal of Power Sources, 2006. **163**(1): p. 509-513.
78. Woodman, A., et al. *Development of corrosion-resistant coatings for fuel cell bipolar plates*. in *AESF SUR FIN-PROCEEDINGS-*. 1999. AMERICAN ELECTROPLATERS AND SURFACE FINISHERS SOCIETY INC.
79. Wang, S.-H., et al., *Performance of the gold-plated titanium bipolar plates for the light weight PEM fuel cells*. Journal of Power Sources, 2006. **162**(1): p. 486-491.
80. Fang, S.-Y., et al., *Enhancement of proton exchange membrane fuel cell performance by titanium-coated anode gas diffusion layer*. International Journal of Hydrogen Energy, 2014. **39**(36): p. 21177-21184.
81. Lyons, K.S. and B.D. Gould. *Lightweight Titanium Metal Bipolar Plates for PEM Fuel Cells*. in *Materials Science Forum*. 2017. Trans Tech Publ.
82. Schweiss, R.M., C.; Damjanovic, T.; Galbiati, I.; Haak, N., *SIGRACET® Gas Diffusion Layers for PEM Fuel Cells, Electrolyzers and Batteries*. . 2016.
83. Zamora, H., et al., *Improving of micro porous layer based on advanced carbon materials for high temperature proton exchange membrane fuel cell electrodes*. Fuel Cells, 2015. **15**(2): p. 375-383.
84. Zhang, Y., et al., *Phosphorus-doped carbon nitride solid: enhanced electrical conductivity and photocurrent generation*. Journal of the American Chemical Society, 2010. **132**(18): p. 6294-6295.
85. Goebel, S.G., *Evaporative cooled fuel cell*. 2005, Google Patents.
86. ElMaraghy, H.A., *Flexible and reconfigurable manufacturing systems paradigms*. International journal of flexible manufacturing systems, 2005. **17**(4): p. 261-276.

87. Swink, M., *Threats to new product manufacturability and the effects of development team integration processes*. Journal of Operations Management, 1999. **17**(6): p. 691-709.
88. Antolini, E., *Graphene as a new carbon support for low-temperature fuel cell catalysts*. Applied Catalysis B: Environmental, 2012. **123**: p. 52-68.
89. Jeon, I.-Y., et al., *Facile, scalable synthesis of edge-halogenated graphene nanoplatelets as efficient metal-free electrocatalysts for oxygen reduction reaction*. Scientific reports, 2013. **3**.
90. Velu, R. and S. Singamneni, *Evaluation of the influences of process parameters while selective laser sintering PMMA powders*. Proceedings of the Institution of Mechanical Engineers, Part C: Journal of Mechanical Engineering Science, 2015. **229**(4): p. 603-613.
91. Lawrence, M. and Y. Jiang, *Porosity, Pore Size Distribution, Micro-structure*, in *Bio-aggregates Based Building Materials*. 2017, Springer. p. 39-71.
92. Novoselov, K., et al., *Two-dimensional gas of massless Dirac fermions in graphene*. nature, 2005. **438**(7065): p. 197-200.
93. Tian, H., et al., *Graphene earphones: Entertainment for both humans and animals*. ACS nano, 2014. **8**(6): p. 5883-5890.
94. Geim, A.K., *Graphene: status and prospects*. science, 2009. **324**(5934): p. 1530-1534.
95. Lundstedt, T., et al., *Experimental design and optimization*. Chemometrics and intelligent laboratory systems, 1998. **42**(1): p. 3-40.
96. Zhang, S. and D. Zhao, *Aerospace materials handbook*. 2012: CRC Press.
97. Lohfeld, S., et al., *A method to fabricate small features on scaffolds for tissue engineering via selective laser sintering*. Journal of Biomedical Science and Engineering, 2010. **3**(02): p. 138.
98. Ramamurti, T., C. Ganapathy, and S. Saran, *Low-temperature sintering of titanium dioxide for ceramic capacitors*. Nature, 1954. **174**(4443): p. 1187-1187.
99. Brezesinski, T., et al., *Ordered mesoporous α -MoO₃ with iso-oriented nanocrystalline walls for thin-film pseudocapacitors*. Nature materials, 2010. **9**(2).

100. Mohammadi, A.V. and M. Halali, *Synthesis and characterization of pure metallic titanium nanoparticles by an electromagnetic levitation melting gas condensation method*. RSC Advances, 2014. **4**(14): p. 7104-7108.
101. Lankoff, A., et al., *The effect of agglomeration state of silver and titanium dioxide nanoparticles on cellular response of HepG2, A549 and THP-1 cells*. Toxicology letters, 2012. **208**(3): p. 197-213.
102. Morgan, R., C. Sutcliffe, and W. O'Neill, *Experimental investigation of nanosecond pulsed Nd: YAG laser re-melted pre-placed powder beds*. Rapid Prototyping Journal, 2001. **7**(3): p. 159-172.
103. Tolochko, N.K., et al., *Balling processes during selective laser treatment of powders*. Rapid Prototyping Journal, 2004. **10**(2): p. 78-87.
104. Gu, D., et al., *Laser additive manufacturing of metallic components: materials, processes and mechanisms*. International materials reviews, 2012. **57**(3): p. 133-164.
105. Sasikumar, G., J. Ihm, and H. Ryu, *Optimum Nafion content in PEM fuel cell electrodes*. Electrochimica Acta, 2004. **50**(2): p. 601-605.
106. Polymers—Properties, M.-F., *Applications*; Bhattacharya, S. K, Ed. 1986, Marcel Dekker: New York.
107. Bazylak, A., et al., *Effect of compression on liquid water transport and microstructure of PEMFC gas diffusion layers*. Journal of Power Sources, 2007. **163**(2): p. 784-792.
108. Kandlikar, S., et al., *Uneven gas diffusion layer intrusion in gas channel arrays of proton exchange membrane fuel cell and its effects on flow distribution*. Journal of Power Sources, 2009. **194**(1): p. 328-337.
109. Sumirat, I., Y. Ando, and S. Shimamura, *Theoretical consideration of the effect of porosity on thermal conductivity of porous materials*. Journal of Porous Materials, 2006. **13**(3-4): p. 439-443.
110. Mavrokefalos, A., et al., *Four-probe measurements of the in-plane thermoelectric properties of nanofilms*. Review of scientific instruments, 2007. **78**(3): p. 034901.
111. Chen, G., *Nonlocal and nonequilibrium heat conduction in the vicinity of nanoparticles*. TRANSACTIONS-AMERICAN SOCIETY OF MECHANICAL ENGINEERS JOURNAL OF HEAT TRANSFER, 1996. **118**: p. 539-545.

112. Henrion, M. and B. Fischhoff, *Assessing uncertainty in physical constants*. American Journal of Physics, 1986. **54**(9): p. 791-798.
113. Panigrahi, B., et al., *Sintering mechanisms of attrition milled titanium nano powder*. Journal of materials research, 2005. **20**(4): p. 827-836.
114. Arif, A.F., et al., *Highly conductive nano-sized Magnéli phases titanium oxide (TiO_x)*. Scientific Reports, 2017. **7**.
115. Schmid, M., A. Amado, and K. Wegener. *Polymer powders for selective laser sintering (SLS)*. in *AIP Conference Proceedings*. 2015. AIP Publishing.
116. Nelson, J. and J. Barlow, *Relating operating parameters between SLS machines which have different scanner geometries and laser spot sizes*. Department of Chemical Engineering, University of Texas at Austin, 1992.
117. Duley, W.W., *Laser processing and analysis of materials*. 2012: Springer Science & Business Media.
118. Alda, J., *Laser and Gaussian beam propagation and transformation*. Encyclopedia of optical engineering, 2003. **2013**: p. 999-1013.
119. Franz, R. and G. Wiedemann, *Ueber die Wärme-Leitungsfähigkeit der Metalle*. Annalen der Physik, 1853. **165**(8): p. 497-531.
120. Tanaka, S. and T. Shudo, *Significant performance improvement in terms of reduced cathode flooding in polymer electrolyte fuel cell using a stainless-steel microcoil gas flow field*. Journal of Power Sources, 2014. **248**: p. 524-532.
121. McNally, T., et al., *Polyethylene multiwalled carbon nanotube composites*. Polymer, 2005. **46**(19): p. 8222-8232.
122. Williams, D., et al., *The effects of zirconium in titanium-base alloys*. Journal of the Less Common Metals, 1964. **6**(3): p. 219-225.
123. Man, H., Z. Cui, and T. Yue, *Corrosion properties of laser surface melted NiTi shape memory alloy*. Scripta Materialia, 2001. **45**(12): p. 1447-1453.
124. Murr, L.E., et al., *Metal fabrication by additive manufacturing using laser and electron beam melting technologies*. Journal of Materials Science & Technology, 2012. **28**(1): p. 1-14.
125. Yahaya, A., M. Gondal, and A. Hameed, *Selective laser enhanced photocatalytic conversion of CO₂ into methanol*. Chemical physics letters, 2004. **400**(1-3): p. 206-212.

APPENDIX A

Broad Base. Best Solutions.



WHITE PAPER

SIGRACET® Gas Diffusion Layers for PEM Fuel Cells, Electrolyzers and Batteries

*Authors: Rüdiger Schwelss, Christian Meiser,
Tanja Damjanovic, Ivano Galbati, Nico Haak*

+ SIGRACET® gas diffusion layer

Introduction

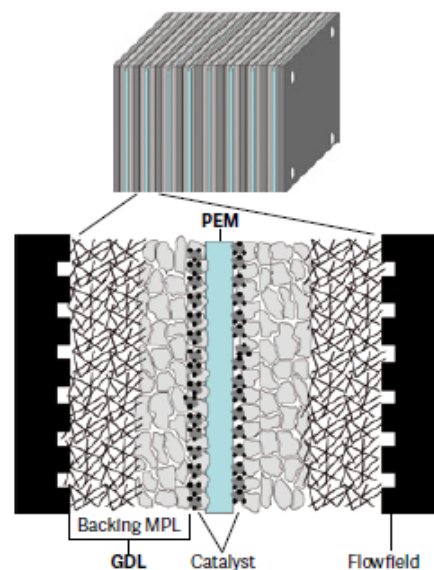
Gas diffusion layers (GDLs) are crucial components for proton exchange membrane fuel cells (PEMFCs), since they modulate all relevant transport processes (fuel, reaction products, electricity, heat) [1 – 2].

Figure 1 shows a typical setup of a single cell PEMFC. It consists of two flowfields, two GDLs, catalyst layers and the proton exchange membrane (PEM). Gas diffusion layers act as an interface between the flow fields (structural cell parts, millimeter-size features) and the electrocatalysts (reaction layers, nanometer-size features), directing the fuel to the active sites while removing heat and reaction products and electrically wiring the reaction layers with the current collectors.

Gas diffusion layers typically consist of a bilayer structure consisting of a macro-porous backing material (carbon fiber paper) and a micro-porous, carbon-based layer (MPL). The fibrous backing material governs the mechanical properties of the GDL (behavior upon compression, bending and shear strength) and also impacts the thermal and electric parameters.

Its hydrophobic properties and its microstructure have a significant effect on the water management via the capillary pressure-saturation relationship. Micro-porous layers are additional mediators of the water management of PEMFCs where pore size distribution, type of carbon and PTFE load can be adjusted to optimize water management under the prevalent operating conditions.

Additionally, the MPL facilitates catalyst deposition and effectively protects the proton exchange membrane against perforation by the carbon fibers.

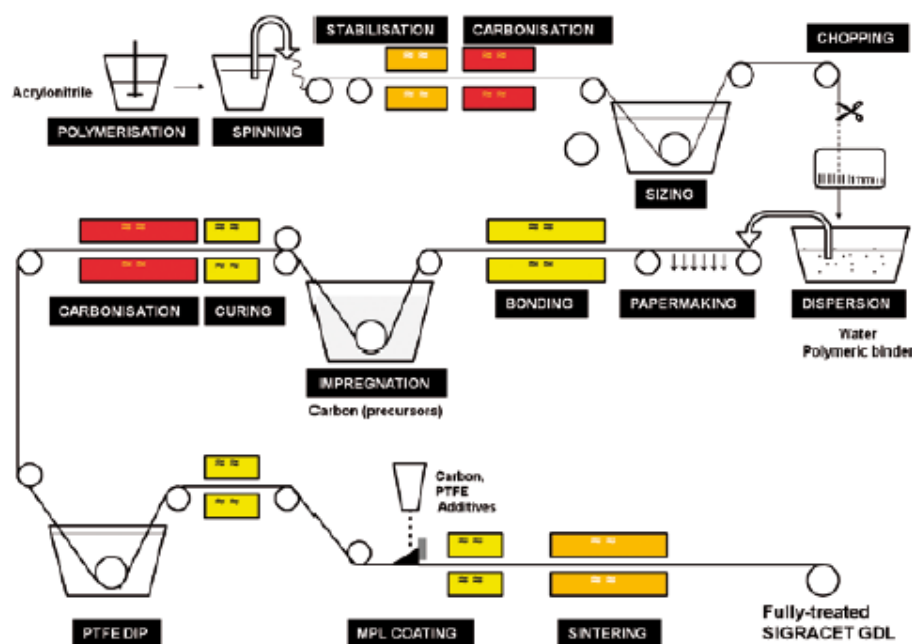


† Figure 1: Structure of a PEMFC single cell

Manufacturing Process

Gas diffusion electrodes can be manufactured by depositing catalysts onto GDLs. Carbon paper-type (prepared by wet-laying of chopped PAN-based carbon fibers) gas diffusion layers are the preferred solutions since they can be manufactured at high volumes (scalability) and low thickness.

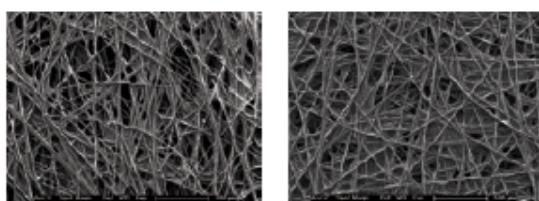
Chopped carbon fibers are processed to a primary carbon fiber web using a papermaking (wet-laying) technology and subsequent thermo bonding. The raw paper is then impregnated with carbonizable resins (carbonizable resins with optional addition of carbon fillers), cured and recarbonized/graphitized. (Figure 2)



† Figure 2: Manufacturing process of SIGRACET (carbon paper-based) gas diffusion layers

This procedure serves to adjust the porosity and to enhance electric and thermal conductivity. Figure 3 shows two GDL backings with different filler content which are the base for the finishing processes hydrophobic treatment with PTFE and coating with a micro-porous layer (MPL).

Sintering (thermal annealing) is applied in order to bond the substrate/MPL and to develop the full hydrophobic properties of the GDL. Proper selection of raw materials and additives ensures that the material is virtually free of heavy metals which are detrimental to fuel cell applications.



A loading of the substrate with 5 wt% PTFE has proven to be sufficient for obtaining a pronounced hydrophobicity (BA types). Nevertheless, higher loads up to 30 wt% are possible.

The standard microporous layer (C-type) is based on 77 wt% carbon black and 23 wt% PTFE. This MPL composition has been identified as the optimum composition in PEMFC tests (optimum level of porosity and hydrophobicity).

Mean pore sizes are in a range from 0.1 to 0.3 μm (mercury intrusion porosimetry) or 1.5 to 3 μm (calculated from capillary flow porometry). The hydrophobic treatment produces water repellent properties for the substrate and for the MPL (water contact angles by sessile drop method >150°).

← Figure 3: SEM images of carbon paper with different filler content (GDL backing with high porosity (left), low porosity (right))

Physical Properties

Table 1 and 2 summarize the most important material properties of GDL backings (AA grades) and fully treated GDLs (BC grades). SIGRACET GDL grades comprise two porosity and thickness levels. This portfolio allows for a wide range of total pore volumes.

Table 1: Typical material data of SIGRACET® GDL backings (SIGRACET® AA grades)

Typical properties	Units	28 AA	29 AA	38 AA	39 AA
Thickness	µm	190	190	280	280
Area weight	gm ⁻²	55	40	75	50
Open porosity	%	82	88	82	89
Mean pore diameter	µm	39 – 44	48 – 51	25 – 29	42 – 44
TP area-specific resistance**	mΩcm ²	< 4	< 5	< 5	< 5
TP electric conductivity**	Scm ⁻¹	4 – 5	3.5 – 4	5 – 6	4 – 5
IP electric conductivity (X/Y)**	Scm ⁻¹	225/200	190/170	270/240	215/180
TP thermal conductivity	Wm ⁻¹ K ⁻¹	0.5 – 0.6	0.4 – 0.5	< 0.4	< 0.3
IP permeability**	10 ⁻¹² m ²	2 – 3	8 – 9	3 – 4	11 – 12
Bending stiffness (X/Y)	mNm	2.1/1.9	2/1.5	5.5/4.3	5.4/4.1
Compressibility (1 MPa)	%	13	31	12	33

Table 2: Typical material data of SIGRACET® GDLs (SIGRACET® BC grades)

Typical properties	Units	28 BC	29 BC	38 BC	39 BC
PTFE load of backing	wt%	5 ± 1	5 ± 1	5 ± 1	5 ± 1
PTFE content of MPL	wt%	23	23	23	23
Thickness	µm	235	235	325	325
Area weight	gm ⁻²	105	90	125	105
Open porosity	%	36 – 37	40 – 41	46 – 47	50 – 52
TP gas permeability (Gurley)*	cm ³ cm ⁻² s ⁻¹	0.5 – 0.7	0.9 – 1.3	0.2 – 0.4	1.0 – 1.5
TP gas permeability*	10 ⁻¹² m ²	5 – 6	6 – 7	7 – 8	12 – 15
IP gas permeability**	10 ⁻¹² m ²	1.4	1.9	2.3	2.7
TP area-specific resistance**	mΩcm ²	7.5 – 8.5	8.5 – 9.5	10 – 11	11 – 12
TP electric conductivity**	Scm ⁻¹	2.4 – 2.7	2.0 – 2.3	2.5 – 2.8	2.0 – 2.2
IP electric conductivity (X/Y)**	Scm ⁻¹	200/180	175/155	225/200	170/145
TP thermal conductivity*	Wm ⁻¹ K ⁻¹	0.6	0.5	0.35	0.25
Compressibility (1 MPa)	%	13	18	13	30
Recovery (2.5 MPa)	%	65	61	65	54
Resiliency (2.5 MPa)	%	13	21	13	30

IP - In plane TP - through plane * uncompressed ** compressed with 1 MPa

Understanding the compression behavior of GDLs is important for minimizing contact resistances and to optimize water management in PEMFCs. Figure 4 and 5 show the effect of compression load on the thickness, the area-specific through-plane resistance and on the in-plane pressure drop.

In order to characterize the compressibility, the difference between uncompressed thickness (compression load of 5 psi) and thickness at a load of 1 MPa (which results in a compression to around 75 to 85 % of the initial thickness) can be used.

$$a_{MPa} (\%) = \left[\frac{d_0 - d_{1MPa}}{d_0} \right] \cdot 100$$

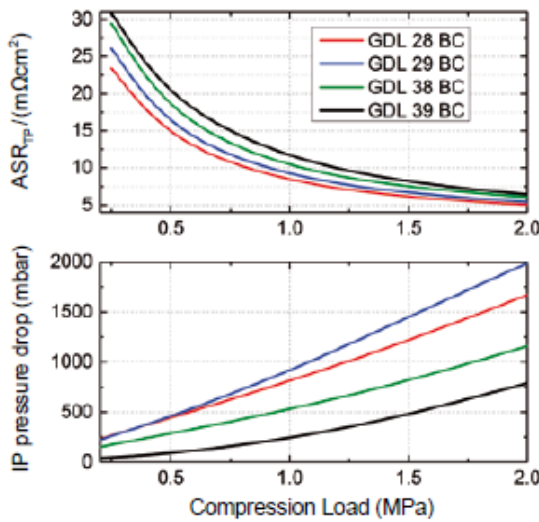
Since a GDL typically shows a certain fraction of elastic and plastic (inelastic) deformation, the recovery

$$rec_{2.5MPa} (\%) = \left[\frac{d_0^{2nd} - d_{2.5MPa}^{1st}}{d_0^{1st} - d_{2.5MPa}^{1st}} \right] \cdot 100$$

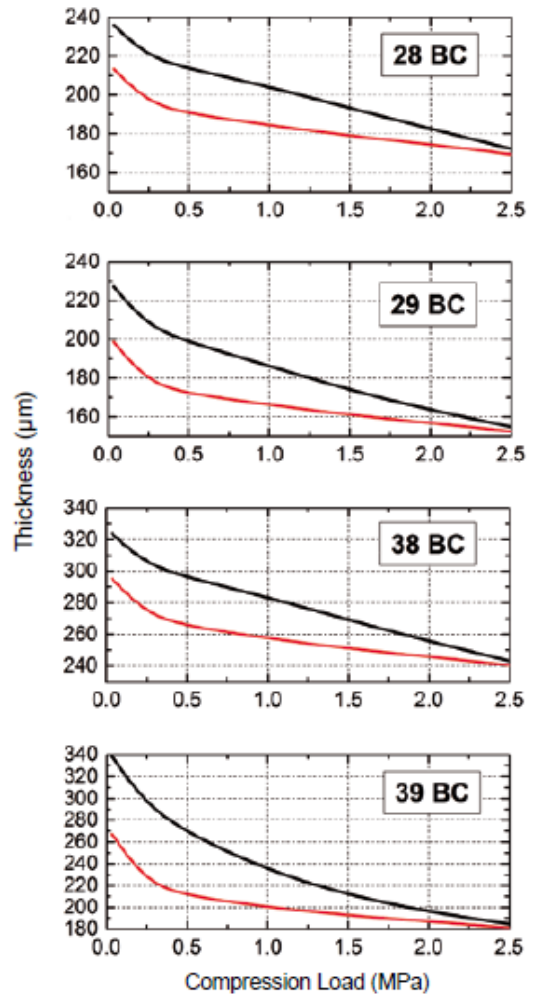
and resiliency of a GDL

$$res_{2.5MPa} (\%) = \left[\frac{d_0^{2nd} - d_{2.5MPa}^{1st}}{d_{2.5MPa}^{1st}} \right] \cdot 100$$

constitute additional metrics for the compression behavior of GDLs.



† Figure 5: Area-specific through-plane resistance and in-plane pressure drop of SIGRACET GDL grades as a function of applied compression load



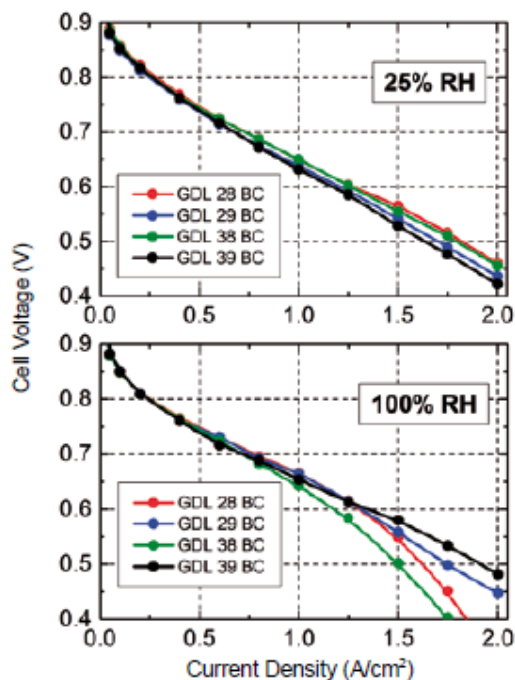
† Figure 4: Compression plots of SIGRACET GDLs (first (black curve) and second (red curve) compression cycle)

Electrochemical Properties

GDLs are effective in supporting the water management in PEM fuel cells. Hence, proper choice of the GDL type is favorable to obtain the optimum cell performance. Figure 6 shows the typical PEMFC single cell performance of different GDLs under dry (25% relative humidity (RH)) and wet (100% RH) operating conditions.

As evident in Figure 6, the GDL platforms 28 and 38 are preferable for dry operation since the denser backing is preventing dehydration of the proton exchange membrane. Similarly, GDL 38 BC is recommended for high temperature PEM fuel cells (HT-PEMFCs) since it prevents leaching of phosphoric acid from PBI membranes.

By contrast, GDL 29 and 39 are recommended if high gas diffusivity is needed (predominantly wet operation, high current densities or low pressure).



→ Figure 6: Polarization curves of single cells (25 cm^2) using different SIGRACET GDLs under dry (25% RH) and wet (100% RH) operating conditions (temperature 80°C , 1.5 bar, stoichiometry H_2/air 1.5/2.5, CCM with $18 \mu\text{m}$ membrane, $0.5 \text{ mg}/\text{cm}^2 \text{ Pt}$)

The following Table 3 presents a recommendation of different SIGRACET GDL platforms for specific PEMFC types.

This has been based on long-term field observations of the PEMFC industry. Further PEMFC application data of SIGRACET GDLs can be found in [8 – 11].

Table 3: Preferred SIGRACET® grade for various applications

Applications	GDL 28 200 μm Low porosity	GDL 29 200 μm High porosity	GDL 38 300 μm Low porosity	GDL 39 300 μm High porosity
PEMFC stationary	•		••	
PEMFC automotive	•	••		
PEMFC portable				•
HT-PEMFC			•	
DMFC		•		•
PEM electrolysis		•		••

Different modifications of finishing treatments could be used for further tailoring of PEMFC performance. For instance, various PTFE load of the backing (5 wt% – 20 wt%) and in the MPL [3] and MPL with carbon blends [5 – 7]. The following MPLs types are available (Table 4).

Table 4: Available MPL types

MPL types	Features
C	Well established MPL – suitable for a variety of operating conditions
B	Low loading MPL for enhanced mass transport

C-type MPL is a widely established industrial standard which is characterized by a low amount of cracks and which can be used for a variety of conditions. The B-type MPL shows better performance under wet conditions and high current densities.

Composite MPLs based on carbon nanotubes (MWCNT) and carbon black or graphite have reproducibly demonstrated excellent PEMFC performance [5 – 7], but still need further refining with respect to cost-efficient manufacturing.

Non-Fuel Cell Applications

Given its high conductivity and surface area, gas diffusion layers can inherently be used in related applications such as microbial fuel cells, PEM electrolysis, metal-air batteries, or redox flow batteries. The following Table 5 presents a selection of non-fuel cell applications and the recommended SIGRACET grades.

Conclusions

Gas diffusion layer technology has attained a high level of maturity. Nevertheless, the complex interactions among various cell components constantly require a design matching of the GDL with adjacent materials and cell operation strategy. Such an optimization is only facilitated by detailed feedback with respect to MEA/cell/stack performance.

Table 5: Selection of non-fuel cell applications and recommended SIGRACET® grades

Applications	Material applied as	Recommended grade(s)
Redox flow batteries	Porous electrode for zero-gap cell design	GDL 39 AA/38 AA
Metal-air batteries	Cathode support (for GDE)	GDL 39 AA/BA/BC
Microbial fuel cells	Electrode support	GDL 39 AA/BC
PEM electrolysis	Cathode support	GDL 39 AA/BA/BC

References

- [1] **Diffusion media and characterization.** M. F. MATHIAS, J. ROTH, J. FLEMING, W. LEHNERT In: W. VIELSTICH, H. A. GASTEIGER, A. LAMM (Eds.) Handbook of Fuel Cells, Vol. 3, 2003, Chapter 6.; Wiley, New York, pp 517-537
- [2] **Ex-situ characterisation of gas diffusion layers for proton exchange membrane fuel cells.** A. EL-KHAROUF, T. J. MASON, D. J. L. BRETT, B. G. POLLET, J. Power Sources 2010, 218, 393-404
- [3] **Effect of polytetrafluoroethylene treatment and microporous layer-coating on the electrical conductivity of gas diffusion layers used in proton exchange membrane fuel cells.** M. S. ISMAIL, T. DAMJANOVIC, D. B. INGHAM, M. POURKASHANIAN, A. WESTWOOD, J. Power Sources 2010, 195, 2700-2708
- [4] **On the through-plane permeability of microporous layer-coated gas diffusion layers used in proton exchange membrane fuel cells.** M. S. ISMAIL, D. S. BORMAN, T. DAMJANOVIC, D. INGHAM, M. POURKASHANIAN, Int. J. Hydrogen Energ. 2011, 36, 10392-10402.
- [5] **Enhancement of proton exchange membrane fuel cell performance by doping of microporous layers of gas diffusion layers with multiwall carbon nanotubes.** R. SCHWEISS, M. STEEB, P. M. WILDE, T. SCHUBERT, J. Power Sources 2012, 220, 79-83
- [6] **Degradation of gas diffusion layers in PEM fuel cells during drive cycle operation.** R. MUKUNDAN, J. DAVEY, K. RAU, D. LANGLOIS, D. SPERNJAK, K. ARTYUSHKOVA, R. SCHWEISS, R. L. BORUP, ECS Trans. 2013, 58, 919-926
- [7] **The importance of carbon materials in micro-porous layer in gas diffusion layers for proton exchange membrane fuel cells.** R. SCHWEISS, O. OETTINGER, TANSO 2015, 268, 131-13
- [8] **The effect of materials on proton exchange membrane fuel cell electrode performance.** B. MILLINGTON, S. DU, B. G. POLLET, J. Power Sources 2011, 192, 9013-9017
- [9] **Gas diffusion layer materials and their effect on polymer electrolyte fuel cell performance – ex-situ and in-situ performance.** A. EL-KHAROUF, N. V. REES, R. STEINBERGER-WILCKENS, Fuel Cells 2014, 14, 735-741
- [10] **Feasibility of in-plane GDL structuration: Impact on current density distribution in large-area Proton Exchange Membrane Fuel Cells.** L. JABBOUR, C. ROBIN, F. NANDJOU R. VINCENT, F. MICOUD, J.-P. POIROT-CROUVEZIER, J. DARBIGNY D M. GERARD, J. Power Sources 2015, 299, 380-390
- [11] **Understanding flexural, mechanical and physico-chemical properties of gas diffusion layers for polymer membrane fuel cell and electrolyzer systems.** S.R. DHANUSHKODI, F. CAPITANIO, T. BIGGS, W. MÉRIDA, Int. J. Hydrogen Energ. 2015, 40, 16846-16859

Contact

SGL CARBON GmbH
Werner-von-Siemens-Strasse 18
86405 Meltingen/Germany
Phone +49 8271 83-3360
fuelcellcomponents@sglgroup.com

* registered trademark of SGL CARBON SE 08 2016/0.5 E Printed in Germany
This information is based on our present state of knowledge and is intended to provide general notes on our products and their uses. It should therefore not be construed as guaranteeing specific properties of the products described or their suitability for a particular application. Any existing industrial property rights must be observed. The quality of our products is guaranteed under our 'General Conditions of Sale'.

Technology & Innovation
SGL CARBON GmbH



Werner-von-Siemens-Strasse 18
86405 Meltingen/Germany
www.sgllacert.com



A technical review on gas diffusion, mechanism and medium of PEM fuel cell

Arunkumar Jayakumar · Sundar Pethaiah Sethu · Maximiano Ramos · John Robertson · Ahmed Al-Jumaily

Received: 15 September 2014 / Revised: 2 November 2014 / Accepted: 17 November 2014 / Published online: 30 November 2014
© Springer-Verlag Berlin Heidelberg 2014

Abstract The operation of polymer electrolyte membrane (PEM)-based fuel cells involves numerous physicochemical processes and components actively governing its function and, among them, gas transport phenomena and gas diffusion layer (GDL) are noteworthy, and the present paper provides a comprehensive assessment on gas diffusion mechanism, geometry of GDL components and related modelling studies involved in GDL fabrication. The impact of GDL on diffusion of reactants, water management and the transport of ions has also been systematically dealt.

Keywords PEM fuel cell · Gas diffusion layer · Microporous layer · Membrane electrode assembly · Carbon cloth · Carbon paper

Introduction

It is believed that there will be a time, in the future, when global energy demands will be met by sources other than fossil fuels, and fuel cells are expected to play a remarkable role in this because of their high fuel conversion efficiency and environmental compatibility [1]. Among the various fuel cells, PEM fuel cells are considered as one of the promising solutions and will attract numerous niche markets due to its superior characteristics and power density compared to conventional generators or advanced batteries. In a PEM fuel cell, hydrogen gas diffuses through the gas diffusion medium or

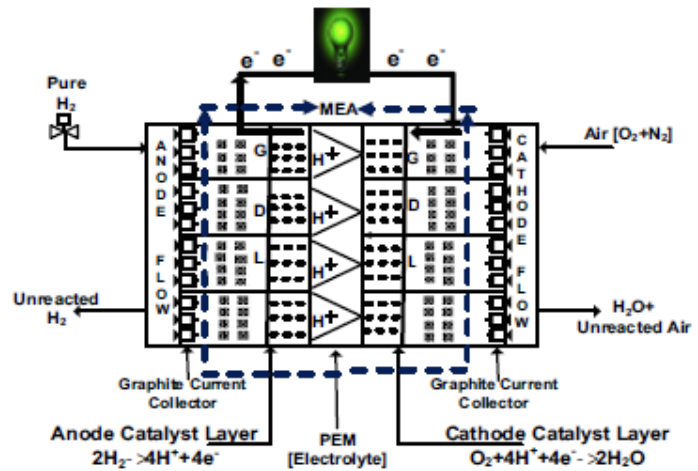
gas diffusion layer (GDL) and reaches the anode catalyst site where it is electrochemically oxidized to protons and electrons. The membrane transports the protons to the cathode, but the electrons are forced to travel in an external circuit (since the membrane is electrically insulating) to generate electric power. At the cathode, oxygen/air gets electrochemically reduced and combines with protons, thereby producing water and heat as the by-products. The typical structure of a PEM fuel cell, with flow field, membrane-electrode-assembly (MEA), catalyst layer (CL), gas diffusion layer (GDL) and electrochemical reactions is illustrated in Fig. 1.

The vital components of a PEM fuel cell are bipolar plates, membrane and electrodes, catalyst and a GDL. The role of bipolar/flow field plates are to distribute the reactant gas over the surface of the electrodes through flow channels. They also collect the current and form the supporting structure of the fuel cell [2]. The function of the membrane is to conduct proton and impede electron. DuPont's Nafion membranes are widely used due to their high proton conductivity and excellent chemical stability [3], and the dimension of state-of-the-art membranes are about 50 μm [4]. Integration of the gas diffusion layer with the microporous layer and catalyst layer is termed as gas diffusion electrode (GDE). The membrane, the catalyst (platinum supported on carbon particle) and the two GDEs are assembled into a sandwich structure to form a MEA [5]. GDL is an integral part of a MEA, and its principal functions are to efficiently transport the reactants and the products to and from the reaction sites as well as to conduct heat and current [6]. GDLs are typically porous composites and have a thickness in the range of 100 to 300 μm [7]. The GDL comprises of carbon for electrical conductivity and PTFE for hydrophobicity [8]. Figure 2 represents the cross section of a gas diffusion layer that provides a physical microporous support for the catalyst layer while allowing gas and water to transport to and from the catalyst layer.

A. Jayakumar (✉) · M. Ramos · J. Robertson · A. Al-Jumaily
Auckland University of Technology, Auckland, New Zealand
e-mail: ajayakum@aut.ac.nz

S. P. Sethu
Technische Universität München - Campus for Research Excellence and Technological Enterprise, 1 CREATE Way, Singapore 138602, Singapore

Fig. 1 Line sketch of PEM fuel cell revealing the vital components and ion transport



Although, GDL significantly influences the performance of a PEM fuel cell in all the three polarization regions, the mass transport characteristics predominantly affect the performance of a gas diffusion layer (GDL) in the proton exchange membrane (PEM) fuel cell [9] as well its durability. An ideal GDL should offer properties such as superior gas diffusion with optimum bending stiffness, porosity, surface contact angle, air permeability, water vapour diffusion, hydrophobicity, hydrophilicity, corrosion resistance, crack-free surface morphology, high mechanical integrity and enhanced oxidative stability along with durability at various operating conditions including freezing [10–14]. Any weak spot in the GDL circuits will adversely impact the gas diffusion processes which in turn affect the performance. Paganin et al. [15] perceived that the diffusion layer has a small effect on the cell performance; however, later it has been revealed that altering the diffusion layer composition can even lead to substantial improvements in the PEMFC performance [16]. Understanding the design and functional characteristics of GDL may provide a significant contribution in the gas diffusion process and components so as to optimize the quality of MEAs and, consecutively, this kind of comprehensive review can lead to the commercialization of PEM fuel cell.

Gas diffusion and structural characteristics of GDL

Gas diffusive transport is a physical process involved in fuel cell stack; Fick's law [17] predicts how diffusion causes the concentration to change with time, and the equation is governed as follows:

$$\frac{\partial C_i}{\partial t} = D_i^{\text{eff}} \frac{\partial^2 C_i}{\partial z^2} \quad (1)$$

Springer

Where

- C_i is the concentration.
- D_i^{eff} is the diffusion coefficient.
- Z is the position [length].

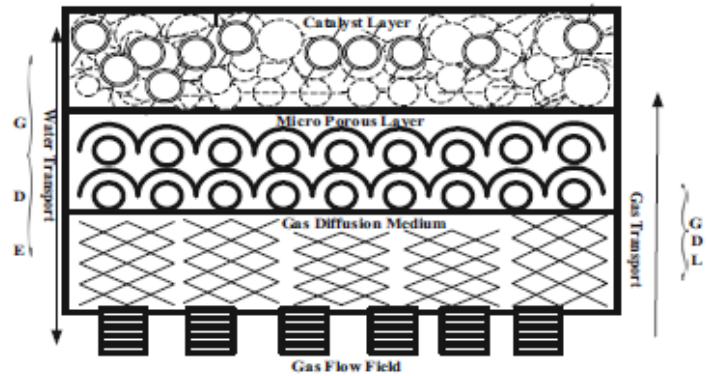
Fick's law is insufficient in approximating the mass diffusion process due to its very fine pore sizes and as a result the effective diffusion coefficient is modified by Bruggeman correction. This alteration is employed in species transport of oxidants and fuels in the porous media of the PEM fuel cells. However, the texture of porous media is very complex and the relative influence of ordinary diffusion or Knudsen diffusion on species transport is governed by the pore geometry [18]. As presented by Nam and Kaviany [19], the effective diffusion coefficient in the porous media in PEM fuel cells is better depicted by using percolation theory, given as;

$$D_g^{\text{eff}} = f(\varepsilon) \times D_g^t \quad (2)$$

$$f(\varepsilon) = \varepsilon \left(\frac{\varepsilon - \varepsilon_p}{1 - \varepsilon_p} \right)^\alpha \quad \alpha = \begin{cases} 0.521 & \text{in-plane} \\ 0.785 & \text{through-plane} \end{cases} \quad (3)$$

Where ε_p is the percolation critical value and has been reported to be 0.11 and 0.13 by Pharoah et al. [20] and Liu and Wang [21], respectively. The results produced by the anisotropic diffusion coefficient reveal that the gas flow is much higher for in-plane direction than through-plane. Mass transfer can take place by Knudsen or Fickian diffusion if the pores are sufficiently small [22] as well as the diffusion characteristics of the macroporous layer can be examined by Fick's laws,

Fig. 2 A cross-sectional view of GDE, GDM, MPL and CL, screening the gas and water transport



while the microporous layer generally exhibits Knudsen diffusion. The Knudsen number, K_n used to characterize the regime of diffusion is defined as

$$K_n = \lambda_g/d_p \tag{4}$$

Where λ_g is the mean molecular free path and d_p is the pore diameter.

An estimate of K_n under practical cell operating conditions, shows that this usually occurs for the gases in a PEM fuel cell when the permeability is in the range of 10^{-16} to 10^{-17} m² and for $\lambda_g/d_p \ll 1$ the Knudsen diffusion effect can be neglected [23].

The effective diffusion coefficient is related to the bulk diffusion coefficient through the MacMullin number and is governed by the equation

$$N_M = D/D_{eff} \tag{5}$$

The MacMullin number is a parameter determined only by the morphology of the GDL and can be expressed as a generalized relationship with tortuosity (τ) and porosity (ϵ):

$$N_M = f(\tau, \epsilon) = \tau^n / \epsilon^m \tag{6}$$

Where n and m are constants that depend on the geometrical model of the porous media; under some conditions of an operating fuel cell, pores in the GDL can be filled with liquid water, which effectively decreases the porosity for the gas stream. To account for this effect, an effective porosity is generally used [24] and described by:

$$\epsilon_{eff} = (1-s)\epsilon \tag{7}$$

Porosity quantifies the reduction in a cross-sectional area available for gaseous transport, while tortuosity characterizes

the convoluted nature of the porous pathways followed by diffusing species. The tortuosity of each sample was estimated using the Bruggeman equation [25]:

$$\tau = \frac{1}{\epsilon^{1/2}} \tag{8}$$

The theoretical determination of tortuosity is model-dependent and extremely cumbersome for all but the simplest geometries. Studies by Springer et al. [26] reveal that the effective tortuous path length for gas diffusion in the cathode backing is about 2.6 times the thickness. The dependence of the permeability of a porous material on its porosity is often described by the Carman–Kozeny equation [27]:

$$K = \frac{\epsilon^3 d_f^2}{16k_{CK}(1-\epsilon)^2} \tag{9}$$

Tamayol and Bahrami predicted that the in-plane permeability of GDLs is directly proportional to its porosity and the fibres diameter squared [28]. The geometry is also correlated to the water and thermal management and was good in a system with high permeability in at least one direction (in-plane or through-plane), while water and thermal management were poor in a system with low permeability in both directions [29]. Observations by Fishman et al. [30] revealed that the GDL has been shown to be an anisotropic and heterogeneous material with transport properties that vary significantly between the in-plane and through-plane directions. Ironically, Gostick et al. [27] claimed that most GDL materials were found to display higher in-plane than through-plane permeability. Measurement of relative permeability of GDL has received little attention; however, some early attempts to measure air relative permeability were reported by Koido et al. [31]. Properties of the GDL such as permeability, porosity, tortuosity and the hydrophobic treatment can affect the degree of flooding, thus changing the total fuel cell performance [8]. The absolute gas permeability of PEM fuel cells using numerous gas diffusion layer (GDL) materials was

measured in three perpendicular directions to investigate the anisotropic properties, and it was observed that most materials were found to display higher in-plane permeability than through-plane. In their study, Hussaini et al. [32] measured the absolute permeability and air–water relative permeability functions for typical fuel cell GDL materials such as Toray carbon paper and E-Tek carbon cloth. Conclusions drawn from this study are that carbon paper materials and absolute permeability in the in-plane directions are found to be higher than their through-plane values by about 18 %, whereas for carbon cloth, through-plane permeability is found to be higher by about 75 %. PEM fuel cell performance may be strongly influenced by in-plane permeability of the GDL [33], and liquid water saturation is found to be a linear function of a capillary number. At a given capillary number, carbon papers show similar saturation in both directions, whereas carbon cloth shows higher saturation in the through-plane than in the in-plane. In general, GDL has a simpler structural configuration than the membrane and catalyst layer. A scanning electron microscope has been used to observe the morphology of the gas diffusion medium, namely carbon cloth and carbon paper as showed in Fig. 3.

Physical characterization of diffusion mediums (Table 1) are characterized by Benziger et al. [34], and their measurements provide details about the pore sizes of different gas diffusion media. Rofaief et al. [35] presented a novel method for measuring heterogeneous through-plane PTFE distributions within the bulk of the GDL using energy dispersive X-ray spectrometry (EDS) imaging.

Electrochemical characteristics of GDL

Electrochemical impedance spectroscopy (EIS) is, perhaps, the most reliable tool for in situ fuel cell characterization [36]. Diffusion can also create impedance called Warburg impedance, which depends on the frequency of the potential perturbation at high frequencies; the Warburg impedance is small since diffusing reactants do not have to move very far and at low frequencies, and the reactants have to diffuse farther, increasing the impedance. The equation for the “infinite” Warburg impedance is:

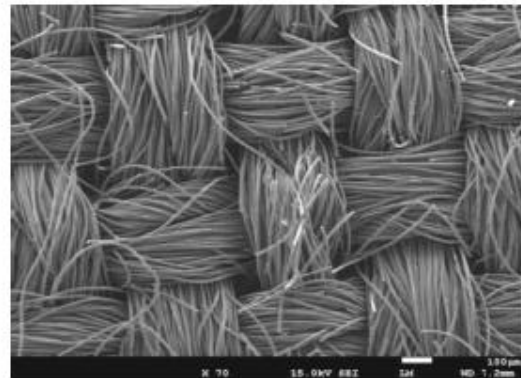
$$Z_W = \sigma(\omega)^{-1/2}(1-j) \quad (10)$$

σ is the Warburg coefficient defined as:

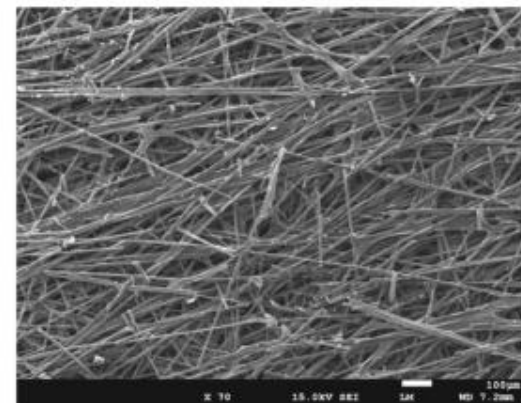
$$\sigma = \frac{RT}{F^2 n^2 A \sqrt{2}} \left(\frac{1}{C^{*O} \sqrt{D_O}} + \frac{1}{C^{*R} \sqrt{D_R}} \right) \quad (11)$$

In which,

- ω radial frequency
- D_O diffusion coefficient of the oxidant
- D_R diffusion coefficient of the reductant



a



b

Fig. 3 SEM image of a carbon cloth and b carbon paper

- A surface area of the electrode
- n number of electrons involved

AC impedance spectroscopy was performed by Springer et al. [26]; the impedance spectra of gas diffusion cathodes are measured under various conditions, and it is inferred that air cathode contains two features: a higher frequency loop or arc determined by interfacial charge-transfer resistance and a lower frequency loop determined by gas-phase transport limitations in the backing.

Carbon paper vs. carbon cloth

A GDL typically consists of a gas diffusion medium (GDM) and a microporous layer (MPL), and carbon cloth or non-woven carbon paper is widely used as a GDM due to its high gas permeability, electronic and heat conductivity. The suitable candidates for diffusion of reactant gases in PEM fuel

Table 1 Physical characterization of diffusion mediums [34]

Media	Dry areal mass (kg/m ²)	Areal mass after liquid water contact (kg/m ²)	Void fraction	Advancing/receding contact angle
Carbon paper (Toray)	0.259±0.007	0.469±0.052	0.72±0.05	115°/30°
Carbon paper + 20 % Teflon	0.374±0.007	0.423±0.035	0.69±0.05	170°/120°
Carbon paper + 40 % Teflon	0.456±0.010	0.525±0.047	0.59±0.05	170°/120°
Carbon paper + 60 % Teflon	0.476±0.009	0.526±0.044	0.50±0.05	170°/120°
Carbon cloth	0.355±0.009	0.484±0.027	0.75±0.05	95°/30°
Carbon cloth + 20 % Teflon	0.476±0.012	0.551±0.047	0.73±0.05	170°/120°
Carbon cloth + 40 % Teflon	0.595±0.011	0.648±0.041	0.68±0.05	170°/120°
Carbon cloth + 60 % Teflon	0.697±0.017	0.839±0.055	0.52±0.05	170°/120°
E-TEK/ELAT electrode	0.435±0.011	0.620±0.036	0.74±0.05	170°/120°

cells is the carbon fibre-based products such as non-woven carbon papers and woven carbon cloths due to their high porosity (>70 %) and electrical conductivity. They are commercially available for many industrial applications and are now being extended to PEM fuel cell applications. The typical properties of these two materials are specified in Table 2.

Gallo Stampino et al. [38] studied the electrical performance of PEM fuel cells with gas diffusion layers made of carbon paper and carbon cloth and demonstrated that carbon paper substrate has superior performance in a vast range of current densities starting from open-circuit voltage to 0.8 A/cm². Sasikumar et al. [39] investigated the performance of gas diffusion electrodes fabricated using carbon paper and carbon cloth and observed better performance when carbon paper was used as the backing material. Their studies showed that the limitation of mass transport was a concern with carbon cloth under non-pressurized operating conditions, especially at higher current densities, due to the higher thickness and density. Yuan-Kai Liao et al. [40] compared the performance of conventional carbon fibre cloth and PAN-based cloth that uses

phenolic resin to improve the characteristics of the gas diffusion layer (GDL). Wang et al. studied the structure–performance relationship of carbon cloth and paper as GDM [37] and revealed that under dry conditions, the carbon paper is found to be better due to its higher tortuous pore structure, which retains product water in the MEA and enhances the membrane conductivity by reducing ohmic loss. However, they have observed that carbon cloth gives a better performance under humidified conditions. The experiment conducted by Williams et al. [41] was also in line with that of Wang et al. stating that the performance of the carbon cloth is superior to that of carbon paper at elevated humidity operations. Park and Popov [42] have analysed the influence of a GDL based on carbon paper/carbon cloth through various electrochemical techniques like mercury porosimetry, surface morphology analysis, polarization techniques, AC impedance spectroscopy, contact angle and water permeation measurement. They have observed that the MEA fabricated using carbon paper exhibited better performance when compared to carbon cloth, because of high water flow resistance owing

Table 2 Comparison of features of carbon paper and carbon cloth [37]

Properties	Method	Carbon paper ^a	Carbon cloth ^b
Thickness (μm)	Callipers at 7 kPa	0.19	0.38
Areal weight (g/m ²)	Gravimetric	85	118
Density (g/cm ³)	At 7 kPa calculated	0.45	0.31
Resistance (through plane, Ω.cm ²)	Two flat graphite blocks at 1.3 MPa	0.009 ^c	0.005 ^c
Bulk resistivity (through plane Ω.cm)	Mercury contacts	0.08	NA
Bulk resistivity (in plane Ω.cm)	Four probe	0.0055 ^d	0.0091 ^d
Gas permeability (through plane, Darcy)	Gurley permeometer	8 ^e	55 ^e
Material description	4301	Toray	Avcarb 1071

^a Reported by Toray (unless indicated otherwise)

^b Reported by Ballard Material Systems (unless indicated otherwise)

^c Measured at general motors (GM), includes diffusion-media bulk resistance and two contact resistances (plate to diffusion media)

^d Measured at GM, uncompressed, average of resistivity in machine and cross-machine direction

^e Measured at GM, uncompressed, 1 Darcy = 10⁻¹² m²

to less permeable macro porous substrate, and more hydrophobic and compact microporous layer. The ac-impedance technique reveals that a microporous layer which has high volume of micropores and more hydrophobic property allows oxygen to diffuse freely towards the catalyst layer due to the effective removal of water from the catalyst layer to the gas flow channels.

Sahu et al. successfully synthesized GDL incorporating a mesoporous carbon with a high specific surface area and pore size [43]. Xie Zhi-yong et al. [44] compared the performance of PEM fuel cells with pyrocarbon and conventional carbon paper composites as GDM. The carbon paper was fabricated using a conventional precursor and coating it with pyrocarbon by pyrolyzing propylene via a chemical vapour deposition (CVD) method. For comparison, conventional carbon paper composites were prepared using PAN-based carbon felt as the precursor followed by impregnation with resin, moulding and thermal treatment. SEM characterization signposted that pyrocarbon was uniformly and tightly bonded on the surface of the fibre; in contrast, cracks were observed in the matrix and debonding of fibres was reported to occur due to carbonization shrinkage in the conventional carbon paper. Measurements showed that the former had much better conductivity and gas permeability than the latter. Additionally, current density–voltage performance revealed that the pyrocarbon coating can also improve the properties of carbon papers used as electrode materials. The carbon fibres of both the cloth and paper are slightly hydrophobic; work must be done to push the water into the hydrophobic pores. The larger the pore, the less work is required to overcome the unfavourable surface energy. Coating the carbon fibres with Teflon makes the pores highly hydrophobic and requires a higher pressure to push the water into the pores. The pressure, P that must be applied to force water into the pores of radius r_{pore} is given by the Young and Laplace equation:

$$\Delta P = \frac{2\gamma_{\text{water}}\cos\theta}{r_{\text{pore}}} \quad (12)$$

Where γ_{water} is the surface tension of water, and θ is the contact angle of water with the surface of the pore [45]. Chunyu Du et al. [46] proposed a new method of fabricating a hierarchy carbon paper with CNTs uniformly grown on carbon fibres and observed it to be good for the self-humidifying PEM fuel cells. They claimed that carbon paper facilitated the self-humidifying characteristics and can be attributed to its higher hydrophobic nature.

Novel gas diffusion medium

So far, limited exploration with other gas diffusion medium apart from carbon cloth and carbon paper is available in the open literature. Few attempts have been made using metallic

thin film as GDM by Fushinobu et al. [47], with micromachined titanium film as GDM due to its high endurance property. A similar sort of experiment was also performed by Hottinen et al. [48] using titanium sinter material and their investigation illustrated the applicability of titanium sinter as a GDM in free-breathing PEM fuel cells. Micromachined silicon has also been used as GDM for microPEM fuel cell applications tested with hydrogen/air [49]. The technique of incorporating sintered stainless steel fibre felt was implemented by Yi et al. [50] and they inferred that the compressive modulus and ductility of GDL were improved. In addition, they claimed that the characteristics of treated stainless steel fibre felt were comparable to carbon paper. Ironically, Glora et al. [51] and Long et al. [http://www.acs.omnibooksonline.com/data/papers/2004_I048.pdf] tried using aerogels to replace conventional GDMs and observed several advantages with aerogels over traditional carbon supports for fuel–cell catalysis including large surface areas (typically $>500 \text{ m}^2/\text{g}$), high-fractional mesoporous pore volumes for gas transport, synthetic control over structural properties and availability in monolithic forms [http://www.acs.omnibooksonline.com/data/papers/2004_I048.pdf]. Glora et al. [51] employed a resorcinol-formaldehyde aerogel with the thickness of less than $500 \mu\text{m}$ and the highest achieved electronic conductivity was about 28 S/cm in an 80 % porous GDL structure. Wang et al.'s experiment [52] was also inline with that of Glora et al. [51], and the carbon aerogel is prepared from a resorcinol-formaldehyde mix by a pyrolysis technique in an inert gas atmosphere, and their properties are in Table 3.

Variation in GDL porosity could result in non-uniform mass transportation and, as a consequence, even a small change in the porosity may severely lower the overall cell current density. In order to circumvent this problem, Roshandel et al. [53] mathematically calculated the porosity variation in the GDL by considering the applied pressure and the amount of water generated in the cell, and they concluded that a decrease in the average porosity causes the reduction in oxygen consumption, resulting in decreased electrical current density. Zhang et al. [54] developed a novel porous gas diffusion medium with improved thermal and electrical conductivity and controllable porosity using MEMS technology. The gas diffusion medium is fabricated with $12.5\text{-}\mu\text{m}$ thick copper foil and by applying a microporous layer (MPL) on it and enhancing the in-plane transport. This novel-designed

Table 3 Properties of carbon aerogels [52]

Parameters	Values
Density (g/cm^3)	0.1–0.6
Surface area (m^2/g)	400–1000
Average pore size (nm)	4–30
Electrical conductivity (S/cm)	1–10

material exhibited multi-functionality such as high thermal and electrical conductivity and controllable permeability.

Treatments in GDM

Treatment methods followed for GDM plays a crucial role in determining the performance of the PEMFCs, and water flooding takes place through the following ways [55]:

- (i) Water vapour from the humidified reactant feeds
- (ii) Product water from cathode side
- (iii) The electro-osmotic drag through the electrolyte membrane.

Carbon substrates used as diffusion media are not generally hydrophobic when received from the supplier, so they are teflonized by pretreating with hydrophobic material usually polytetrafluoroethylene (PTFE) in order to increase the hydrophobicity. Staiti et al. was a pioneer to reveal the relationship between the water transport and the amount of hydrophobic agent in the gas diffusion electrodes [56]. Teflonization is one of the most commonly used methods, by which the gas diffusion media is immersed into an aqueous PTFE suspension where the excess suspension is allowed to drip off, and the remaining solvent is removed by oven drying. Finally, the PTFE is heated above 350 °C to sinter and to bind the PTFE particles onto the GDL surface. The homogeneous PTFE distribution throughout the thickness of the gas diffusion media is very sensitive to the drying process. Rapid drying in a convective oven tends to result in PTFE concentrated in the exposed surfaces of the diffusion media. On the other hand, slow diffusive drying (e.g. air drying) results in the even distribution throughout the bulk [57]. Bevers et al.'s [58] exploratory analysis has led to an imperative conclusion that PTFE content and sinter temperature both correlate negatively with conductivity and positively with hydrophobicity. Park et al. [59] studied the effects of PTFE content in the carbon paper under various operating conditions in a H₂/Air PEMFC system and investigated to explore which driving forces (capillary, shear or evaporation) are dominant in controlling water transport. Their results are summarized in Table 4 at various porosity, which shows that lesser thickness and larger pore diameter in GDM are the factors which support good reactant gas permeation and water management. A similar study by Prasanna et al. [60] was also in line and concluded that the gas permeability and pore diameter of the GDM are the vital factors to be controlled for achieving acceptable performance. In addition, they demonstrated that if hydrophobicity is less, then the reactant gas permeability is affected by poor water removal. However, there would be a severe gas diffusion loss if hydrophobicity is high. The technique of employing

fluorinated ethylene propylene (FEP) for introducing hydrophobicity in GDM was examined by Lim and Wang [61], and they reported that lower polymer content (<10 %) is sufficient to facilitate liquid water removal but at the same time leaves the GDM surfaces relatively accessible for the reactants and product moving in and out. On the contrary, excess of FEP impregnation results in significant blockage of surface pores of carbon paper, highly restricted surface area for the reactant transport and product removal.

Lin and Nguyen [62] also investigated the effect of thickness and hydrophobic polymer content of GDM on flooding and observed that adding PTFE to the GDM could enhance reactant gas and water transport when a cell operates under flooding conditions. On the contrary, excess PTFE can reduce the hydrophilic pathway and make it more difficult for water to diffuse out of the catalyst layer and within the GDM, which results in electrode flooding. Generally, GDM with lower thickness is beneficial due to low gas diffusion loss than materials with higher thickness, whereas very thin GDM is susceptible to mass transfer limitation, contact resistance and losses in mechanical properties. A study by Park et al. [63] indicated that the optimized PTFE content of GDM resulted in an effective water management and improved oxygen gas diffusion kinetics in the membrane-electrode assembly. Pai et al. [64] observed that the usage of carbon tetra fluoride plasma will effectively improve the hydrophobic property of GDM and the plasma treatment can modify the surface morphologies of the wet-proofed GDL to enhance the fuel cell performance without the usage of expensive electro catalytic elements. The method of coating the GDL with an entirely new chemical, namely fluoro alkyl silane (FAS) having strong hydrophobic ligands as well as siloxane bonds was introduced by Yoon et al. [65] and they inferred that FAS-treated carbon paper has an extremely thin and uniform coating surface compared to PTFE, showing that they are firmly formed on carbon fibres without any flaking-off.

Significance of microporous layer (MPL) and its fabrication

A microporous layer (MPL) is a critical component sandwiched between the GDL and the CL and usually comprises of carbon black Teflon as a hydrophobic binder and pore-forming agent. The binders such as Teflon or PTFE serve two functions, namely (i) binding the high-surface-area carbon particles into a cohesive layer and (ii) imparting hydrophobicity to the layer in order to facilitate the removal of water [66]. The MPL also reduces the ohmic resistance between the catalyst layer and the GDM, providing non-permeable support during catalyst deposition and manages liquid water flow during fuel cell operation [15, 67–69]. The micropores in the layer provide sufficient surface pores and hydrophobicity to

Table 4 Effect of PTFE content on gas diffusion medium properties [59]

Gas diffusion medium	Thickness (μm)	PTFE content (wt.%)	Pore diameters (μm)	Porosity (%)	Air permeability ($\text{cm}^3/\text{cm}^2\cdot\text{sec}$)	Break through pressure (kPa)
Carbon paper	190	0	25.933	77.73	7.5	11.25
		5.86	26.19	77.09	15.75	5.57
		17.19	27.43	75.30	17	5.32
		27.19	25.05	71.67	12	5.82
		34.75	24.02	69.45	8.5	6.07
Carbon cloth	250	49.32	20.79	62.85	2.5	7.02
		0	22.09	72.10	6.0	13.21
		4.72	22.49	71.34	9.0	6.48
		14.24	21.10	69.43	6.25	6.91
		27.93	20.94	64.83	6.5	6.97
		28.02	20.77	65.13	5.5	7.02
		44.32	9.18	55.62	1.0	9.39

avoid flooding and also reduce the liquid saturation in the catalyst layer. In addition, the MPL on the anode side can serve as a diffusion barrier, preventing membrane dehydration under low humidity conditions [70]. Another positive impact of adding a MPL is the prevention of diffusion media fibre intrusion into the CL. Due to its critical role in improving water management, prior research efforts [63, 71–73] have been focused on investigating the effect of physical properties of the MPL (i.e. carbon black, hydrophobic agent, thickness, etc.) on fuel cell performance. In addition, it is also intended to prevent the catalyst ink from leaking into the GDM, thereby increasing the catalyst utilization. PEM fuel cell performance can be improved by altering the properties of MPL and this can be achieved by modifying the amounts, nature and characteristics of the above components. Several authors examined diverse properties of the microporous layer for near-saturated ($\sim 100\%$ R.H.) operation in various aspects. PTFE has been the most commonly used hydrophobic agent in the diffusion layer and as its content increases, the porosity decreases, resulting in higher oxygen transport resistance. However, as the PTFE content gets too low, there is inadequate water removal capability and the optimum PTFE content for near-saturated operation was found between 15 and 20 wt.% [41]. If the thickness of the microporous layer is too low, the cell total resistance increases due to an insufficient carbon/PTFE layer to establish good electronic contact between the rough macroporous substrate and the catalyst layer. Thus, it is evident that the thickness of the microporous layer is a critical parameter for fuel cell performance [41]. Different kinds of carbon powder, besides the widely used Vulcan carbon black powder in the microporous layer, have been studied. Acetylene black was found to be superior just because of its characteristics involving surface area, pore volume and pore-size distribution [61]. The microporous carbon layer should have optimum hydrophobicity to remove the product water

effectively from the active layer [74]. Pasaogullari and Wang [70] inferred that placing a MPL between GDL and membrane enhances liquid water removal and reduces the liquid saturation in the catalyst layer. However, analysis of MPL effect is limited to liquid water transport in the cathode gas diffusion medium. Wang et al. [75] performed an extensive characterization on the effect of various carbon powders such as acetylene black, black pearls 2000 and composite carbon black in the microporous layer (MPL) and inferred a superior fuel cell performance with peak power density of $0.91\text{ W}/\text{cm}^2$ with 10 wt.% Black Pearls 2000 in composite carbon black. Giorgi et al. [76] studied the performance operated with both oxygen and air as oxidants with the insertion of MPL in GDL fabrication and observed that GDL porosity decreases considerably with increasing PTFE content. In a similar study, Passalacqua et al. [77] established a better performance when a hydrophobic MPL was used with a hydrogen/air system. Investigation on several carbons, namely Vulcan XC-72, Shawinigan acetylene black (SAB), Mogul L and Asbury 850 graphite with different specific surface areas were used for the diffusion layers. SAB which has a high pore volume and a small average pore size exhibited better performance; this may be attributed to reduced mass transport problems, probably connected to improved water transport.

The remarkable effect of MPL on water management of fuel cells was also explained by Chen et al. [78]. It reveals a more uniform water profile throughout the fuel cell operation, when MPL was used than when it was absent. The effects were particularly imperative for a non-humidified fuel. Karan et al. [79] investigated the effect of a MPL at the cathode on the net water transport in a PEM fuel cell and established that the MPL on the cathode neither enhances back-diffusion nor water removal from the cathode catalyst layer to the gas diffusion medium; their experimental results were in contrary to the frequently asserted hypothesis that the MPL enhances

back-diffusion of water from the cathode to the anode [80]. Studies on the effect of varying carbon loadings in MPL fabrication were carried out to achieve higher performance in PEM fuel cell operation, and there are numerous publications discussing various types of carbon for MPLs [49]. Table 5 shows the properties of various carbons used to fabricate MPL.

Passalacqua et al. [85] investigated the effect of using carbon blacks and graphite as candidates for diffusion layer fabrication in PEMFC electrode and a power density of about 360 mWcm^{-2} in hydrogen-/air-operated at 70°C using SAB as carbon which has a high pore volume and a small average pore size. An improvement in the performance of PEM fuel cell was observed by Jordan [86] and Antolini et al. [87] using MEA with electrode diffusion-layers made from acetylene black as a substitute of Vulcan carbon. Literatures of Wang et al. [75] reveals that a novel MPL prepared with composite carbon black consisting of acetylene black and Black Pearls 2000 (10 wt.%) form an effective bi-functional pore structure and gave a maximum power density of 910 mWcm^{-2} in hydrogen/air operation. An article by Park et al. [88] adopted carbon nanotube (CNT) and carbon nanofibre (CNF) to facilitate thin microlayers and concluded that a composition of 25 % CNF and 75 % Vulcan XC-72 in the microporous layer gives higher performance by enhancing the electronic conductivity and gas permeability. Kannan et al. [89] have also studied the usage of single-walled CNT as an effective MPL for fabricating GDL. The GDL fabricated by the use of pure black carbon (jointly developed by a superior graphite company and Columbian Chemicals Company) exhibits superior performance in hydrogen/air system without any back pressure [64]. The PEM fuel cell performance has been compared using non-processed Ketjenblack EC-600JD and Vulcan XC-72 as the MPL material [90, 91], and better performances were observed with high-surface-area Ketjen black. Apart from the effect of various carbons in MPL preparation on PEM fuel cell performance, researchers have also focused on influence of carbon loading in MPL, and the results accomplished by various researchers in this area have been summarized in Table 6.

Han et al. [92] discussed the influence of PTFE content in the carbon-filled diffusion layer at optimal carbon loadings, and their result reveals that increasing the carbon loading can

reduce the internal resistance of the cell and, hence, improve the fuel cell performance by decreasing the contact resistance between the interfaces of GDL/CL. In addition, it can also reduce the mass transport limitation due to the improvement of water management. However, they also suggest that excessive loading in such carbon-filled GDL would decrease the porosity and increase the concentration over-potential, in particular, in the H_2 /air-fed fuel cell. The results acquired by various researchers by varying PTFE loading in MPL are summarized in Table 7. The literature [67, 92, 93, 96] shows that the pre-eminent performances are obtained with the lowest PTFE loading, but it is not possible to totally eliminate it. Yan et al. [94] used fluorinated ethylene propylene (FEP) as a hydrophobic agent in GDL preparation and achieved the best performance with 20 % FEP content in MPL.

From diverse literatures [72, 74, 97–100], we infer that the use of MPL's typically results in a better fuel cell performance, increases electrical conductivity and improves water management and in turn the power density. MPL improves performance by reducing mass transport limitations, especially with the air feed and also by reducing ohmic losses especially with oxygen feed [76]. Latorrata et al. [101] coated the microporous layers (MPLs) prepared with and without carboxymethylcellulose (CMC), a unique technique, and compared their electrical performances with a single fuel cell. They revealed that at high current density (CD), the CMC-based GDLs suffer water management, and such behaviour was attributed to a hydrophilic character of the GDL due to residual amounts of CMC in MPL coating [101].

Impact of pore former in MPL fabrication

Porosity of the GDL is a critical parameter for determining the mass transport process which in turn impacts PEM fuel cell performance especially at high current density regions for which a pore former such as ammonium bicarbonate, lithium carbonate and sucrose is included during the fabrication process of the diffusion layer. Chebbi et al. [102] studied the effects of pore-size distribution on reactant transport by introducing lithium carbonate as a pore former and suggested that pore distribution should be bi-modal, facilitating the water discharge through large pores and gas diffusion through small pores. However, complete removal of Li-ions from the

Table 5 Physical properties of various carbon blacks used to fabricate MPL [81–84]

Type of carbon	Particle size (nm)	Surface area (m^2/g)	Pore volume (cm^3/g)	Averaged pore radius (μm)
Shawinigan acetylene black (SAB)	40–50	70	0.594	1.7
Vulcan XC-72	30	250	0.489	1.8
Black Pearl 2000 carbon	15	1501.8	2.67	–
Asbury graphite 850	–	13	0.346	3.5
Mogul L	–	140	0.276	6.0

Table 6 Influence of Carbon loading in microporous layer of PEM fuel cell performance [75, 86, 91–95]

Types of carbon powder	Gas diffusion medium	Loading (mg/cm ²)		Reactant	Power density (W/cm ²)	Electrolyte
		Range	Optimum			
Acetylene black	Carbon paper	0.7–2.5	1.25	H ₂ /Air	0.51	Nafion-112
Acetylene black	Carbon paper	0.7–2.5	1.9	H ₂ /Air	0.3	Nafion-112
Acetylene black	Carbon paper	0–2.0	0.5	H ₂ /Air	0.51	Nafion-112
Vulcan XC-72	Carbon paper	0–8.0	6.0	H ₂ /Air	0.48	Nafion-112
Carbon black	Carbon paper	0–4.04	4.04	H ₂ /Air	0.38	Nafion-112
Vulcan XC-72	Carbon paper	1.0–3.0	1.0	H ₂ /Air	0.66	GORE
Vulcan XC-72	Carbon paper	1.5–10.0	3.5	H ₂ /O ₂	0.24	Nafion-115

electrode needs to be ensured and to circumvent these issues. Selvarani et al. [103] introduced sucrose as a pore former during the GDL fabrication process and reported that the un-leached pore former can be easily burned as a carbon during the gas diffusion electrode-backing process. They found the optimum content of pore former in the GDL to be 50 w/o for effective gas transport and product removal. Kong et al. controlled the pore-size distribution by adding isopropyl alcohol and lithium carbonate as a pore former, together with carbon powder and PTFE [98] and followed by the heat treatment led to a dual functionality, namely higher porosity and bimodal water transport. Tang et al. [104] examined the effect of porosity graded microporous layer prepared by using ammonium chloride as pore former. Their result disclosed that, MPL with graded porosity is beneficial for the electrode process of fuel cell reaction by facilitating the liquid water transportation through large pores, increasing the capillary force of graded microporous layer and gas diffusion via small porous in graded microporous layers. Kitahara et al. [105] made a physical analysis compared to the adding of chemical pore former by varying the mean pore diameter of MPL from 1 to 10 μm and observed that the through-plane permeability increases with MPL mean pore size. The performance was investigated at low and high cathode humidity with anode humidification to be 100 % in both cases. At low humidity, the performance was the best where the GDL had the smallest MPL pore size and lowest through-plane permeability because the MPL prevented MEA dehydration. At high humidity, the pre-eminent performance was found using GDLs with a mean

MPL pore diameter of 3 μm and had an intermediate through-plane permeability value as it was also reported in [106]. Such kind of GDLs facilitates the transport of reagents from a gas channel to a catalyst surface as well as water transport from an electrode to the gas phase.

Assessment on compression and thermal conductivity of GDL

GDL compression and thermal conductivity are also significant factors that should be precisely controlled and, as a result, are briefly dealt with. The effects of changing the bolt torque on the performance of a PEM fuel cells gas diffusion layer have been investigated at fixed stoichiometric flow rates for the reactant by Lee et al. [107], and they observed that the thickness of the GDL may also be affected by the amount of torque exerted on the bolts. In addition, the change in GDL thickness during compression can be converted to porosity and the relationship between measured permeability and porosity can be compared. Jiabin Ge et al. [107] performed a similar correlation study on the GDL compression and fuel cell performance by evaluating two different GDL materials. Their experimental results implied that the fuel cell performance decreases with the increase in compression and, in addition, a unique fuel cell test fixture was designed; it was concluded that the effect of GDL compression is significant for both carbon cloth and paper and significantly in the high

Table 7 Effect of PTFE content in microporous layer on PEM fuel cell performance [52, 61, 75, 96]

Gas diffusion medium	Reactants	PTFE (%)		Membrane	Power density (W/cm ²)
		Range	Optimum		
Carbon paper	H ₂ /Air	25–45	35	Nafion-112	0.360
Carbon paper	H ₂ /Air	10–60	30–40	Nafion-112	0.493
Carbon paper	H ₂ /O ₂	10–40	30	Nafion-115	0.250
Carbon paper	H ₂ /Air	10–60	20	Nafion-117	0.360

current density region. GDL is subjected to compressive stress at high temperatures along with polymer electrolyte membrane in the fabrication process and in assembling the fuel cell stacks. Lee et al. [107] asserted from experimental results that an optimal bolt torque was acquired for a soft commercial diffusion layer because of porosity and electrical contact resistance changes. In addition, both the bolt torque and the gas diffusion layer type are significant factors for the PEM fuel cell performance. A similar experiment by Senthil Velan et al. describes that compressive stress decreases the GDL thickness, electrical conductivity, permeability and affects the pores [108]. Lee and Merida studied [109] GDL compressive strain under steady-state and freezing conditions. GDL strain was measured to occur under steady-state aging conditions. An increase in in-plane and through-plane air permeability (18 and 80 %, respectively) was attributed to material loss during permeability measurements and the ex situ tests showed that convective airflow can cause material loss, resulting in increased permeability and further convection. Effective thermal conductivity is also a vital transport parameter that plays an important role in fuel cell performance analysis [110]. A recent study shows that the thermal conductivity increases gradually with the water content [111]. In another study, it has been shown experimentally as well as numerically that a temperature gradient across diffusion media induces additional water transport due to phase change [112–114]. Yablacki et al. examined the anisotropic thermal conductivity of the GDL using the two- and three-dimensional two-phase conjugate fluid–solid thermal lattice Boltzmann model and concluded that the anisotropic structure of the GDL causes anisotropic thermal conductivity, with a higher value for the in-plane thermal conductivity than the through-plane thermal conductivity [112]. Khandelwal and Mench [115] measured the through-plane thermal conductivity of GDLs by examining two dissimilar commercial GDLs with a variety of thicknesses and porosities. They studied the effect of temperature and polytetrafluoroethylene (PTFE) content on the effective thermal conductivity and obtained values in close agreement with the manufacturer data. Ironically, Sadeghi et al. [116] studied on the parameter's that determine the effective thermal conductivity as well as the thermal contact resistance associated with the interface between the GDL and adjacent layers by building a test bed and observed that effective thermal conductivity increases with the compressive load and decreases with an increase with operating temperature, however, independent to ambient air pressure.

Durability of GDL

Durability is one of the most significant issues impeding successful commercialization of PEM fuel cell systems, and studies on GDL degradation and dry operation might provide

more insight into fuel cell performance as there are only a limited number of studies currently in open literature. Specifically, the GDL plays an important role concerning the durability of the MEAs, which is a critical concern for the end users [117] as well as an abnormally high current density which significantly accelerates the deterioration of the gas diffusion medium. Also, corrosion on the GDL will increase resistance and decrease electrical conductivity. Wu et al. compared the physical characteristics of the GDLs before and after corrosion tests and validated that GDLs are susceptible to electrochemical oxidation [118]. Chen et al. [119] performed an effective ex situ method for characterizing electrochemical durability of a gas diffusion layer (GDL). Wood et al. [120] discussed the physical properties required to understand GDL durability and long-term performance for next-generation GDL components. Yi et al. [121] have studied a numerical model for predicting gas diffusion layer failure in proton exchange membrane fuel cells. Correlations between performance loss and deviations in GDL properties might contribute to enhanced understanding on durability.

Results extrapolated from various modelling studies

Dawn M. Bernardi and Mark W. Verbrugge [122] were the pioneers in performing the one-dimensional model on the gas diffusion medium. They modelled both membrane and gas diffusion electrodes so that it follows extensions to account for heat transfer and pressure gradients. In their subsequent research, they claimed that the anode diffusion layer needs to be included in the cell model to properly account for water transport. It is referred to as BV, and the value of the gas diffusion electrode thickness is 0.26 mm [123].

One of the initially used PEFC models capable of predicting both membrane resistance and water balance is described by Springer et al. [124]. Preliminary research papers on GDL modelling used the Bruggeman expression, which determines an effective diffusive coefficient in porous medium by multiplying the binary gas coefficient by $\epsilon^{1.5}$ [124], and these approximations were initiated by De La Rue and Tobias [125] to hold for conduction through a heterogeneous mixture of random non-conducting spheres. Forthcoming, modelling works have revealed that mass transport in the gas diffusion porous medium constitutes a significant performance loss in the fuel cell, especially when liquid water is present [23, 68, 124].

Chiang and Chu [126] investigated the effects of transport phenomena and performance of PEM fuel cells by using a three-dimensional model and found that a thin GDL generates more current at low cell voltage due to the merits of better reactant gas transport and liquid water delivery.

Um et al. [127] developed a computational fuel cell dynamics model, and their results show that forced convection of

gases through GDL helps to improve performance at high current densities. Gurau et al. [128] presented a computational fluid dynamic model to capture multiphase phenomena at the cathode gas diffusion layer–channel interface, and their analyses provides insight for designing diffusion media with controlled structural properties at the interface with the channel, such as pore-size distribution or pattern of orifices punctured during the fabrication process.

Yi et al. [121] studied a numerical model for predicting gas diffusion layer failure in proton exchange membrane fuel cells basic mechanism and concluded that assembly pressure on the bipolar plate should be below 2.0 MPa to ensure the integrity of GDL. Zhou et al. [129] developed a numerical model and observed that large GDL compression deformation and porosity variation reduced the transport ability of the reactant gas and liquid water in the GDL. Sadeghi et al. [116] also proposed a model to compute the thermal resistances, which was in line with experimental data over a wide range of compressive loads from 0.2 to 1.5 MPa. Table 8 provides the transport equations for the gas and liquid phase in GDL. Wang et al. [130] presented a novel model that encompasses both single- and two-phase regimes and concluded that transport of both liquid and vapour water is controlled by capillary action and molecular diffusion, respectively, due to negligible small air velocity within the porous GDL.

The potential distribution in the GDL is described by [135]:

$$\frac{1}{\rho_x} \frac{\partial^2 \varphi}{\partial x^2} + \frac{1}{\rho_y} \frac{\partial^2 \varphi}{\partial y^2} = 0 \tag{19}$$

The boundary conditions are

$$x = 0, \quad 0yh : \frac{\partial \varphi}{\partial x} = 0$$

$$x = \frac{d_r + d_c}{2}, \quad 0yh : \frac{\partial \varphi}{\partial x} = 0$$

$$y = h, \quad 0x < \frac{d_r}{2} : \varphi = U_{out}$$

$$y = h, \quad \frac{d_r}{2}x < \frac{d_r + d_c}{2} : \frac{\partial \varphi}{\partial y} = 0$$

Nitta et al. [136] developed a two-dimensional model to study the effects of inhomogeneous compression of GDLs on local transport phenomena within a PEM fuel cell and predicted a uniform temperature profile along the active area, with a variation of ca. 1 °C. The compressed GDL thickness under the rib affects the current density distribution and the temperature profile. Su et al. [137] investigated numerically and developed a three-dimensional model to analyse the

Table 8 Transport equations in GDL [13, 128, 131–134]

	For gas phase	For liquid phase
Mass	$\frac{\partial(\epsilon_s \rho_g \rho_g)}{\partial t} + \nabla(\epsilon_s U_g \rho_g) = \epsilon_s (S^{themp} - S^{gcond})$ (13)	$\frac{\partial(\epsilon_l \rho_l \rho_l)}{\partial t} + \nabla(\epsilon_l U_l \rho_l) = \epsilon_l (-S^{themp} + S^{gcond})$ (14)
Momentum	$\frac{\partial(\epsilon_s U_g \rho_g)}{\partial t} = -\epsilon_s S_g \nabla \rho_g + \epsilon_s S_g \frac{\partial U_g}{\partial x} + \epsilon_s (S^{themp} U_g + \epsilon_s (S^{gcond} U_g))$ (15)	$\frac{\partial(\epsilon_l U_l \rho_l)}{\partial t} = -\epsilon_l S_l (\nabla \rho_l + \nabla \rho_c + \nabla \rho_e) + \epsilon_l S_l \frac{\partial U_l}{\partial x} + \epsilon_l (S^{themp} U_l - S^{gcond} U_l)$ (16)
Oxygen	$\frac{\partial(\epsilon_s Y_{O_2} \rho_g)}{\partial t} + \nabla(\epsilon_s Y_{O_2} U_g \rho_g) - \nabla(\epsilon_s D_{O_2} \rho_g \nabla Y_{O_2}) = 0$ (17)	
Water vapour	$\frac{\partial(\epsilon_s Y_{H_2O} \rho_g)}{\partial t} + \nabla(\epsilon_s Y_{H_2O} U_g \rho_g) - \nabla(\epsilon_s D_{H_2O} \rho_g \nabla Y_{H_2O}) = \epsilon_s (S^{themp} - S^{gcond})$ (18)	

Table 9 Difference in general characteristics of carbon cloth and paper observed from literatures

Carbon papers	Carbon cloth
Quite brittle	Mechanically robust
Less thickness and causes less ohmic loss	High thickness and causes high ohmic loss
Optimal for non-humid operation	Optimal for humid operation
Very little compressibility	Good compressibility

impact of transport properties of the GDL, specifically porosity and permeability. Three different configurations of transport properties were tested, i.e. uniform uncompressed GDL properties, uniform compressed GDL properties and non-homogeneous GDL properties and found that the non-homogeneous structure shows noticeable differences in predicted cell performance. Dotelli et al. [138] compared two gas diffusion layers of PEM fuel cells based on the same carbon cloth substrate, coated with microporous layers of different hydrophobicities assembled in. Each configuration of polarization curves were recorded; in order to evaluate the role of different GDLs, AC impedance spectroscopy of the running cell was also performed and inferred that higher compression ratio worsened the cell performances at a higher temperatures and the presence of the microporous layer onto the carbon cloth resulted in extremely beneficial operations especially at high current density. Moreover, it sensibly reduces the high frequency resistance. Pasaogullari et al. developed an analytical model and inferred that capillary transport is the dominant transport process to remove water from flooded GDLs. In addition, flooding diminishes the cell performance as a result of decreased oxygen transport and surface coverage of active catalyst by liquid water [139]. Modelling of GDL by lattice Boltzmann simulation technique for understanding the behaviour of two-phase flow of complex fluid in porous medium was studied by Koido et al. [31] and Tabe et al. [140], and they asserted that capillary–pressure saturation relationship and wettability of the channel are the two phenomena that can severely influence the GDL performance. Investigation on the anisotropic permeability of a carbon cloth GDL [141] based on the integration of X-ray micro-tomography and lattice Boltzmann (LB) simulation was performed by Rama et al., and their results demonstrated that the simulated through-plane permeability is about four times higher than the in-plane permeability. The simulated results are also applied to generate a parametric coefficient for the Kozeny–Carman (KC) method of determining permeability. Niu et al. [4] examined a model to simulate water–gas transportations in the GDL based on the diffuse interface theory and employed two distributions so that multiphase flows with large density ratios and various viscosities can be controlled. To numerically realize the boundary conditions for the complicated structure like GDL, besides the standard bounce back condition used for the nonslip condition, an approximated average scheme

based on the extrapolation method is derived to mimic wetting boundaries.

Summary and recommendation

Dynamic behaviour is a key property of PEM fuel cells to be used for automotive application [142], and the structural design of GDL significantly influences the dynamic response [143]. From the various studies in open literature [42–57], it is observed that though carbon cloth and carbon paper have their own pros and cons, carbon paper has been recommended by most of the authors especially for low humidity operation and carbon cloth for high humidity operation. The worst performance of the carbon cloth is likely to be attributed to contact resistances; however, at high current density, carbon papers have some issues pertaining to water management. The modified carbon fibre cloth can eliminate assembly difficulties with a relatively low resin content and exhibits good through-plane resistance, resulting in good cell performance [40]. Carbon papers are brittle and quite compressible and, as results, are good for designs where a tighter tolerance is permitted in the compression and where the thin GDL is a critical factor. However, in general characteristics such as fraction of hydrophobic pore-size distribution, gas permeability, surface morphology and electronic resistivity predominantly defines the functionality of the GDL, despite the fact that some limitations may occur for measurement of each quantities. Table 9 provides a difference in characteristics of carbon cloth and paper perceived from various literatures.

The cathode electrochemical reactions produce a large amount of liquid water at low-operating voltages, and if the liquid water is not appropriately purged it may accumulate in the pores of the diffusion layers and restrict the oxygen transport to the gas diffusion and the catalyst layer, thereby reducing the reaction rate. Diffusion media characterization and development still rely heavily on in situ testing because well-established correlations between in situ performance results and ex situ characterization data are not yet available. The carbon cloth is the most flexible and is generally robust but results in higher ohmic loss due to its thickness and, in contrast, novel materials like pyrocarbons are yet to achieve significant performance levels. Modified carbon paper can be a clear winner among the gas diffusion layer if precise water

management strategies and gas flow designs are formulated. Increased carbon loadings in MPL can reduce contact resistance between the interfaces of GDL/catalyst layer and hence improve the fuel cell performance. However, excessive carbon loading in GDL tends to decrease the porosity and increase the concentration over potential, in particular, for hydrogen/air-fed PEM fuel cell, which is due to an increased diffusion path in carbon-filled GDL. Hence, care should be taken for carbon loading in GDL fabrication for attaining optimal performance. An optimized carbon loading had a significant positive impact on the PEMFC performance. Acetylene black was chosen for most MPLs because of the favourable combination of water management and corrosion resistance [144]. Assessment of cathode and anode GDL has been performed by several authors, and it has been concluded that the cathode GDL determines the maximum possible current and power density [26, 145, 146]. Transport equations pertinent to GDL [13, 128, 131–134] clarified the impact of operational parameters on the thermal properties of GDLs and provided new insights on the importance of a key interfacial phenomenon. Flooding can drastically decline the fuel cell performance by hindering the gas diffusion and blocking the electro-catalyst sites [139]. In specific, cathode flooding can result in a catastrophic decrease of performance by reducing the oxygen transport to the reaction sites and decreasing the effective catalyst area which has been observed over a wide range of operating conditions. Cathode flooding can be detected experimentally and significantly depends on GDL properties (e.g. porosity and hydrophobicity) [147–150]. In a hydrophilic GDL, there would be no restriction to liquid flow and it would begin with any applied pressure and, for example, thick diffusion layer attributes to a long reactant transport passage and the flooding problem, whereas thin layers are susceptible to mass transfer and contact resistance losses. Another significant factor studied from the review is that the contact resistance could be higher between the bipolar plates and the GDLs due to the flow channels compared to that between GDLs and catalyst layers. Materials with the most highly aligned fibres showed the highest anisotropy and the permeability. There is a lack of fundamental experiments on water transport in GDLs, and the most challenging issue in the GDL fabrication is to develop a compatible GDL for both hydrophilic and hydrophobic operations. GDL components of PEMFCs degrade in different manners, and the mechanisms involved in the degradation are not completely implicit. This might be because there are different techniques employed in preparing those functional components and operating conditions are not well declared. The various mechanisms are related, so one degradation mechanism may trigger or exacerbate another. Future designs could integrate the GDL, current collector and flow field to be manufactured seamlessly by automated MEMS processes [54], and this would be a key to address numerous challenges including the hydrophilic and hydrophobic conditions. The

forementioned details evidently validate the role of GDL in the design and performance of the PEM fuel cells, especially pertaining to the characteristics, fabrication techniques and related components. Incorporation of carbon nanotube as gas diffusion electrode for the next-generation PEM fuel cells due to its exceptionally high transport rates are shown to be as a result of the inherent smoothness of the nanotubes [151] and will be one of the cornerstones of the cutting edge research and may guide PEM fuel cells to a successful level of commercialization.

Conclusions

Despite its critical function, the role of GDL in PEM fuel cell performance is not well asserted and this has been an impetus for the authors to review the GDL characteristics, geometry, fabrication techniques and related components. The best components for each functionality cannot make the best GDL; a trade-off between the properties will evolve the ideal GDL. The review of the authors may pave the way for the future research to be concentrated on a holistic approach in the evolution of GDL.

Acknowledgments This work was supported by the IBTeC, Auckland University of Technology (AUT) grant by the Doctoral Fellowship and the authors would like to acknowledge their support. The authors are also grateful to Ms. Jo Stone for an effective proofreading.

References

- Pethaiah SS, Kalaighan GP, Ulaganathan M, Arunkumar J (2011) Preparation of durable nanocatalyzed MEA for PEM fuel cell applications. *Ionics* 17(4):361–366
- Chiu L-Y, Diong B, Genmen RS (2004) An improved small-signal model of the dynamic behavior of PEM fuel cells. *IEEE Trans Ind Appl* 40(4):970–977
- Tang H, Peikang S, Jiang SP, Wang F, Pan M (2007) A degradation study of Nafion proton exchange membrane of PEM fuel cells. *J Power Sources* 170(1):85–92. doi:10.1016/j.jpowsour.2007.03.061
- Niu X-D, Munekata T, Hyodo S-A, Suga K (2007) An investigation of water-gas transport processes in the gas-diffusion-layer of a PEM fuel cell by a multiphase multiple-relaxation-time lattice Boltzmann model. *J Power Sources* 172(2):542–552
- Berning T, Lu DM, Djilali N (2002) Three-dimensional computational analysis of transport phenomena in a PEM fuel cell. *J Power Sources* 106(1–2):284–294. doi:10.1016/S0378-7753(01)01057-6
- Neergat M, Shukla A (2002) Effect of diffusion-layer morphology on the performance of solid-polymer-electrolyte direct methanol fuel cells. *J Power Sources* 104(2):289–294
- Secanell M, Songprakorp R, Djilali N, Suleman A (2010) Optimization of a proton exchange membrane fuel cell membrane electrode assembly. *Struct Multidiscip Optim* 40(1–6):563–583
- Shimpalee S, Beuscher U, Van Zee JW (2007) Analysis of GDL flooding effects on PEMFC performance. *Electrochim Acta* 52(24):6748–6754. doi:10.1016/j.electacta.2007.04.115

9. Cho J, Oh H, Park J, Min K, Lee E, Jyoung J-Y (2014) Effect of the micro porous layer design on the dynamic performance of a proton exchange membrane fuel cell. *Int J Hydrog Energy* 39(1): 459–468
10. Wilson MS, Valerio JA, Gottesfeld S (1995) Low platinum loading electrodes for polymer electrolyte fuel cells fabricated using thermoplastic ionomers. *Electrochim Acta* 40(3):355–363
11. Spiegel C (2011) PEM fuel cell modeling and simulation using MATLAB. Academic
12. Jordan L, Shukla A, Behrsing T, Avery N, Muddle B, Forsyth M (2000) Effect of diffusion-layer morphology on the performance of polymer electrolyte fuel cells operating at atmospheric pressure. *J Appl Electrochem* 30(6):641–646
13. Gurau V, Blumle MJ, De Castro ES, Tsou Y-M, Zawodzinski TA Jr, Mann JA Jr (2007) Characterization of transport properties in gas diffusion layers for proton exchange membrane fuel cells: 2. Absolute permeability. *J Power Sources* 165(2):793–802. doi:10.1016/j.jpowsour.2006.12.068
14. Wishart J, Dong Z, Secanell M (2006) Optimization of a PEM fuel cell system based on empirical data and a generalized electrochemical semi-empirical model. *J Power Sources* 161(2):1041–1055
15. Paganin V, Ticianelli E, Gonzalez E (1996) Development and electrochemical studies of gas diffusion electrodes for polymer electrolyte fuel cells. *J Appl Electrochem* 26(3):297–304
16. Tan Z, Jia L, Zhang Z (2011) A study on the transport process in gas diffusion layer of proton exchange membrane fuel cells. *J Therm Sci* 20(5):449–453
17. Rohling J, Shen J, Wang C, Zhou J, Gu C (2007) Determination of binary diffusion coefficients of gases using photothermal deflection technique. *Appl Phys B* 87(2):355–362
18. Johnson MF, Stewart WE (1965) Pore structure and gaseous diffusion in solid catalysts. *J Catal* 4(2):248–252
19. Nam JH, Kaviani M (2003) Effective diffusivity and water-saturation distribution in single and two-layer PEMFC diffusion medium. *Int J Heat Mass Transf* 46(24):4595–4611
20. Pharoah J, Karan K, Sun W (2006) On effective transport coefficients in PEM fuel cell electrodes: anisotropy of the porous transport layers. *J Power Sources* 161(1):214–224
21. Liu F, Wang C-Y (2006) Optimization of cathode catalyst layer for direct methanol fuel cells: part II: computational modeling and design. *Electrochim Acta* 52(3):1409–1416
22. Kast W, Hohenthanner C-R (2000) Mass transfer within the gas-phase of porous media. *Int J Heat Mass Transf* 43(5):807–823
23. Djilali N, Lu D (2002) Influence of heat transfer on gas and water transport in fuel cells. *Int J Therm Sci* 41(1):29–40
24. Martínez-Rodríguez MJ, Cui T, Shimpakee S, Seraphin S, Duong B, Van Zee JW (2012) Effect of microporous layer on MacMullin number of carbon paper gas diffusion layer. *J Power Sources* 207: 91–100. doi:10.1016/j.jpowsour.2012.01.132
25. Van Brakel J, Heertjes P (1974) Analysis of diffusion in macroporous media in terms of a porosity, a tortuosity and a constrictivity factor. *Int J Heat Mass Transf* 17(9):1093–1103
26. Springer T, Zawodzinski T, Wilson M, Gottesfeld S (1996) Characterization of polymer electrolyte fuel cells using AC impedance spectroscopy. *J Electrochem Soc* 143(2):587–599
27. Gostick JT, Fowler MW, Pritzker MD, Ioannidis MA, Behra LM (2006) In-plane and through-plane gas permeability of carbon fiber electrode backing layers. *J Power Sources* 162(1):228–238. doi:10.1016/j.jpowsour.2006.06.096
28. Tamayol A, Bahrami M (2011) In-plane gas permeability of proton exchange membrane fuel cell gas diffusion layers. *J Power Sources* 196(7):3559–3564
29. Ahmed DH, Sung HJ, Bae J (2008) Effect of GDL permeability on water and thermal management in PEMFCs—I. Isotropic and anisotropic permeability. *Int J Hydrog Energy* 33(14):3767–3785
30. Fishman Z, Hinebaugh J, Bazyak A (2010) Microscale tomography investigations of heterogeneous porosity distributions of PEMFC GDLs. *J Electrochem Soc* 157(11):B1643–B1650
31. Koido T, Furusawa T, Moriyama K, Takato K (2006) Two-phase transport properties and transport simulation of the gas diffusion layer of a PEFC. *ECS Trans* 3(1):425–434
32. Hussaini I, Wang C (2010) Measurement of relative permeability of fuel cell diffusion media. *J Power Sources* 195(12):3830–3840
33. Feser J, Prasad A, Advani S (2006) Experimental characterization of in-plane permeability of gas diffusion layers. *J Power Sources* 162(2):1226–1231
34. Benziger J, Nehlsen J, Blackwell D, Brennan T, Iescu J (2005) Water flow in the gas diffusion layer of PEM fuel cells. *J Membr Sci* 261(1):98–106
35. Rofaiel A, Ellis J, Challa P, Bazyak A (2012) Heterogeneous through-plane distributions of polytetrafluoroethylene in polymer electrolyte membrane fuel cell gas diffusion layers. *J Power Sources* 201:219–225
36. Hirschorn B, Tribollet B, Orazem ME (2008) On selection of the perturbation amplitude required to avoid nonlinear effects in impedance measurements. *Isr J Chem* 48(3–4):133–142
37. Wang Y, Wang C-Y, Chen K (2007) Elucidating differences between carbon paper and carbon cloth in polymer electrolyte fuel cells. *Electrochim Acta* 52(12):3965–3975
38. Stampino PG, Omati L, Dotelli G (2011) Electrical performance of PEM fuel cells with different gas diffusion layers. *J Fuel Cell Sci Technol* 8(4):041005
39. Sasikumar G, Ryu H (2003) Comparison of electrode backing materials for polymer electrolyte membrane fuel cells. *J Korean Electrochem Soc* 6(No.3):183–186
40. Liao Y-K, Ko T-H, Liu C-H (2008) Performance of a polymer electrolyte membrane fuel cell with fabricated carbon fiber cloth electrode. *Energy Fuel* 22(5):3351–3354
41. Williams MV, Begg E, Bonville L, Kunz HR, Fenton JM (2004) Characterization of gas diffusion layers for PEMFC. *J Electrochem Soc* 151(8):A1173–A1180
42. Park S, Popov BN (2011) Effect of a GDL based on carbon paper or carbon cloth on PEM fuel cell performance. *Fuel* 90(1):436–440
43. Sahu A, Nishanth K, Selvarani G, Sridhar P, Pitchumani S, Shukla A (2009) Polymer electrolyte fuel cells employing electrodes with gas-diffusion layers of mesoporous carbon derived from a sol-gel route. *Carbon* 47(1):102–108
44. Xie Z-Y, Jin G-Y, Zhang M, Su Z-A, Zhang M-Y, Chen J-X, Huang Q-Z (2010) Improved properties of carbon fiber paper as electrode for fuel cell by coating pyrocarbon via CVD method. *Trans Nonferrous Metals Soc China* 20(8):1412–1417
45. Wang C-Y (2004) Fundamental models for fuel cell engineering. *Chem Rev* 104(10):4727–4766
46. Du C, Wang B, Cheng X (2009) Hierarchy carbon paper for the gas diffusion layer of proton exchange membrane fuel cells. *J Power Sources* 187(2):505–508. doi:10.1016/j.jpowsour.2008.11.046
47. Fushinobu K, Takahashi D, Okazaki K (2006) Micromachined metallic thin films for the gas diffusion layer of PEFCs. *J Power Sources* 158(2):1240–1245
48. Hottinen T, Mikkola M, Mennola T, Lund P (2003) Titanium sinter as gas diffusion backing in PEMFC. *J Power Sources* 118(1):183–188
49. Modroukas D, Modi V, Fréchet LG (2005) Micromachined silicon structures for free-convection PEM fuel cells. *J Micromech Microeng* 15(9):S193
50. Yi P, Peng L, Lai X, Li M, Ni J (2012) Investigation of sintered stainless steel fiber felt as gas diffusion layer in proton exchange membrane fuel cells. *Int J Hydrog Energy* 37(15):11334–11344. doi:10.1016/j.ijhydene.2012.04.161
51. Giora M, Wiener M, Petričević R, Pröbstle H, Fricke J (2001) Integration of carbon aerogels in PEM fuel cells. *J Non-Cryst Solids* 285(1):283–287

52. Wang J, Glora M, Petricevic R, Saliger R, Proebstle H, Fricke J (2001) Carbon cloth reinforced carbon aerogel films derived from resorcinol formaldehyde. *J Porous Mater* 8(2): 159–165
53. Roshandel R, Farhanieh B, Saievar-Iranizad E (2005) The effects of porosity distribution variation on PEM fuel cell performance. *Renew Energy* 30(10):1557–1572
54. Zhang F-Y, Advani SG, Prasad AK (2008) Performance of a metallic gas diffusion layer for PEM fuel cells. *J Power Sources* 176(1): 293–298
55. Ren X, Gottesfeld S (2001) Electro-osmotic drag of water in poly(perfluorosulfonic acid) membranes. *J Electrochem Soc* 148(1): A87–A93
56. Staiti P, Poltarzewski Z, Alderucci V, Maggio G, Giordano N, Fasulo A (1992) Influence of electrode properties on water management in a solid polymer electrolyte fuel cell. *J Appl Electrochem* 22(7):663–667
57. Quick C, Ritzinger D, Lehnert W, Hartnig C (2009) Characterization of water transport in gas diffusion media. *J Power Sources* 190(1):110–120
58. Bevers D, Rogers R, Von Bradke M (1996) Examination of the influence of PTFE coating on the properties of carbon paper in polymer electrolyte fuel cells. *J Power Sources* 63(2): 193–201
59. Park G-G, Sohn Y-J, Yang T-H, Yoon Y-G, Lee W-Y, Kim C-S (2004) Effect of PTFE contents in the gas diffusion media on the performance of PEMFC. *J Power Sources* 131(1):182–187
60. Prasanna M, Ha H, Cho E, Hong S-A, Oh I-H (2004) Influence of cathode gas diffusion media on the performance of the PEMFCs. *J Power Sources* 131(1):147–154
61. Lim C, Wang C (2004) Effects of hydrophobic polymer content in GDL on power performance of a PEM fuel cell. *Electrochim Acta* 49(24):4149–4156
62. Lin G, Van Nguyen T (2005) Effect of thickness and hydrophobic polymer content of the gas diffusion layer on electrode flooding level in a PEMFC. *J Electrochem Soc* 152(10):A1942–A1948
63. Park S, Lee J-W, Popov BN (2008) Effect of PTFE content in microporous layer on water management in PEM fuel cells. *J Power Sources* 177(2):457–463
64. Pai Y, Ke J, Huang H, Lee C, Zen J, Shieu F (2006) CF4 plasma treatment for preparing gas diffusion layers in membrane electrode assemblies. *J Power Sources* 161(1):275–281
65. Yoon GH, Park SB, Kim EH, Kim S, Park Y-I (2007) Effect of fluoroalkylsilane coating on the properties of gas diffusion layer in PEMFCs. In: Meeting Abstracts, vol 20. The Electrochemical Society, pp 898–898
66. Thoben B, Siebke A (2004) Influence of different gas diffusion layers on the water management of the PEFC cathode. *J New Mater Electrochem Syst* 7(1):13–20
67. Lee H-K, Park J-H, Kim D-Y, Lee T-H (2004) A study on the characteristics of the diffusion layer thickness and porosity of the PEMFC. *J Power Sources* 131(1):200–206
68. Mathias M, Roth J, Fleming J, Lehnert W (2003) Diffusion media materials and characterisation. *Handbook of fuel cells*
69. Rajalakshmi N, Velayutham G, Ramya K, Subramaniam C, Dhathathreyan K Characterisation and optimisation of low cost activated carbon fabric as a substrate layer for PEMFC electrodes. In: ASME 2005 3rd International Conference on Fuel Cell Science, Engineering and Technology, 2005. American Society of Mechanical Engineers, pp 169–173
70. Passagullari U, Wang C-Y (2004) Two-phase transport and the role of micro-porous layer in polymer electrolyte fuel cells. *Electrochim Acta* 49(25):4359–4369
71. Nakajima H, Konomi T, Kitahara T (2007) Direct water balance analysis on a polymer electrolyte fuel cell (PEFC): effects of hydrophobic treatment and micro-porous layer addition to the gas diffusion layer of a PEFC on its performance during a simulated start-up operation. *J Power Sources* 171(2):457–463. doi:10.1016/j.jpowsour.2007.06.004
72. Weber AZ, Newman J (2005) Effects of microporous layers in polymer electrolyte fuel cells. *J Electrochem Soc* 152(4):A677–A688
73. Ihonen J, Mikkola M, Lindbergh G (2004) Flooding of gas diffusion backing in PEFCs: physical and electrochemical characterization. *J Electrochem Soc* 151(8):A1152–A1161
74. Velayutham G, Kaushik J, Rajalakshmi N, Dhathathreyan K (2007) Effect of PTFE content in gas diffusion media and microlayer on the performance of PEMFC tested under ambient pressure. *Fuel Cells* 7(4):314–318
75. Wang X, Zhang H, Zhang J, Xu H, Tian Z, Chen J, Zhong H, Liang Y, Yi B (2006) Micro-porous layer with composite carbon black for PEM fuel cells. *Electrochim Acta* 51(23):4909–4915
76. Giorgi L, Antolini E, Pozio A, Passalacqua E (1998) Influence of the PTFE content in the diffusion layer of low-Pt loading electrodes for polymer electrolyte fuel cells. *Electrochim Acta* 43(24):3675–3680
77. Passalacqua E, Lufano F, Squadrito G, Patti A, Giorgi L (1998) Influence of the structure in low-Pt loading electrodes for polymer electrolyte fuel cells. *Electrochim Acta* 43(24):3665–3673
78. Chen J, Matsuura T, Hori M (2004) Novel gas diffusion layer with water management function for PEMFC. *J Power Sources* 131(1): 155–161
79. Karan K, Atiyeh H, Phoenix A, Halliop E, Pharoah J, Peppley B (2007) An experimental investigation of water transport in PEMFCs: the role of microporous layers. *Electrochem Solid-State Lett* 10(2): B34–B38
80. Lin G, Van Nguyen T (2006) A two-dimensional two-phase model of a PEM fuel cell. *J Electrochem Soc* 153(2):A372–A382
81. Ong AL, Bottino A, Capannelli G, Comite A (2008) Effect of preparative parameters on the characteristic of poly(vinylidene fluoride)-based microporous layer for proton exchange membrane fuel cells. *J Power Sources* 183(1):62–68
82. Chen J, Xu H, Zhang H, Yi B (2008) Facilitating mass transport in gas diffusion layer of PEMFC by fabricating micro-porous layer with dry layer preparation. *J Power Sources* 182(2):531–539
83. Hung T, Huang J, Chuang H, Bai S, Lai Y, Chen-Yang Y (2008) Highly efficient single-layer gas diffusion layers for the proton exchange membrane fuel cell. *J Power Sources* 184(1):165–171
84. Andersen SM, Borghei M, Lund P, Elina Y-R, Pasanen A, Kauppinen E, Ruiz V, Kauranen P, Skou EM (2013) Durability of carbon nanofiber (CNF) & carbon nanotube (CNT) as catalyst support for proton exchange membrane fuel cells. *Solid State Ionics* 231:94–101
85. Passalacqua E, Squadrito G, Lufano F, Patti A, Giorgi L (2001) Effects of the diffusion layer characteristics on the performance of polymer electrolyte fuel cell electrodes. *J Appl Electrochem* 31(4): 449–454
86. Jordan L, Shukla A, Behring T, Avery N, Muddle B, Forsyth M (2000) Diffusion layer parameters influencing optimal fuel cell performance. *J Power Sources* 86(1):250–254
87. Antolini E, Passos R, Ticianelli EA (2002) Effects of the carbon powder characteristics in the cathode gas diffusion layer on the performance of polymer electrolyte fuel cells. *J Power Sources* 109(2):477–482
88. Park G-G, Sohn Y-J, Yim S-D, Yang T-H, Yoon Y-G, Lee W-Y, Eguchi K, Kim C-S (2006) Adoption of nano-materials for the micro-layer in gas diffusion layers of PEMFCs. *J Power Sources* 163(1):113–118
89. Kannan AM, Menghal A, Barsukov IV (2006) Gas diffusion layer using a new type of graphitized nano-carbon PUREBLACK® for proton exchange membrane fuel cells. *Electrochem Commun* 8(5): 887–891

90. Song Y, Wei Y, Xu H, Williams M, Liu Y, Bonville LJ, Russell Kunz H, Fenton JM (2005) Improvement in high temperature proton exchange membrane fuel cells cathode performance with ammonium carbonate. *J Power Sources* 141(2):250–257
91. Park S, Lee J-W, Popov BN (2006) Effect of carbon loading in microporous layer on PEM fuel cell performance. *J Power Sources* 163(1):357–363
92. Han M, Chan S, Jiang S (2006) Development of carbon-filled gas diffusion layer for polymer electrolyte fuel cells. *J Power Sources* 159(2):1005–1014
93. Qi Z, Kaufman A (2002) Improvement of water management by a microporous sublayer for PEM fuel cells. *J Power Sources* 109(1): 38–46
94. Yan W-M, Hsueh C-Y, Soong C-Y, Chen F, Cheng C-H, Mei S-C (2007) Effects of fabrication processes and material parameters of GDL on cell performance of PEM fuel cell. *Int J Hydrog Energy* 32(17):4452–4458
95. Song J, Cha S, Lee W (2001) Optimal composition of polymer electrolyte fuel cell electrodes determined by the AC impedance method. *J Power Sources* 94(1):78–84
96. Wang X, Zhang H, Zhang J, Xu H, Zhu X, Chen J, Yi B (2006) A bi-functional micro-porous layer with composite carbon black for PEM fuel cells. *J Power Sources* 162(1):474–479
97. Lufano F, Passalacqua E, Squadrito G, Patì A, Giorgi L (1999) Improvement in the diffusion characteristics of low Pt-loaded electrodes for PEMFCs. *J Appl Electrochem* 29(4):445–448
98. Kong CS, Kim D-Y, Lee H-K, Shul Y-G, Lee T-H (2002) Influence of pore-size distribution of diffusion layer on mass-transport problems of proton exchange membrane fuel cells. *J Power Sources* 108(1):185–191
99. Cindrella L, Kannan A, Lin J, Saminathan K, Ho Y, Lin C, Wertz J (2009) Gas diffusion layer for proton exchange membrane fuel cells—a review. *J Power Sources* 194(1):146–160
100. Janssen GJM, Overvelde MLJ (2001) Water transport in the proton-exchange-membrane fuel cell: measurements of the effective drag coefficient. *J Power Sources* 101(1):117–125. doi:10.1016/S0378-7753(01)00708-X
101. Latorrata S, Stampino PG, Amici E, Pelosato R, Cristiani C, Dotelli G (2012) Effect of rheology controller agent addition to microporous layers on PEMFC performances. *Solid State Ionics* 216: 73–77. doi:10.1016/j.ssi.2012.03.030
102. Chebbi R, Wan Daud WR, Mohamad AB, Kadhum AAH (2011) Review of parameters affecting performance of (PVC) electrode for proton exchange membrane fuel cells (PEMFCs). *Adv Mater Res* 233:43–49
103. Selvarani G, Sahu A, Sridhar P, Pitchumani S, Shukla A (2008) Effect of diffusion-layer porosity on the performance of polymer electrolyte fuel cells. *J Appl Electrochem* 38(3): 357–362
104. Tang H, Wang S, Pan M, Yuan R (2007) Porosity-graded microporous layers for polymer electrolyte membrane fuel cells. *J Power Sources* 166(1):41–46
105. Kitahara T, Konomi T, Nakajima H (2010) Microporous layer coated gas diffusion layers for enhanced performance of polymer electrolyte fuel cells. *J Power Sources* 195(8):2202–2211
106. Tseng C-J, Lo S-K (2010) Effects of microstructure characteristics of gas diffusion layer and microporous layer on the performance of PEMFC. *Energy Convers Manag* 51(4):677–684
107. W-k L, Ho C-H, Van Zee J, Murthy M (1999) The effects of compression and gas diffusion layers on the performance of a PEM fuel cell. *J Power Sources* 84(1):45–51. doi:10.1016/S0378-7753(99)00298-0
108. Senthil Velan V, Velayutham G, Rajalakshmi N, Dhathathreyan K (2014) Influence of compressive stress on the pore structure of carbon cloth based gas diffusion layer investigated by capillary flow porosimetry. *Int J Hydrog Energy* 39(4):1752–1759
109. Lee C, Mérida W (2007) Gas diffusion layer durability under steady-state and freezing conditions. *J Power Sources* 164(1):141–153
110. Radhakrishnan A, Lu Z, Kandlikar SG (2010) Effective thermal conductivity of gas diffusion layers used in PEMFC: measured with guarded-hot-plate method and predicted by a fractal model. *ECS Trans* 33(1):1163–1176
111. Xu G, LaManna JM, Clement JT, Mench MM (2014) Direct measurement of through-plane thermal conductivity of partially saturated fuel cell diffusion media. *J Power Sources* 256:212–219. doi:10.1016/j.jpowsour.2014.01.015
112. Yáblecki J, Nabovati A, Bazylak A (2012) Modeling the effective thermal conductivity of an anisotropic gas diffusion layer in a polymer electrolyte membrane fuel cell. *J Electrochem Soc* 159(6):B647–B653
113. Weber AZ, Hickner MA (2008) Modeling and high-resolution-imaging studies of water-content profiles in a polymer-electrolyte-fuel-cell membrane-electrode assembly. *Electrochim Acta* 53(26): 7668–7674. doi:10.1016/j.electacta.2008.05.018
114. Wang Y, Wang C-Y (2006) A nonisothermal, two-phase model for polymer electrolyte fuel cells. *J Electrochem Soc* 153(6):A1193–A1200
115. Khandelwal M, Mench MM (2006) Direct measurement of through-plane thermal conductivity and contact resistance in fuel cell materials. *J Power Sources* 161(2):1106–1115. doi:10.1016/j.jpowsour.2006.06.092
116. Sadeghi E, Djilali N, Balrami M (2011) Effective thermal conductivity and thermal contact resistance of gas diffusion layers in proton exchange membrane fuel cells. Part 1: effect of compressive load. *J Power Sources* 196(1):246–254
117. Escibano S, Blachot J-F, Ethève J, Morin A, Mosdale R (2006) Characterization of PEMFCs gas diffusion layers properties. *J Power Sources* 156(1):8–13
118. Wu J, Yuan XZ, Martin JJ, Wang H, Zhang J, Shen J, Wu S, Merida W (2008) A review of PEM fuel cell durability: degradation mechanisms and mitigation strategies. *J Power Sources* 184(1):104–119. doi:10.1016/j.jpowsour.2008.06.006
119. Chen G, Zhang H, Ma H, Zhong H (2009) Electrochemical durability of gas diffusion layer under simulated proton exchange membrane fuel cell conditions. *Int J Hydrog Energy* 34(19):8185–8192
120. Wood DL III, Borup RL (2009) Durability aspects of gas-diffusion and microporous layers. In: *Polymer electrolyte fuel cell durability*. Springer, New York, pp 159–195
121. Yi P, Ni J, Peng L, Lai X (2011) A numerical model for predicting gas diffusion layer failure in proton exchange membrane fuel cells. *J Fuel Cell Sci Technol* 8(1):011011
122. Bernardi DM, Verbrugge MW (1991) Mathematical model of a gas diffusion electrode bonded to a polymer electrolyte. *AIChE J* 37(8): 1151–1163
123. Bernardi DM, Verbrugge MW (1992) A mathematical model of the solid-polymer-electrolyte fuel cell. *J Electrochem Soc* 139(9):2477–2491
124. Springer T, Wilson M, Gottesfeld S (1993) Modeling and experimental diagnostics in polymer electrolyte fuel cells. *J Electrochem Soc* 140(12):3513–3526
125. Tobias CW (1959) Effect of gas evolution on current distribution and ohmic resistance in electrolyzers. *J Electrochem Soc* 106(9): 833–838
126. Chiang M-S, Chu H-S (2006) Numerical investigation of transport component design effect on a proton exchange membrane fuel cell. *J Power Sources* 160(1):340–352
127. Um S, Wang C (2004) Three-dimensional analysis of transport and electrochemical reactions in polymer electrolyte fuel cells. *J Power Sources* 125(1):40–51
128. Gurau V, Mann JA (2010) Effect of interfacial phenomena at the gas diffusion layer-channel interface on the water evolution in a PEMFC. *J Electrochem Soc* 157(4):B512–B521

129. Zhou P, Wu C (2007) Numerical study on the compression effect of gas diffusion layer on PEMFC performance. *J Power Sources* 170(1):93–100
130. Wang Z, Wang C, Chen K (2001) Two-phase flow and transport in the air cathode of proton exchange membrane fuel cells. *J Power Sources* 94(1):40–50
131. Gurau V, Zawodzinski TA, Mann JA (2008) Two-phase transport in PEM fuel cell cathodes. *J Fuel Cell Sci Technol* 5(2):021009
132. Hartnig C, Manke I, Kuhn R, Kardjilov N, Banhart J, Lelmer W (2008) Cross-sectional insight in the water evolution and transport in polymer electrolyte fuel cells. *Appl Phys Lett* 92(13):134106
133. Pasaogullari U, Wang C-Y (2005) Two-phase modeling and flooding prediction of polymer electrolyte fuel cells. *J Electrochem Soc* 152(2):A380–A390
134. Meng H, Wang C-Y (2005) Model of two-phase flow and flooding dynamics in polymer electrolyte fuel cells. *J Electrochem Soc* 152(9):A1733–A1741
135. Grigoriev S, Kalinnikov A, Fateev V, Wragg A (2006) Numerical optimization of bipolar plates and gas diffusion layers for PEM fuel cells. *J Appl Electrochem* 36(9):991–996
136. Nitta I, Karvonen S, Himanen O, Mikkola M (2008) Modelling the effect of inhomogeneous compression of GDL on local transport phenomena in a PEM fuel cell. *Fuel Cells* 8(6):410–421
137. Su Z, Liu C, Chang H, Li C, Huang K, Sui P (2008) A numerical investigation of the effects of compression force on PEM fuel cell performance. *J Power Sources* 183(1):182–192
138. Dotelli G, Omati L, Gallo Stampino P, Grassini P, Brivio D (2011) Investigation of gas diffusion layer compression by electrochemical impedance spectroscopy on running polymer electrolyte membrane fuel cells. *J Power Sources* 196(21):8955–8966. doi:10.1016/j.jpowsour.2011.01.078
139. Pasaogullari U, Wang C (2004) Liquid water transport in gas diffusion layer of polymer electrolyte fuel cells. *J Electrochem Soc* 151(3):A399–A406
140. Tabe Y, Lee Y, Chikahisa T, Kozakai M (2009) Numerical simulation of liquid water and gas flow in a channel and a simplified gas diffusion layer model of polymer electrolyte membrane fuel cells using the lattice Boltzmann method. *J Power Sources* 193(1):24–31. doi:10.1016/j.jpowsour.2009.01.068
141. Rama P, Liu Y, Chen R, Ostadi H, Jiang K, Zhang X, Gao Y, Grassini P, Brivio D (2011) Determination of the anisotropic permeability of a carbon cloth gas diffusion layer through X-ray computer micro-tomography and single-phase lattice Boltzmann simulation. *Int J Numer Methods Fluids* 67(4):518–530
142. Kim Y, Kang S (2010) Time delay control for fuel cells with bidirectional DC/DC converter and battery. *Int J Hydrog Energy* 35(16):8792–8803
143. Cho J, Park J, Oh H, Min K, Lee E, Jyoung J-Y (2013) Analysis of the transient response and durability characteristics of a proton exchange membrane fuel cell with different micro-porous layer penetration thicknesses. *Appl Energy* 111:300–309. doi:10.1016/j.apenergy.2013.05.022
144. Mandle M, Wilde P (2001) SGL Carbon Group. SGL TECHNOLOGIES GmbH, Private communication
145. Bultel Y, Wiezell K, Jaouen F, Ozil P, Lindbergh G (2005) Investigation of mass transport in gas diffusion layer at the air cathode of a PEMFC. *Electrochim Acta* 51(3):474–488. doi:10.1016/j.electacta.2005.05.007
146. Baker DR, Wieser C, Neyerlin KC, Murphy MW (2006) The use of limiting current to determine transport resistance in PEM fuel cells. *ECS Trans* 3(1):989–999
147. Berning T, Djilali N (2003) A 3D, multiphase, multicomponent model of the cathode and anode of a PEM fuel cell. *J Electrochem Soc* 150(12):A1589–A1598
148. Gloaguen F, Durand R (1997) Simulations of PEFC cathodes: an effectiveness factor approach. *J Appl Electrochem* 27(9):1029–1035
149. Yu HM, Ziegler C, Oszcipok M, Zobel M, Hebling C (2006) Hydrophilicity and hydrophobicity study of catalyst layers in proton exchange membrane fuel cells. *Electrochim Acta* 51(7):1199–1207. doi:10.1016/j.electacta.2005.06.036
150. Li H, Tang Y, Wang Z, Shi Z, Wu S, Song D, Zhang J, Fatih K, Zhang J, Wang H, Liu Z, Abouattallah R, Mazza A (2008) A review of water flooding issues in the proton exchange membrane fuel cell. *J Power Sources* 178(1):103–117. doi:10.1016/j.jpowsour.2007.12.068
151. Skoulidas AI, Ackerman DM, Johnson JK, Sholl DS (2002) Rapid transport of gases in carbon nanotubes. *Phys Rev Lett* 89(18):185901

Article

Manufacturing the Gas Diffusion Layer for PEM Fuel Cell Using a Novel 3D Printing Technique and Critical Assessment of the Challenges Encountered

Arunkumar Jayakumar ^{1,*} , Sarat Singamneni ¹, Maximiano Ramos ¹, Ahmed M Al-Jumaily ¹ and Sethu Sundar Pethaiah ² 

¹ Mechanical Engineering Department, Auckland University of Technology, Auckland 1010, New Zealand; sarat.singamneni@aut.ac.nz (S.S.); maximiano.ramos@aut.ac.nz (M.R.); ahmed.aljumaily@aut.ac.nz (A.M.A.-J.)

² Gashubin Engineering Pte. Ltd., 8 New Industrial Road, Singapore 536200, Singapore; sundar.energy@gmail.com

* Correspondence: ajayakum@aut.ac.nz; Tel.: +64-223896308

Received: 7 June 2017; Accepted: 10 July 2017; Published: 14 July 2017

Abstract: The conventional gas diffusion layer (GDL) of polymer electrolyte membrane (PEM) fuel cells incorporates a carbon-based substrate, which suffers from electrochemical oxidation as well as mechanical degradation, resulting in reduced durability and performance. In addition, it involves a complex manufacturing process to produce it. The proposed technique aims to resolve both these issues by an advanced 3D printing technique, namely selective laser sintering (SLS). In the proposed work, polyamide (PA) is used as the base powder and titanium metal powder is added at an optimised level to enhance the electrical conductivity, thermal, and mechanical properties. The application of selective laser sintering to fabricate a robust gas diffusion substrate for PEM fuel cell applications is quite novel and is attempted here for the first time.

Keywords: PEM fuel cell; gas diffusion layer; membrane and electrode assembly; polyamide; titanium; carbon paper; selective laser sintering

1. Introduction

Among the various fuel cell types, polymer electrolyte membrane (PEM) fuel cells are expected for future technology applications due to their versatile characteristics such as high power density (compatible for transportation), low operating temperature (60–90 °C), and dynamic response [1]. In addition, PEM fuel cells retain the best attributes of both batteries and internal combustion (IC) engines, making them a versatile energy conversion system [2].

The membrane and electrode assembly (MEA) is the prime component/heart of a PEM fuel cell stack, and consists of an electrolyte (proton-exchange membrane) sandwiched between two gas diffusion electrodes (GDEs). Figure 1 provides a 2D view of all the key functional components of a GDE. It is apparent from the figure that gas diffusion layers (GDLs) serve as an armour to protect the principal components—namely, the catalyst layer and membrane of the PEM fuel cell stack [3].

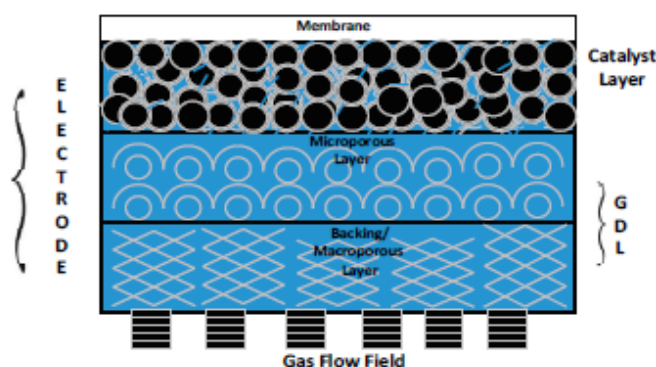
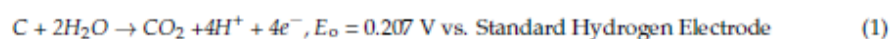


Figure 1. A 2D view of a gas diffusion electrode (GDE) indicating the catalyst layer and gas diffusion layer (GDL; comprising a backing layer and mesoporous layer, MPL).

The desirable characteristics of a GDL include (i) relative stability in the fuel cell environment; (ii) good electrical conductivity; (iii) high permeability for gases and liquids; and (iv) elastic property under compression [4]. Carbon in the form of either paper or cloth are widely used GDL base materials, and both them have their own pros and cons [3]. Though the conventional carbon-based GDLs (non-woven carbon paper and carbon cloth) are functionally similar, they possess different structural characteristics, which might significantly influence the transport of heat, current, reactant gas, and water. Conventional GDLs are typically porous composites and comprise carbon-based material to enhance the electrical conductivity and polytetrafluoroethylene (PTFE) to improve hydrophobicity characteristics [5]. However, these materials contribute to the durability issues. Apart from the durability, the complex manufacturing process also augments the issues pertaining to PEM fuel cell commercialization.

2. GDL Degradation

The conventional GDL material suffers from several degradation issues, and the predominant ones are mechanical and electrochemical degradation. Mechanical degradation is due to the high compression and results in GDL deformation and changes in thickness due to the breakage and displacement of fibres under high pressures. Electrochemical degradation is due to the oxidation of carbon to carbon dioxide, and is illustrated in Equation (1):



However, operating a PEM fuel cell stack at such a low voltage (<0.207 V) is not practically possible. Incorporating a GDL that is free from carbon can be a promising solution to evade this issue.

Excess water accumulation (flooding) can accelerate the degradation of the catalyst and the gas diffusion layer due to polytetrafluoroethylene loss [6,7]. Apart from degradation issues, conventional GDL materials are fabricated by a multifaceted manufacturing process as shown in Figure 2, which is one of the prime reasons for its high cost.

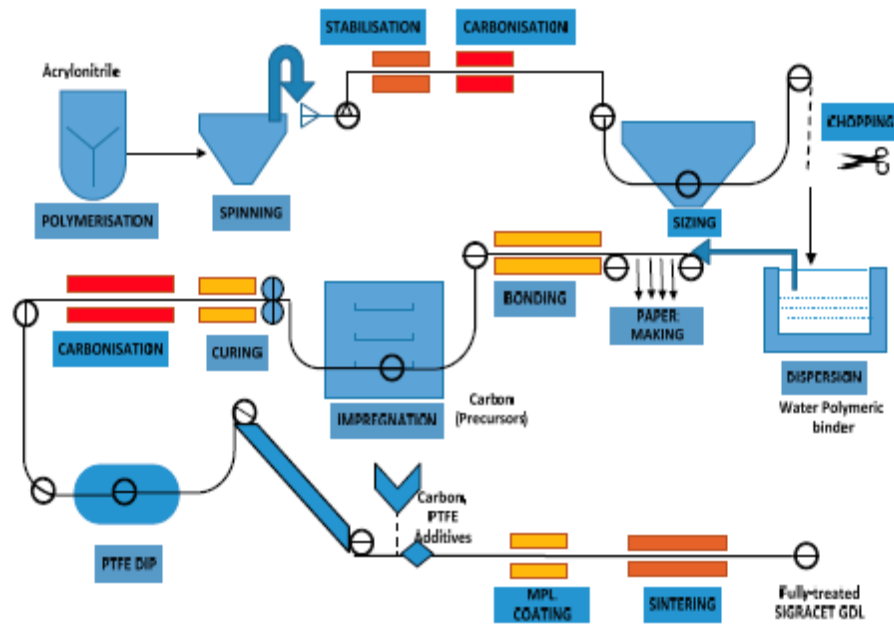


Figure 2. Manufacturing steps involved in conventional GDL fabrication (SGL 39 BC) [8]. PTFE: polytetrafluoroethylene.

The hypothesis of the present work is that the durability, complexity, and cost can be significantly improved in a positive manner by the 3D printing manufacturing technique. Therefore, the contribution to knowledge in the proposed work is to:

- i. Improve the durability of GDL as they are susceptible to electrochemical oxidation [9].
- ii. Simplify the manufacturing process by an advanced 3D printing technique, which can be a promising solution to drastically reduce the costs and lead-time.

3. Experimental Procedure

The manufacturing process employed in the present work involves the use of a selective laser sintering (SLS) system, where the desired material in the powder form can be consolidated layer upon layer through laser heating. Sufficient inter-particle and inter-layer consolidation are achieved by optimising the laser energy flowing into the powder substrate [10]. The energy density (E_D , $J \cdot mm^{-2}$) per unit area along the scan line can be evaluated as per Equation (2) [11]:

$$E_D = P / (D \times v). \quad (2)$$

The three critical parameters governing the SLS (3D printing) mechanism are laser power (P), scan speed (v) and beam diameter (D) [11]. The SLS system used for the work employs a beam deflection system (galvano mirrors) to achieve the laser scanning as required.

Material Selection for SLS

Not all the materials that can be processed using the existing SLS infrastructure can be used to synthesize the gas diffusion material for the PEM fuel cell application. In the previous investigation, alumide [12] was used as the base material since it is stiffer than many other materials used in 3D printing and it contributes to good flexural strength and higher thermal load [13].

Though the mechanical and electrical characteristics of alumide are compatible for PEM operating conditions, one of the severe limitations from the fundamental chemistry perspective is that the aluminium present in the alumide is prone to oxidation in the PEM fuel cell environment, resulting in the possibility that metal ions formed could potentially damage the expensive membrane component. Other researchers [14–16] reported that aluminium bipolar plates exposed to a PEM fuel cell operating environment are prone to such a corrosion. Consequently, in the following work polyamide (PA) is used as the base material to develop the thin film samples.

The utilization of titanium structures has already been proposed by Hottinen et al. [17], and it is a safe material for GDL application. Titanium powder (US Research Nanomaterials, Houston, TX, USA) was added to polyamide in appropriate percentages to infuse appropriate conductivity, as polyamide is a non-conducting polymer, however well compatible with the SLS process.

In this present study, the base powder (PA) was sintered in a precise mode; appropriate functional material (Ti in the present study) was added to the base powder to attain the desirable functional characteristics. In the preliminary investigations, it was observed that sufficient electrical conductivity was not attained with 10% titanium, and consequently the experiment was performed with 20% and 30% titanium. For the 30% titanium composition, the laser was not able to sinter the composite powder, as the laser power oxidised the titanium metallic powder in the composite instead of selectively binding it. Thus, the composite with 30% titanium was too brittle and was left out of the subsequent investigation.

Based on this, the 20% Ti and 80% polyamide composite was considered for further evaluation. The composite powder was spread on the build platform layer upon layer, achieving a uniform dispersion and a flat top surface. The initial temperature of the powder bed was kept at around 70 degrees to keep the powder substrate dry and free of moisture. To study the diffusion and bonding of the titanium powder, the experiments were executed by varying the power as illustrated in Table 1 for a fixed scanning speed of 450 mm/s. These combinations of laser power and material composition were established based on trial and error experimentation and the resulting sintered structures. It may be noted that with increasing titanium content, the laser power required is decreased in order to achieve a continuous sintered layer. This is because the titanium component absorbs the heat from the laser and burns partly, which is an exothermic reaction, resulting in excessive thermal energies. Consequently, the higher the titanium content, the lower the energy density level for laser sintering.

Table 1. Laser power required to sinter various configurations of polyamide (PA)/titanium.

Laser Power (W)	Polyamide/Titanium Composition (%)
15	10/90
12	20/80
9	30/70

4. Characterization

The characterization studies were performed to investigate the mechanical, physical, and electrical properties of the proposed gas diffusion material. The characterization studies involved in the present work are as follows:

- Surface and Elemental Energy Dispersive X-ray Analysis (EDX) characterization to investigate morphology and composition, Hydrophobicity, and Porosity measurement.
- Electrical characterization to investigate in-plane resistance.
- Thermal characterization to investigate thermal conductivity.
- Tensile characterization to investigate tensile strength.

The proposed paper considers SIGRACET[®] grade GDL 39 BC (325- μ m thickness) as a baseline material. The unique characteristics of SGL 39 BC to consider is that it is denser and has a better

water-retaining capability than its precursors (SGL 10 BC) [8]. Therefore, it is observed that SIGRACET® grade GDL 39 will be an appropriate material for baseline consideration.

4.1. Surface Morphology—SEM

Surface characterization: The sample produced using SLS process was investigated and characterised using a Schottky field emission scanning electron microscope (SEM) (Hitachi SU-70, Tokyo, Japan). Figure 3 reveals the SEM image of (a) surface and (b) cross-section of the novel carbon-free gas diffusion material.

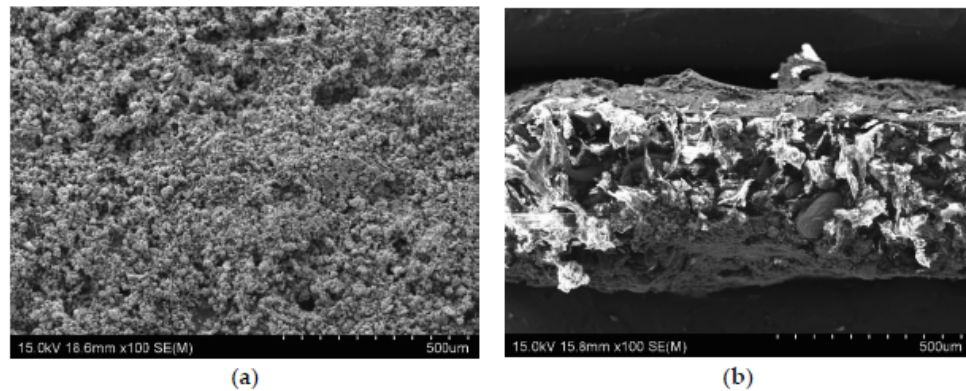


Figure 3. SEM image of the proposed gas diffusion material. (a) Surface; (b) Cross-section.

The Table 2 provides the elemental analysis of the proposed composite material.

Table 2. The elemental analysis of the proposed composite material after selective laser sintering (SLS).

	C	N	O	Ti	Zr
S7-PA	66.1	8.3	9.1	14.8	1.7

4.2. Hydrophobicity

Contact angle measurement is a powerful diagnostic for understanding the interaction of GDL material with water. The degree of hydrophobicity is determined by the simple concept proposed by Zamora et al. [18], in which a 20- μ L drop was deposited on a sample and after stand-up for 1 h, zoom shooting was conducted for the sample and the contact angle was measured between the droplet and the surface. The material exhibited predominantly hydrophilic nature with the contact angle measurement [$\theta \sim 20^\circ$].

4.3. Electrical Characterization

Electrical conductivity is a key property which directly influences the fuel cell performance [19]. Polymers filled with metal are of substantial interest because the electrical characteristics of such composites are close to metal properties with mechanical properties and processing procedures typical to that of plastics [20]. The figure of merit of the electrical characterization signifies the ease with which electrons transfer along the in-plane.

The electrical conductivity of the substrate was measured to be 1–10 S/cm; however, it was sensed to be low and consequently a nano-conductive platinum coating was provided by means of an ion sputter coater (Hitachi-E-1045, Tokyo, Japan) along both surfaces for few minutes, which surged the in-plane electrical conductivity of the substrate. The surface roughness of the substrate (as shown in the SEM image of Figure 3a) might be one of the factors that caused an effective physical

absorption/diffusion of Pt towards the 3D matrix of the substrate; In addition, the grain sizes of Pt are smaller than gold, which validate the advantage of Pt over gold in ion sputtering. The four-wire Kelvin method was used to measure the electrical properties (in-plane resistance) of the GDL using the DMM 4040 meter (Tektronix, OR, USA).

4.4. Thermal Characterization

The thermal diffusivity of the sample material was measured using the laser flash apparatus LFA 467 *HyperFlash*[®] (NETZSCH, Bavaria, Germany). The sample was tested at several temperatures according to their behaviour in the desired temperature range of 25–160 °C. The measurements were carried out in a foil sample holder (Φ 25.4 mm) at the values of 25 °C, 80 °C, and 140 °C. In agreement with theory, the thermal diffusivity of the material decreased with higher temperatures, while specific heat values increased. Table 3 provides the thermophysical properties of polyamide-titanium composite.

Table 3. Thermophysical properties of polyamide-titanium composite.

Temperature/°C	Thermal Diffusivity mm ² /s	Specific Heat kJ/(kg·K)	Thermal Conductivity W/(m·K)
25	0.680	1.289	0.588
80	0.521	1.559	0.544
140	0.408	1.870	0.512

4.5. Tensile Strength

Tensile test was performed using a TA.XT Plus texture analyser (Stable Micro Systems Ltd. Godalming, Surrey GU7 1YL, UK) to analyse the mechanical strength characteristics of the proposed material. ASTM D882 test method was piloted to estimate the tensile properties of the proposed thin films (as the thickness is less than 1.0 mm). To avoid tearing and premature specimen failure, the tensile test was conducted at a speed of 0.5 mm/s. The thin film material was clamped between two fixtures and tested to measure its tensile strength and was found to be approximately (ca.) 4 N/cm.

5. Polarization Curve

The MEA was fabricated as follows. Catalyst-coated membrane (CCM) was prepared by giving a coating of 0.5 mg Pt/cm² on either side of the Nafion membrane. The fabricated GDL (by 3D printer) was attached on both sides of the CCM, after applying a thin coating of Pt black on the GDL side facing the membrane, such that the additional Pt loading was about 0.1 mg/cm². The above MEA was placed in the fuel cell test fixture. The graphite plates with a serpentine flow channel were used for the single cell studies. The experiments were performed in both dry and humidified conditions (100% humidity at a cell temperature of 75 °C). The reactant gases—namely H₂ and O₂—were fed at a pressure of 15 psi. The cell was connected to a Hewlett Packard DC electronic load bank for the polarization studies. All the operating parameters were kept constant throughout the course of the experiment.

Figure 4 displays the polarization curve, and it is obvious that the cell performance with 3D printed GDL showed a much more inferior performance than the commercial SGL-based GDL. However, it is inferred that the performance of the 3D printed GDL displayed a marginally improved performance with humidified conditions.

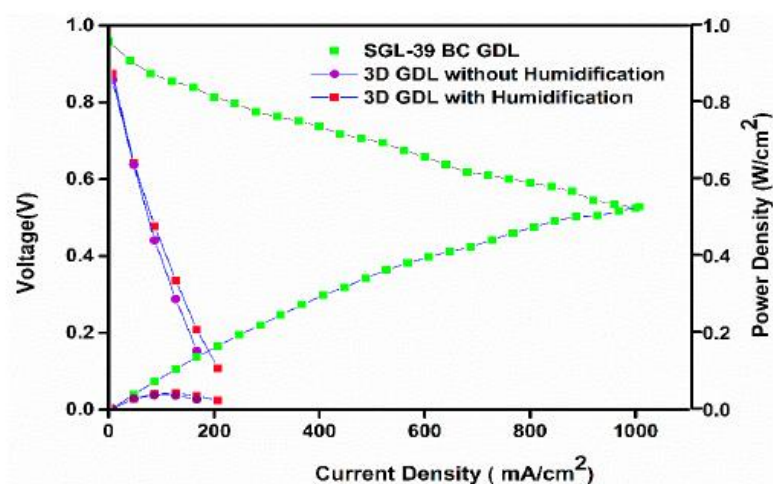


Figure 4. Polarization plots for the 3D-printed GDL [80% PA + 20% Ti] used membrane and electrode assembly (MEA) and normal MEA tested with humidified H_2/O_2 at 75 °C and 15 psi pressure.

6. Discussion and Limitation

The values of the proposed material were compared against a wide range of conventional GDLs, and their values are illustrated in Table 4, which compares the properties of the proposed material (fabricated by 3D printing) and Carbon paper Sigracet™ 39 BC. The functional characteristics as specified in Table 4 authenticate that this material can be a hopeful candidate for GDL, as it is carbon free and possesses optimal multifunctional characteristics such as thickness, porosity, and conductivity. The low electrical conductivity is one of the prime limitations in this study, which might be attributed to the porous nature of 3D-printed GDL.

Table 4. Comparison of functional properties of the proposed material with Sigracet™ 39 BC [8].

Material Properties	Proposed Material (Polyamide-80% & Titanium-20%) Fabricated by SLS	Sigracet™ 39 BC
Thickness (μm)	430	325
Basic Weight (gm^{-2})	380	105
In-Plane Conductivity (S/cm)	1–10 * S/cm	170 **
Thermal Conductivity (W/(mK))	0.588–0.512 (Using Laser Flash Analysis)	0.25
Porosity (%)	ca. 42% (Using ImageJ)	52
Tensile Strength (N/cm)	≥ 4	NA

* Uncompressed; ** Compressed with 1 MPa.

The characterization studies authenticate that the proposed material can be an economical alternative to the conventional carbon-based GDLs (woven carbon cloth and non-woven carbon paper) preparation route. One of the unique features of SLS to be compatible for GDL application is its porosity characteristics by default [21]. The numerical values of the various characteristics of the proposed GDL exhibited a minor deviation as elaborated in Table 4 due to the material's anisotropic nature.

Though titanium has been previously used in the literature by Hottinen et al. [17], they were unable to achieve the desired thickness and porosity. However, in the proposed technique the thickness was around 430 μm , which is around 15% less than that made by Hottinen et al. The incorporation of the 3D printing technique is the prime factor to attain this level of fitness, where the complexity of the binder requirement is eliminated by the heat produced in the laser to bind the base powder to the metallic powder.

Though 20% titanium was the actual weight proportion used for the substrate preparation, it was sensed in the EDX (in Table 2) that weight as low as 14.8% actually contributed to the substrate formation. The following possibilities might have happened in the process:

- i. An increase in the Ti alone does not provide a feasible solution to enhance the conductivity, because with the present experimental set-up (non-inert atmospheric condition) the titanium present in the composite might be oxidised to titanium oxide (evident from the EDX of Table 2).
- ii. Performing the experiment in argon conditions can drastically enhance the electrical conductivity, and under such an operating condition the increase in the Ti can actually enhance the electrical conductivity of the gas diffusion material and a higher percentage such as 30% or 40% can be feasible. In addition, the incorporation of ion sputtering to enhance the surface conductivity can be totally eliminated under that circumstance.

The authors assert that appropriate mixing of titanium particles with the base powder material using an advanced ball mill can also enhance the electrical conductivity, unlike in the present study where a manual mortar was used to mix the Ti powder to PA. Though in the proposed research the performance of the proposed GDL was much lower than the conventional GDL (SGL 39 BC), its manufacturing complexity is very simple and straight-forward. The DOE target of \$5.5/m² for a mass GDL production of 500,000 [22] can be very easily accomplished through this technique because the process is predominantly single-stage (as ion sputtering can be possibly eliminated in future), unlike multiple stages in the conventional route (evident from Figure 2), less residue is produced, and there is reduced lead time (improving the productivity) and complexity.

7. Conclusions

The principal implication of this work is that the carbon-based gas diffusion layer—which is the integral constituent in a PEM fuel cell stack—is prone to electrochemical degradation. To circumvent that, a novel additive manufacturing approach incorporating selective laser sintering was used to fabricate a non-carbon-based GDL directly from a 3D printing technique (additive manufacturing). This manufacturing route is an economical option, and has the substantial potential to achieve the Department of Energy ((DOE), USA target in the future by appropriately selecting the material and optimising the operating parameters. Though the performance is currently low, the authors ascertain that the fine-tuning of the SLS process parameters (such as SLS printer speed and laser power) and appropriate material selection and performing the experiment in the inert atmosphere can match its characteristics to be on-par with or superior to that of conventional GDL.

Acknowledgments: This work was supported by IBTec, Auckland University of Technology (AUT) grant by the Doctoral Fellowship and the author would like to acknowledge their support. The authors would like to thank NETZSCH, Germany for performing the thermal characterization study on the proposed materials. The authors would also like to thank Jo Stone for an effective proof reading.

Author Contributions: Arunkumar Jayakumar conceived the project, purchased the materials, performed the characterisation studies and composed the paper. Sarat Singamneni planned and performed the Selective Laser Sintering experiments. Maximiano Ramos assessed the paper. Ahmed M Al-Jumaily contributed to the discussion of the data and Sethu Sundar Pethaiah performed the PEM fuel cell polarisation experiment.

Conflicts of Interest: The authors declare no conflict of interest.

References

1. Kumar, J.A.; Kalyani, P.; Saravanan, R. Studies on PEM fuel cells using various alcohols for low power applications. *Int. J. Electrochem. Sci.* **2008**, *3*, 961–969.
2. Jayakumar, A.; Chalmers, A.; Lie, T.T. A Review of Prospects for Adoption of Fuel Cell Electric Vehicles in New Zealand. *IET Electr. Syst. Transp.* **2017**. [[CrossRef](#)]
3. Jayakumar, A.; Sethu, S.P.; Ramos, M.; Robertson, J.; Al-Jumaily, A. A technical review on gas diffusion, mechanism and medium of PEM fuel cell. *Ionics* **2015**, *21*, 1–18. [[CrossRef](#)]

4. Park, S.; Lee, J.-W.; Popov, B.N. A review of gas diffusion layer in PEM fuel cells: Materials and designs. *Int. J. Hydrogen Energy* **2012**, *37*, 5850–5865. [CrossRef]
5. Shimpalee, S.; Beuscher, U.; Van Zee, J.W. Analysis of GDL flooding effects on PEMFC performance. *Electrochim. Acta* **2007**, *52*, 6748–6754. [CrossRef]
6. Borup, R.; Meyers, J.; Pivovar, B.; Kim, Y.S.; Mukundan, R.; Garland, N.; Myers, D.; Wilson, M.; Garzon, F.; Wood, D.; et al. Scientific aspects of polymer electrolyte fuel cell durability and degradation. *Chem. Rev.* **2007**, *107*, 3904–3951. [CrossRef] [PubMed]
7. Seidenberger, K.; Wilhelm, E.; Schmitt, T.; Lehnert, W.; Scholta, J. Estimation of water distribution and degradation mechanisms in polymer electrolyte membrane fuel cell gas diffusion layers using a 3D Monte Carlo model. *J. Power Sources* **2011**, *196*, 5317–5324. [CrossRef]
8. Schweiss, R.; Meiser, C.; Damjanovic, T.; Galbiati, I.; Haak, N. Sigracet® Gas Diffusion Layers for PEM Fuel Cells, Electrolyzers and Batteries. 2016. Available online: https://www.researchgate.net/profile/Ruediger_Schweiss/publication/295859224_SIGRACETR_Gas_Diffusion_Layers_for_PEM_Fuel_Cells_Electrolyzers_and_Batteries_White_Paper/links/56cece8308aeb52500c5416a.pdf (accessed on 11 July 2017).
9. Wu, J.; Yuan, X.Z.; Martin, J.J.; Wang, H.; Zhang, J.; Shen, J.; Wu, S.H.; Merida, W. A review of PEM fuel cell durability: Degradation mechanisms and mitigation strategies. *J. Power Sources* **2008**, *184*, 104–119. [CrossRef]
10. Kruth, J.P.; Mercelis, P.; Van Vaerenbergh, J.; Froyen, L.; Rombouts, M. Binding mechanisms in selective laser sintering and selective laser melting. *Rapid Prototyp. J.* **2005**, *11*, 26–36. [CrossRef]
11. Velu, R.; Singamneni, S. Evaluation of the influences of process parameters while selective laser sintering PMMA powders. *J. Mech. Eng. Sci.* **2015**, *229*, 603–613. [CrossRef]
12. Jayakumar, A.; Ramos, M.; Al-Jumaily, A. A novel 3D printing technique to synthesise gas diffusion layer for PEM fuel cell application. In Proceedings of the ASME 2016 International Mechanical Engineering Congress and Exposition, Phoenix, AZ, USA, 11–17 November 2016.
13. Ju, H.; Meng, H.; Wang, C.-Y. A single-phase, non-isothermal model for PEM fuel cells. *Int. J. Heat Mass Trans.* **2005**, *48*, 1303–1315. [CrossRef]
14. Hermann, A.; Chaudhuri, T.; Spagnol, P. Bipolar plates for PEM fuel cells: A review. *Int. J. Hydrogen Energy* **2005**, *30*, 1297–1302. [CrossRef]
15. Hung, Y.; El-Khatib, K.; Tawfik, H. Testing and evaluation of aluminum coated bipolar plates of PEM fuel cells operating at 70 °C. *J. Power Sources* **2006**, *163*, 509–513. [CrossRef]
16. Woodman, A.S.; Jayne, K.D.; Anderson, E.B.; Kimble, M.C. Development of corrosion-resistant coatings for fuel cell bipolar plates. In Proceedings of the American Electroplaters and Surface Finishers (AESF) SUR/FIN '99, Annual International Technical Conference, Cincinnati, OH, USA, 21–24 June 1999.
17. Hottinen, T.; Mikkola, M.; Mennola, T.; Lund, P. Titanium sinter as gas diffusion backing in PEMFC. *J. Power Sources* **2003**, *118*, 183–188. [CrossRef]
18. Zamora, H.; Canizares, P.; Rodrigo, M.A.; Lobato, J. Improving of micro porous layer based on advanced carbon materials for high temperature proton exchange membrane fuel cell electrodes. *Fuel Cells* **2015**, *15*, 375–383. [CrossRef]
19. Mathias, M.F.; Roth, J.; Fleming, J.; Lehnert, W. *Diffusion Media Materials and Characterisation, Handbook of Fuel Cells*; John Wiley & Sons, Ltd: Hoboken, NJ, USA, 2003.
20. Mamunya, Y.P.; Davydenko, V.V.; Pissis, P.; Lebedev, E.V. Electrical and thermal conductivity of polymers filled with metal powders. *Eur. Polym. J.* **2002**, *38*, 1887–1897. [CrossRef]
21. Lohfeld, S.; Tyndyk, M.A.; Cahill, S.; Flaherty, N.; Barron, V.; McHugh, P.E. A method to fabricate small features on scaffolds for tissue engineering via selective laser sintering. *J. Biomed. Sci. Eng.* **2010**, *3*. [CrossRef]
22. James, B.D.; Spisak, A.B. *Mass Production Cost Estimation of Direct H₂ PEM Fuel Cell Systems for Transportation Applications: 2013 Update*; Under Award Number DEEE0005236 for the US Department of Energy; Strategic Analysis, Inc.: Arlington, VA, USA, 2013.



© 2017 by the authors. Licensee MDPI, Basel, Switzerland. This article is an open access article distributed under the terms and conditions of the Creative Commons Attribution (CC BY) license (<http://creativecommons.org/licenses/by/4.0/>).